Politecnico di Torino

Corso di Laurea Magistrale in Ingegneria Aerospaziale

Academic year 2020/2021

Sessione di Laurea Ottobre 2021

Sonic boom Sensitivity analysis for different type of configuration

Bow shock overpressure and time duration for different type of supersonic aircraft with Carlson's Method

Relatori:

N. Viola

R. Fusaro

Candidato

Samuele Graziani

Sonic boom Sensitivity analysis for different type of configuration

Bow shock overpressure and time duration for different type of supersonic aircraft with Carlson's Method

Samuele Graziani

Abstract

In the last decades, the effort of scientist and engineer have result in the creation of reliable methods for the prediction of sonic-boom phenomena. In particular for this work it was used Carlson's method that provides estimates of sonic-boom pressure and time duration over the entire exposed ground area for vehicles in level flight or in moderate climb or descent flight profiles. This thesis studied the sonic boom pressure level and duration time for Concorde, Stratofly and GreenHawk3 concept. A sensitivity analysis was first carried out by varying altitude, aircraft length, Mach number and flight path angle. The previous parameters were varied simultaneously in order to determine what had the greatest influence on the sonic boom analysis. Regarding GreenHawk3 conceptual design, the reduction of shape factor was investigated by positioning the wings two metres forward.The influence of the positioning of a canard was also studied. Finally, regarding Stratofly project, an analysis was carried out for an aircraft with a length of 70% of the original.

Dedication

To my twin Brenno

Contents

List of Figures

List of Tables

Nomenclature

Δp Pressure increase due to sonic boom [Pa]

Δp_{max} Pressure increase due to sonic boom at N-wave bow shock [Pa]

γ Flight path angle [deg]

ϕ Angle between aircraft ground track and ground projection of ray path [deg]

θ Ray path azimuth angle [deg]

$A(x)$ area of aircraft cross section normal to flight direction at a given value of longitudinal coordinate x

$A_{e,1}$ total effective area at the half of effective aircraft length l_e $[m^2]$

$A_{e,max}$ maximum effective area $[m^2]$

$A_e(x)$ effective area of aircraft at a given x coordinate

a_v speed of sound at the given altitude $[\frac{m}{s}]$

$B(x)$ Equivalent area due to lift

$b(x)$ local span of the aircraft planform at a given value of x coordinate

d Distance between aircraft ground track position at time of sonic boom generation and location of the ground impact [km]

d_x Component of d in direction of the aircraft ground track [km]

d_y Component of d in direction perpendicular of the aircraft ground track [km]

h altitude of aircraft above the ground and equal to $h_v - h_g$ $[km]$

h_e Effective altitude[km]

h_e effective altitude $[km]$

h_g altitude of ground above sea level $[km]$

h_v altitude of aircraft above sea level$[km]$

K_d Ray path distance factor

K_L Lift parameter

K_P Pressure amplification factor

K_R	reflection factor, equal to 2.0
K_S	Aircraft shape factor
K_t	signature duration factor
l	Aircraft fuselage length [m]
l_e	effective length of aircraft [m]
M	Mach number
M_c	Cut off Mach numbe below which sonic boom will not reach ground
M_e	Effective Mach number
p	Atmospheric pressure [Pa]
p_g	Atmospheric pressure at ground level [Pa]
p_v	Atmospheric pressure at aircraft altitude [Pa]
S	Aircraft planeform area, m^2
W	Aicraft weight [kg]
x	Distance from aicraft nose measured backward along flight path [m]

1

Sonic Boom Phenomena

1.1 Description of sonic boom

Any body moving with a speed greater than the local speed of sound a_v generates a shock wave system. For a supersonic aircraft there is the formation of a series of shock waves, which at a great distance will coalescence into a bow and tail shock.

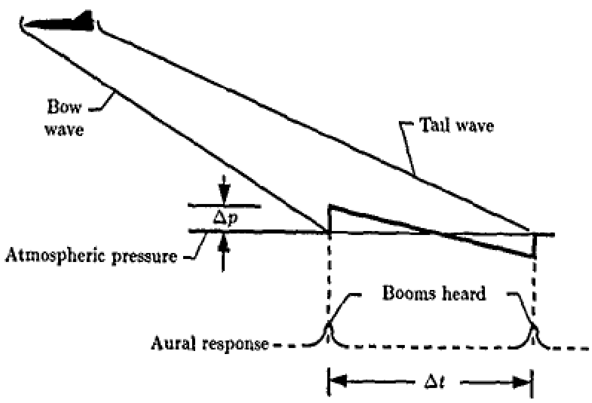

Figure 1.1: Far field wave patterns

In figure 1.1 there is the representation of a system of shock waves that manage to reach the ground. At the bow wave it occurs a compression that are able to increase the local pressure from a value of atmospheric pressure p to $p + \Delta p$.
Following this initial compression, there is an approximately linear expansion wave that produces a decrease in local pressure to values below atmospheric pressure p. In conclusion, there is a second compression wave or tail shock that brings the pressure back up to atmospheric pressure.
In the vast majority of cases the two compression waves are of the same order of intensity, with the expansion wave being approximately linear: this type of wave system is called *N-wave* because of its shape and it moves with the aircraft in continuous supersonic flight.
A sonic boom carpet is defined as that portion of the ground which is affected by this wave system and whose amplitude depends on the operational flight conditions and the characteristics

of the aircraft itself. The duration of the sonic boom Δt influences the perception of a listener on the ground, in particular if this value is higher than 0.15 seconds the human ear manage to distinguish two different booms.
Generally, a large supersonic aircraft flying at high altitudes produces a time duration Δt greater than 0.15 seconds and consequently two different booms can generally be distinguished by a listener on the ground.
The peaks of Δp are also often associated with certain aircraft elements such as wings and inlets. It can be seen that as the distance from the aircraft increases, these waves become coalescent with also a marked difference between the wave system generated above the aircraft and those below.

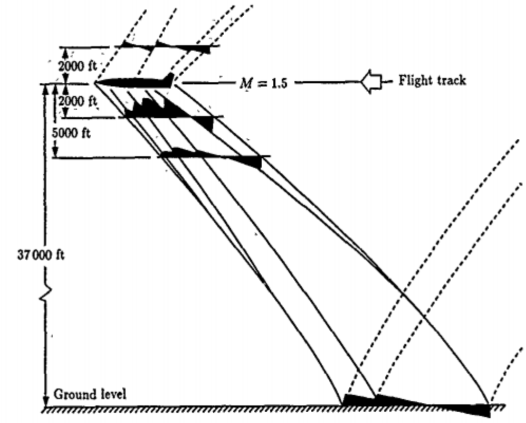

Figure 1.2: Evolution of pressure signature

1.2 Sonic boom carpets

A first description of the ground exposed pattern was given in section 1.1. Usually, however, there is not just one zone in which sonic boom overpressure is present, but two ground exposure patterns are distinguished.
Primary boom carpet contains the observed sonic boom overpressure of only the propagating wave below the aircraft, while secondary boom carpet contains both the portion of the atmosphere above the aircraft and the portion below the aircraft itself.Between these two regions, there is an area where there is no sonic boom.
Generally, the secondary boom carpet is located at large distances from the aircraft(could be hundreds of km) and the value of overpressure is considerably lower than on the primary boom carpet.

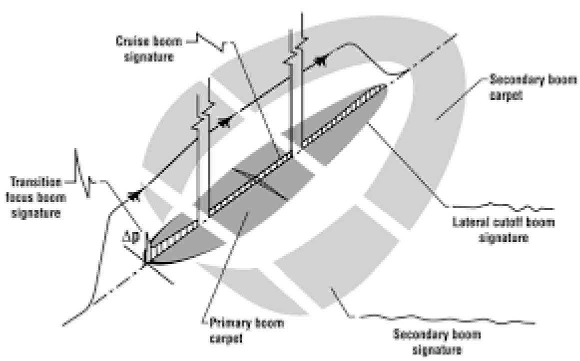

Figure 1.3: Sonic boom carpets

It should be notice that lateral cutoff booms and secondary booms don't have a *N-wave* characteristic. Moreover, secondary boom are not audible due to their frequency(between 0.1 and 1.0 Hz). The last signature type is the focus boom and it could be visible when the aircraft accelerates, which will lead to a coalescence of the wave system causing a higher value of sonic boom pressure.

1.2.1 Primary boom carpet

Over the years, numerous studies have been conducted regarding the calculation of the peak amplitude of primary boom carpet overpressures under various flight conditions.

Lateral spread Measurements

It is also important the lateral evolution of the primary boom carpet and whose intensity decrease as the distance of the aircraft increase. The extent of the primary carpet is the point at which the ray refracts away from the ground and is independent of aircraft configuration.
It is a function of the flight altitude of the aircraft, the Mach number and the atmospheric characteristics below the aircraft.

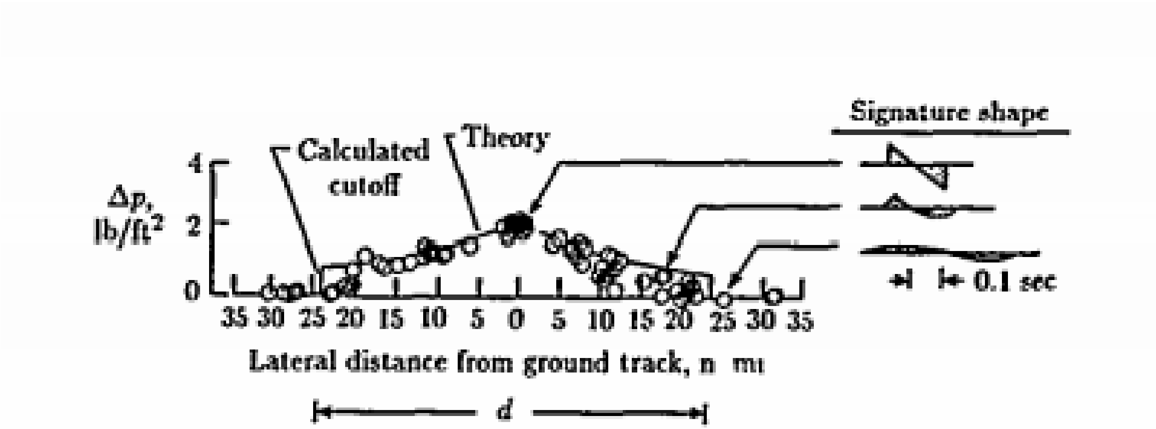

Figure 1.4: Sonic boom overpressure for XB-70 at 60000ft as function of lateral distance

It should be notice that the width of sonic boom carpet increase with the increase of altitude and Mach number. However, consideration should be given to any important atmospheric variations especially in the first few thousand feet above the ground. In fact, it can cause a distortion of the sonic boom signature by varying from a classic *N-wave* configuration to a *peaked* or *rounded-type* signature.
Moreover, with a peaked signature higher overpressure values will be obtained than with a rounded type. In particular, rounded waveform signatures are typically associated with bow shock overpressures value below 1.0 lb/ft^2, on the other hand the peaked ones have as previously highlighted have higher values and are typically greater than 1.0 lb/ft^2.

1.2.2 Secondary boom carpet

The secondary sonic boom is the second configuration of disturbance due to the presence of a supersonic aircraft and has different features from the primary both from the point of view of the mode of its propagation and signature.

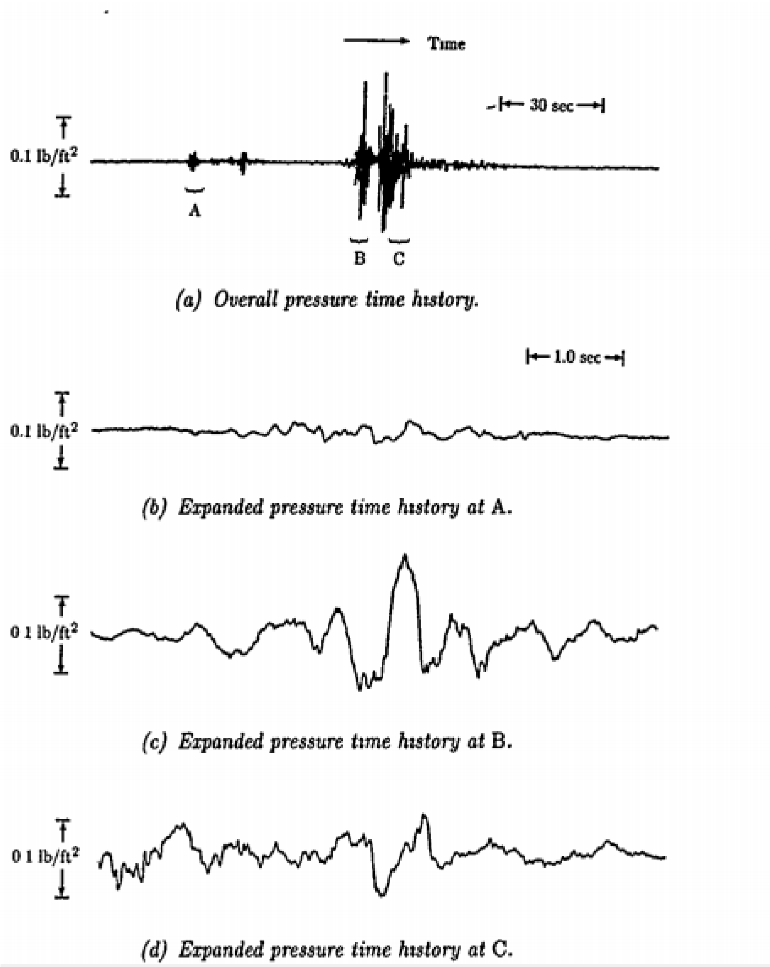

Figure 1.5: Secondary sonic boom Concorde

In figure 1.5 there is the representation of the secondary sonic boom signature from Concorde, the first civil supersonic aircraft.
From the figure it could be see that the signal is complex with numerous perturbations observed having a much longer duration time than the primary sonic boom(hundreds of time) and with maximum peak intensity 0.2 psf, which is more than 10 times lower than the intensity of the primary sonic boom.
It could be seen that the fundamental frequency of the secondary sonic boom is between 1.5 and 2.0 Hz. In addition, for secondary sonic boom the pressure variation is very slow and has a subaudible frequency value. Moreover, the fact of having very low amplitudes makes it very complicated for the human ear to distinguish this sound, in fact its presence remained unknown until the end of the 70s with the first flights of Concorde. However by modifying the path of the aircraft and its operating conditions according to atmospheric and seasonal conditions the disturbance was eliminated.
Like the primary sonic boom, their perception varies according to the sensitivity of the subject. In addition, in indoor cases the perception is stronger due to the vibration of the structure and the various elements inside the building that causes movements and rattling.
These disturbances affect both the upper and lower parts of the atmosphere during propagation it has a very small overpressure value and a low frequency content.The distance in which this disturbance propagates could be in the order of 150 or more km from the position of the aircraft itself but there are not yet detailed studies on the human response to these disturbances.

1.3 Role of atmosphere

1.3.1 Influence of a stratified atmosphere

In a stratified atmosphere, two types of effects of the atmosphere on the primary boom carpet can be distinguished:

1. macro effects

2. micro effects

Macro effects are related to characteristics such as pressure, temperature and wind profile while micro effects to turbulence, especially at lower altitude. In figure 1.6 are represented the major atmospheric effects on sonic boom overpressure.
Viscous losses, conduction, turbulence effects and heat effects influence in the first thousand feet of earth's surface while atmospheric absorption is important from ground to tropopause, instead at higher altitude humidity is not anymore relevant.

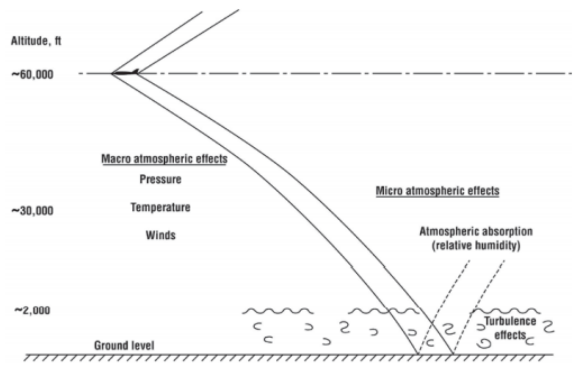

Figure 1.6: Atmospheric effects

Macro effects

The atmospheric temperature variation between the aircraft and the ground will cause the refraction of the ray path, which describes the path of the shock-wave.
As far as the temperature gradient is concerned, a negative gradient will result in the ray path bending upwards while in the case of a positive gradient the ray path bending downwards. The distortion of the ray path leads to the formation of a shadow zone after the primary boom carpet that was already described in the previous section.
As for the variation of wind speed and direction between the aircraft and the ground, this variation leads to a change in the direction of the ray path similarly to the variation of temperature. In particular, in case of head winds they tend to bend the rays upwards while the opposite occurs with tail winds.

Regarding the effects of these two factors described on sonic boom pressure, for Mach number values greater than 1.5, sonic boom overpressure along the aircraft ground track could results in a variation of up to 5% rather the standard atmosphere case.
The value increases for ground temperatures lower than the standard temperature and with the presence of tailwinds at altitude. On the other hand, the value will decrease for temperatures higher than the standard temperature and with the presence of headwinds at flight altitude.

Micro effects

Micro effects are correlated to the turbulent processes in the atmosphere and lead to forms of instability. They can result from wind shear, flying over large obstacles or thermal instability due to solar heating of the ground.

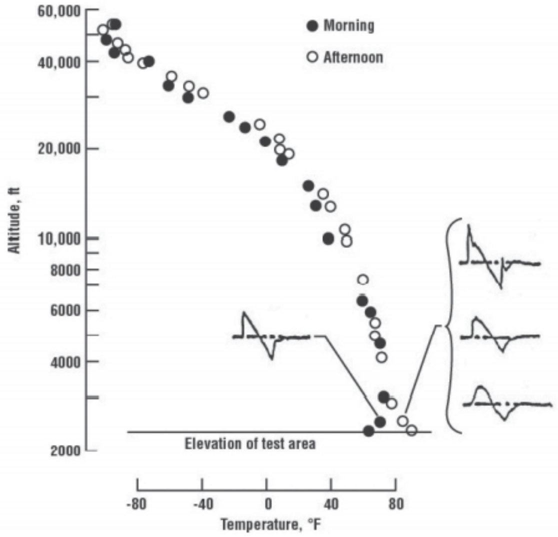

Figure 1.7: Effect of earth's boundary leyer on temperature profile

Figure 1.7 represent the temperature variation in function of altitude between morning and afternoon. It could be seen that in the upper part of atmosphere the variation in temperature is not marked throughout the day, while in the first thousand of feet above the groumd, in the lower part of atmosphere the temperature profile is different.
With this particular type of temperature profile, the surface layer of the atmosphere is unstable and could generate thermal-induced turbulence. In fact, there is a correlation between the type of signature and the temperature profile in the lower layers of the atmosphere.
In particular, there is the presence of the classic N-waves when the lower atmosphere is quiescent, while there are the presence of distortions and variations in the shape of the signature when the lower part of atmosphere is unstable.

1.4 Sonic Boom Theory

A slender axisymmetric body in a uniform supersonic flow generates a cylindrical acoustic wave field with a value of overpressures given by the following equation:

$$\Delta p(x-\beta r, r) = p_0 \cdot \frac{\gamma M^2 F(x-\beta r)}{(2\beta r)^{\frac{1}{2}}} \tag{1.1}$$

In equation 1.1 p is the atmospheric pressure, p_0 is the ambient pressure, x is the axial coordinate, r is the radius of the cylinder, γ is the ratio of specific heat and β is the Prandtl-Glauert factor equal to

$$\beta = \sqrt{M^2-1}$$

Also in equation 1.1 Whitham F-function is equal to:

$$F(x) = \frac{1}{2\pi}\int_0^x \frac{A''(\xi)}{(x-\xi)^{\frac{1}{2}}} d\xi \tag{1.2}$$

In equation 1.2 A is the cross sectional area and ξ is a variable of integration.
These equations are respectively derived from the linearised supersonic flow theory and the area rule for axisymmetric bodies. Moreover, this formulation could be also appropriate for non-axisymmetrical body by replacing the actual cross sectionl area A(x) by an equivalent area function of the azimuth angle with an axis which passes through the body of the aircraft in the direction of flight.
This equivalent area is composed by two parts:

- area of the aircraft cross sectional normal to flight direction $A(x)$ or *equivalent area due to volume*
- equivalent area proportional to axial distribution of lift $B(x)$ or *equivalent area due to lift*

Whitham described the acoustic overpressure as

$$\frac{p - p_0}{p_0} = \frac{F(\tau)}{\sqrt{S}} \tag{1.3}$$

In equation 1.3:

- τ: t - $(\frac{s}{c_0})$
- t: time
- s: distance along a ray
- S: ray tube area
- c_0: speed of sound

Whitham's rule requires the substitution of c_0 with $c+u$, where c is the perturbed sound speed and u is the velocity perturbation. For an isentropic acoustic wave the propagation speed is

$$c + u = c_0 \cdot \left(1 + \frac{\gamma+1}{2\gamma} \cdot \frac{p - p_0}{p_0}\right) \tag{1.4}$$

The parameter τ represent a point on the acoustic wave while t is its arrival time at location s that could be obtained by integrating equation 1.4:

$$t = \tau + \frac{s}{c_0} - \frac{\gamma+1}{2\gamma c_0} F(\tau) \int_0^s \frac{ds}{\sqrt{S}} \tag{1.5}$$

Linearizing the Rankine Hugoniot equation we obtain the velocity u_s which in the case of a weak shock is equal to:

$$u_s = c_0 \cdot \left(1 + \frac{\gamma+1}{4\gamma} \cdot \frac{\Delta p}{p_0}\right) \tag{1.6}$$

The final evaluation for the far field bow shock overpressure made by Whitham is equal to

$$\Delta p_{shock} = \frac{p_0}{s}\left[2\int_0^{\tau_0} F(\tau)d\tau\right]^{\frac{1}{2}} \left(\frac{\gamma+1}{2\gamma c_0}\int_0^s \frac{ds}{\sqrt{S}}\right)^{\frac{1}{2}} \tag{1.7}$$

In equation 1.7 τ_0 is the value of τ at the end of the positive phase of F-function. In case of uniform atmosphere that equation is proportional to $r^{-\frac{3}{4}}$.
Moreover it contains terms related to the ray tube area dependence of acoustic overpressure. These considerations lead to the suggestion that the far field sonic boom is not affected by the

detailed conformation of the aircraft itself.
This hypothesis was verified through flight tests in which it was noted that the shape of the classic N waves is not different for conventional aircraft of analogous size and weight. A first expression used for the calculation of volume induced sonic boom was given by:

$$\Delta p = K_r \cdot K_s \cdot \sqrt{p_v \cdot p_g} \cdot (M^2 - 1)^{\frac{1}{8}} \cdot \frac{D}{l^{\frac{1}{4}}} \cdot r^{-\frac{3}{4}} \tag{1.8}$$

Equation 1.8 is base on the Walkden theory and similar equation were developed for calculating the lift induced sonic boom.
A mach more used method for sonic booming in stationary flight is through the simplified Carlson's method which will be explained in chapter 2. His formulation for a N wave are:

$$\begin{cases} \Delta p_{max} = K_P \cdot K_R \cdot \sqrt{p_v p_g} \cdot (M^2 - 1)^{\frac{1}{8}} \cdot h_e^{-\frac{3}{4}} \cdot l^{\frac{3}{4}} \cdot K_s \\ \Delta t = K_t \cdot \frac{3.42}{a_v} \cdot \frac{M}{(M^2-1)^{\frac{3}{8}}} \cdot h_e^{\frac{1}{4}} \cdot l^{\frac{3}{4}} \cdot K_s \end{cases} \tag{1.9}$$

In the case of level flight in stationary conditions, Carlson's simplified method has an accuracy of the order of 5% compared to computer-calculated values and it could be used for sonic boom analysis during the conceptual design phase of the project.

1.5 Maneuvers and focus boom

Any change in flight condition from the stationary condition in level flight produces a sudden variation in the intensity, location and number of ground shock wave patterns.

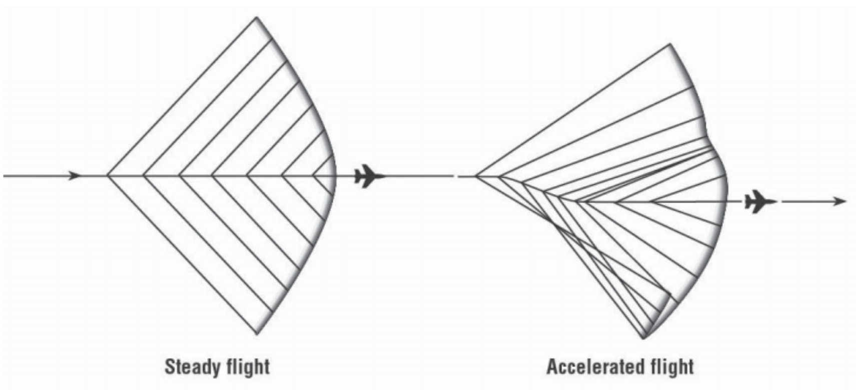

Figure 1.8: Bow shock wave ground footprint

As can be seen on the left-hand side of the figure 1.8, the ray paths represented by the lines are parallel to each other and in addiction the bow shock wave ground-intersection pattern is essentially hyperbolic in shape.
In the right-hand side of the figure there is the representation of an acceleration flight and it could bee see that the ray path are not anymore parallel and tend to converge or diverge. Moreover the shock wave ground intersection is not anymore hyperbolic.

1.5.1 Example of the F16 during some maneuver

Diving acceleration

There is the study of the increase in sonic boom pressure for a F16-B during the maneuver of a dive. The studied average value of overpressure in the primary carpet was about 3.5 lbs/ft^2

during the entire maneuver while in the focus region the peak overpressure was just above 7.2 lbs/ft^2 with a focus factor of about 2.0.

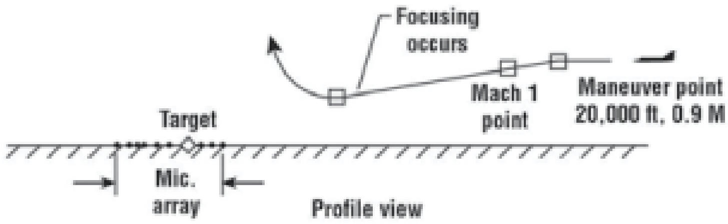

Figure 1.9: Flight Profile

Climbout

Regarding the climbout maneuver, the F16 aircraft started the maneuver itself from a Mach number of 1.2 at 10,000 ft of altitude. The pilot then brought the aircraft down to a load factor of 0.5 and kept the Mach number constant at 1.2 until the aircraft reached the imposed altitude.
The peak overpressure was about 11.6 lbs/ft^2 which is four times higher rather the value of the pre and post focus region.

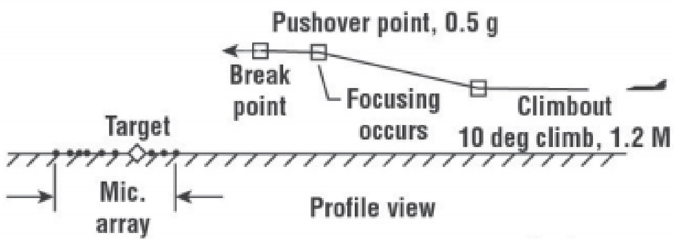

Figure 1.10: Flight Profile

Turns

For the following test it was imposed to have a maximum load factor n equal to 4 while keeping a Mach number of 1.2 at 10000 ft of altitude and the end of the maneuver was after a 50 degree turn.
The maximum overpressure recorded was just below $9 lbs/ft^2$, with a focus factor of about 2.5.

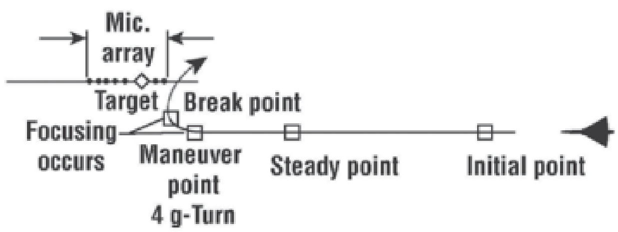

Figure 1.11: Flight Profile

Transition flight

Any supersonic aircraft has an initial part of the mission in subsonic regime before starting the supersonic flight phase.
During this transition phase between subsonic and supersonic regime there is always the presence of a focus region.

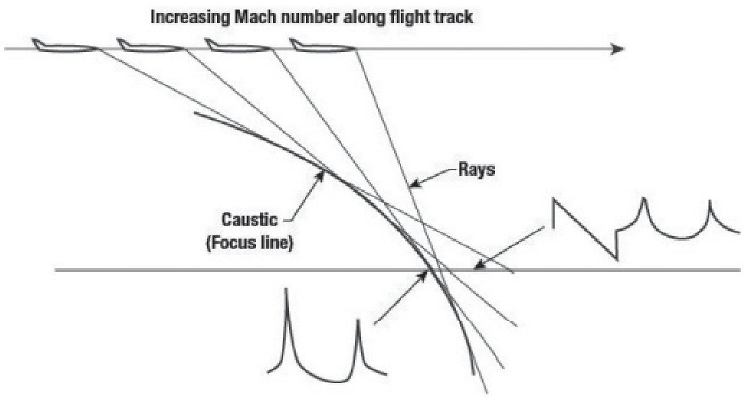

Figure 1.12: Focus boom

During the acceleration phase the Mach number increase and this cause that the Mach angle decrease and rays converge into a focus boom at a certain location from the aircraft. The focus tends to move away from the aircraft during the acceleration and it is spread out over a line referred to as a caustic.
A focused boom condition exist every time that a certain number of rays converge along the focus line, in addition the maximum focus boom occurs along the caustic and on the ground is small.
There are three different type of focus:

1. the simple focus, regarding a to a smooth caustic
2. the superfocus, corresponding to a cusp between two caustics
3. the perfect lens-like focus

Generally, the simple focus is the most common scenario for focus sonic boom. The formulation for the maximum shock overpressure in case of a simple focus is given by Guiraud's law and it is equal to:

$$\frac{p_{max}}{p_{ref}} = C\left[\frac{y_{ref}}{(\gamma+1)p_{ref}R}\right]^{\frac{1}{5}} \tag{1.10}$$

In equation 1.10 p_{ref} is the boom pressure at a distance y_{ref} from the caustic, R is the curvature between the caustic and the rays while C is a constant.

1.6 Hypersonic flight

Sonic boom theory is also applicable for hypersonic Mach number values. On the other hand, for high Mach numbers and slender bodies, the calculation of the F-function is difficult.
There are three ways to consider hypersonic flight in the case of the F-function:

1. hypersonic finite-difference calculations for the near-field flow

2. wind tunnel for obtaining F function
3. theoretical analyses based

Wind tunnel measurements demonstrated the capability to measure F-function even for hypersonic flight regimes.

1.7 Sonic boom minimization

1.7.1 Flight condition optimization

The ability to minimize sonic boom has always been at the centre of the designer's attention in order to allow flying over the land and populated areas without annoying the population. Sonic boom minimization include modification to the aircraft length, weight, shape, altitude and Mach operative number in order that ray path aren't able to reach the ground. Unlike their predecessors such as Concorde or Tupolev Tu-144, the new supersonic civil transport aircraft will have a sonic boom minimization requirement.

Influence of altitude and Mach number

Both the altitude at which the aircraft operates and the Mach number are important to minimize sonic boom for every type of supersonic vehicle.

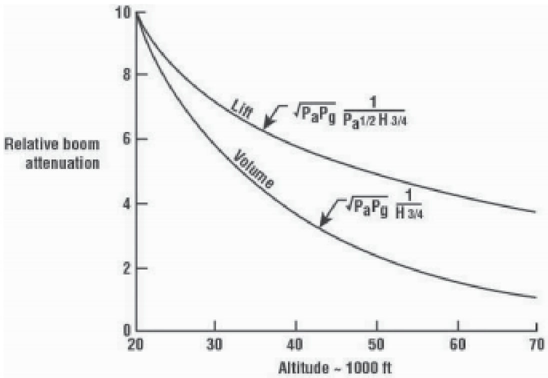

Figure 1.13: Sonic boom attenuation with operative altitude

Figure 1.13 shows the attenuation of equivalent area due to lift and volume for sonic boom phenomena as operating altitude increases.

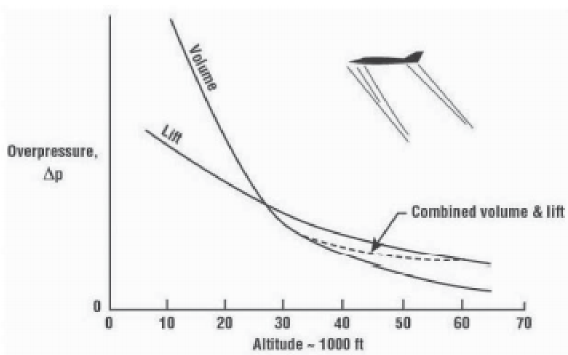

Figure 1.14: Contribution of aircraft volume and lift on boom level

In figure 1.14 overpressure is plotted as a function of altitude and it can be seen that at low flight altitudes the contribution of equivalent area due to volume is much more important than the lift contribution. On the other hand as altitude increase, the importance of the contributions is reversed with a reduction of the overpressure value rather zero ft of altitude.

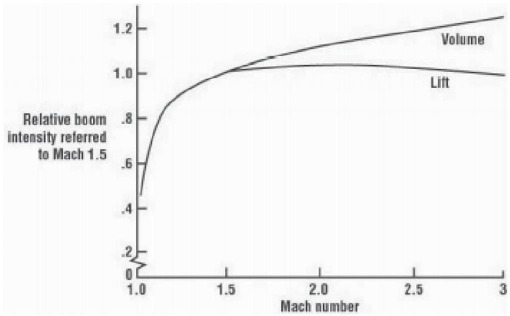

Figure 1.15: Influence of Mach number

Figure 1.15 represent the effect of the increase of Mach number in boom intensity referred to the Mach number equal to 1.5. From the figure it can be seen that for increasing Mach number values the greatest increase is in the equivalent area due to volume with a minimum decrease in the equivalent area due to lift. This will lead to later evidence that increasing the Mach number does not significantly affect the value of bow shock overpressure.

Flight path angle γ

In addition to Mach number and flight altitude, the flight path angle also plays an important role in the minimization of sonic boom. It could also be used to delay the arrival of the sonic boom until the aircraft has reached a higher flight altitude.

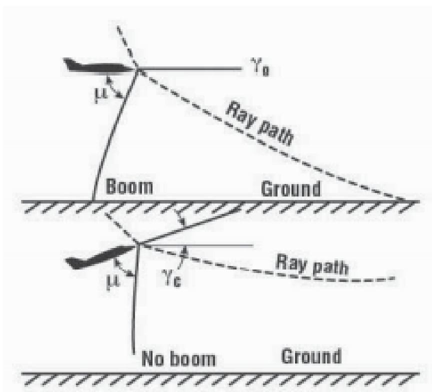

Figure 1.16: Shock ray pattern

Figure 1.16 represents the same aircraft at the same Mach number with two different profile: the first is in a level flight condition while the second one has a certain flight path angle that is not equal to 0 deg. For the first configuration in level flight, the correlation between Mach number and altitude is such that the bow shock is visible and audible to an observer on the ground. For the second illustration the aircraft has a flight path angle $\gamma \neq 0$ deg the bow shock becomes normal to the ground and will result in the fact that it will not be able to reach the ground.
The variation of flight path angle γ is visible as a variation of Mach number as can be seen in equation 2.8: positive value of flight path angle are beneficial regarding sonic boom minimization, while negative angle do not minimize the value of bow shock overpressure.

Tailoring flight path

A technique studied for minimising the sonic boom for short periods of time is the one studied by Ferri and it is not applicable for longer portion of the flight. The maneuver consists with the reduction of the lift component with a series of manoeuvres: firstly an aircraft moving in supersonic regime will perform a pull-up manoeuvre of a few degrees before reaching the zone where it has sonic boom minimization. Secondly it will follow a particular trajectory with very low lift values to reduce the boom above that desired zone. It is easy to understand that this type of condition is no applicable for long portion of the flight.

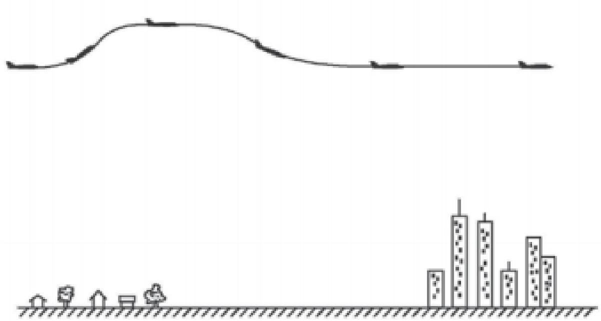

Figure 1.17: Example of the maneuver

1.7.2 Aircraft Shaping

In addition to flying under certain operating conditions, the shape of the aircraft itself can also produce important improvements in minimising sonic boom. In fact, one of the key aspect in the reduction of sonic boom overpressure and time duration is the reduction of the shape factor parameter K_s, that is function of the aircraft geometrical characteristics.

Volume and lift distribution

Most of the sonic boom minimization modelling for aircraft is based on the equivalent body theories made by Whitham and Walkden. The basic concept is related to the fact that if the real aircraft is replaced by an equivalent body of revolution with the same effective area distribution $A_e(x)$,the sonic boom signature would be similar with small differences in the tail shock re-compression.

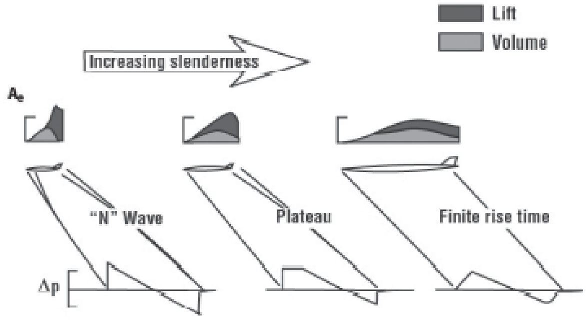

Figure 1.18: Signature in relation with area development

Figure 1.18 represent three different type of equivalent area distribution with the resulting far field boom signatures. In the past, the first supersonic aircraft were designed in order to have an N-wave on the ground as could be seen in the left part of figure 1.18. On the other hand, current minimization techniques for sonic boom are based on having an effective area $A_e(x)$ that progressively grows in order to increase the slenderness ratio with a finite rise time.

Flight test result for vehicle shaping

In the early 2000s, the american company Northtrop Grumman carried out a large amount of tests with a modified version of the F-5E aircraft to investigate the minimization effects of modelling the vehicle with a real atmosphere. The modification to the aircraft's geometry concerned the front part of the aircraft itself in order to obtain a flat-top signature on the ground.

Figure 1.19: F5-SSBD

Regarding the classic F5-E it was known that it produced a classic N-wave on the ground, while as I said before, for the modified version the target was to achieve a flat top signature. As can be seen in the left-hand side of the figure 1.20, the shapes of the signature are different between the two aircraft in the initial part, however, in the final part they are similar due to the fact that no changes have been made to the aft end of the aircraft.

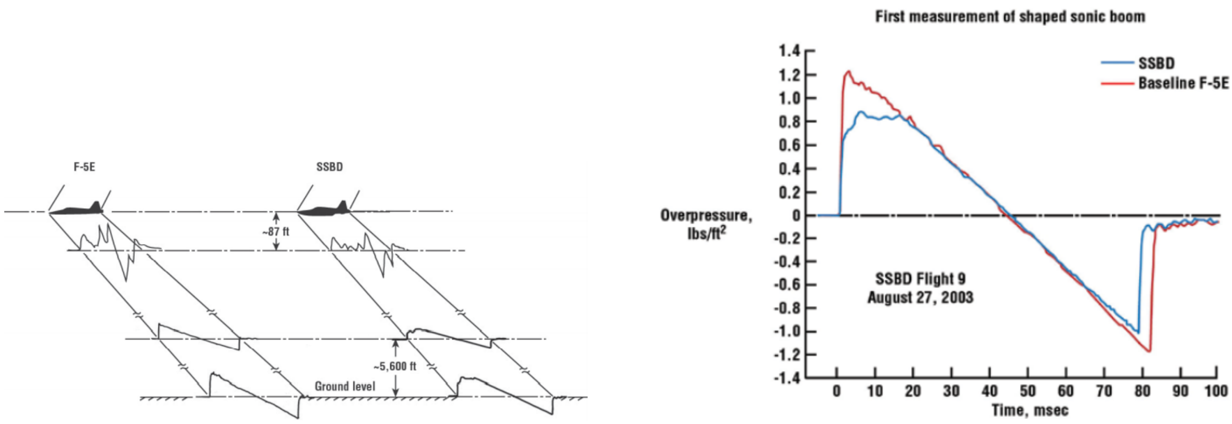

(a) Signature of the two aircraft

(b) Overpressure evaluation

Figure 1.20: Signature and overpressure evaluation of F-5E and SSBD

During the various tests, the aircraft flew for about 45 seconds apart at the same Mach number, flight track and altitude of the classic F5-E.

Wing planform

Another important aspect is that lift distribution can also be used to control the intensity and location of shocks through changes in wing planform, wing section thickness, wing twist and wing dihedral. The two contributions of volume and lift must be optimised together in order to achieve the best possible optimisation. In fact, as it will explained later in chapter 2 it will be a strong correlation between the value of equivalent area in various points of the aircraft and the sonic boom overpressure.
The main wing characteristics that can be pointed out are:

1. A relatively large spread in overpressures was obtained for this series of wings ranging from the unswept trapezoidal down to the highly sweptback arrow
2. Camber is advantageous for the arrow wing in the case of high lift coefficients
3. The changing effectiveness of lift in overpressure is significant
4. The dihedral wing has a very high reduction in overpressure for delta wings

Dihedral angle

The concepts of sonic boom minimization do not only apply to the area below the aircraft but also laterally to it: the presence of a dihedral angle Γ have shown a benign effect for both on and off-track locations.

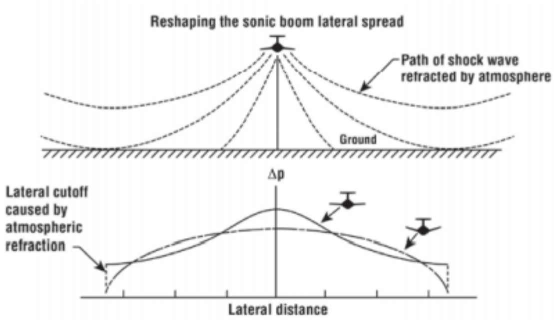

Figure 1.21: Influence of dihedral

The figure 1.21 shows the representation of the lateral distribution of sonic boom pressure with the curve with the presence of a dihedral angle showing a much more uniform distribution. The normal Δp distribution by a wing without dihedral angle could be considered flexible with lower boom levels off track then under the aircraft while a flattering of the curve would cause a more uniform boom level laterally.
With negative dihedral angle values there is an increase of the overpressure levels compared to the flat wing case, whereas with positive angles there is an important decrease.

1.8 Boomless and Low Altitude transonic flight

1.8.1 Boomless flight

A particular flight condition in which there is no sonic boom is through flight for Mach number values just above the unit: under these conditions the wave does not impact against the ground

due to atmospheric refraction or cutoff.
However, it should be remembered that these are flight conditions where the drag coefficient value C_D is much higher and consequently there would be a reduction in bow shock overpressure but a net increase in resistance.

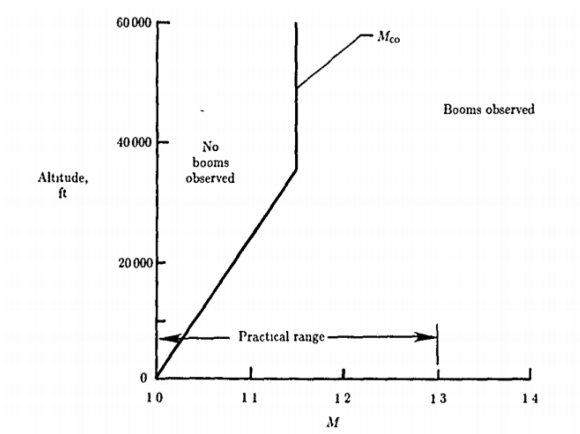

Figure 1.22: Mach number and altitude for Boomless flight

There are specific regions with particular combinations of flight altitude and Mach number for which these phenomena occur and generally they are for Mach number values below 1.15 considering the standard atmosphere. In the case that a real atmosphere is considered, there are also temperature gradients and winds that lead to a variation of the speed of sound. The cutoff Mach value goes up to values of 1.25/1.30 for very high altitude in level flight conditions. Mach cutoff values are exclusively a function of the operating conditions of the aircraft and the atmosphere in which it is located, so it does not depend on the geometry of the aircraft itself. As I said before the drag coefficient value is very high at Mach numbers slightly above unity.

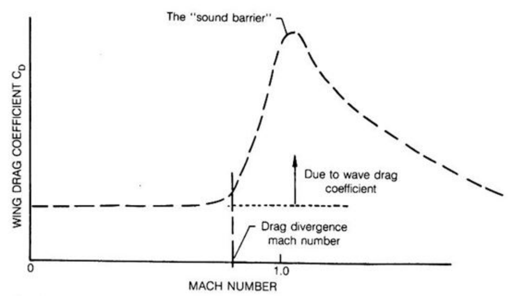

Figure 1.23: Drag coefficient as a function of Mach number

1.8.2 Low altitude transonic flight

The presence of the sonic boom is not exclusively for aircraft moving at a speed greater than the local speed of sound. In fact, sonic boom is possible even for aircraft moving at a Mach number between 0.95 to 0.99 with an altitude below 2000 ft. It could happen if the aircraft is flying in a cloud of water vapor condensed by a shock wave created when the local Mach number exceed 1.0 where the shock attaches.
The intensity of the sonic boom is important because of the low altitude with a different signature to the classic N-wave.

1.9 Sonic boom response

In addition to the acoustic disturbance to humans caused by the sonic boom phenomena, it can also lead to structural disturbances to infrastructure as well as to animals. In particular, reducing the annoyance caused by supersonic aircraft to people and infrastructure will be the focus of future discussions on the acceptability over the land and populated area of these vehicles. Moreover, the response of humans should be studied whether they are inside or outside buildings, since for most of the time people are indoor.
In the case where the subject is outside a building, he is directly exposed to the wave, while in the second case it will first pass through the structure of the building itself, whose presence will act as a filter and influence the response of the observer.
The structural vibration caused by the sonic boom is measured by accelerometers mounted on the windows and walls of buildings. If the observer is inside a building, he will be subjected to a series of complex stimuli such as visual, auditory ad vibratory inputs that are considerably different from those outside the building.
It turns out that the incident sonic boom puts some energy into the structure which will cause vibrations for longer periods than the duration of the incident boom. This vibration is mainly function to the angle of incidence of the sonic boom, the type of construction, the materials used and the age of the construction.

1.9.1 Effects on people and animals

The effects of sonic booms on humans are mainly a function of their sensitivity and the boundary conditions in which they will find themselves. The intensity of the sonic boom is directly related to the rise time of the sonic boom, defined as the time to go from 10 to 90% of the response finished transient, in fact a very low rise time will lead to a very high intensity value of shock overpressure.
In addition, it has been shown that the greatest annoyance for humans comes from concern about the possibility of damage to their property. Responses depend also on age, time of the day, geographic location and previous exposure.

1.9.2 Indoor and outdoor response

Most of the studies related to sonic boom disturbance have been done outdoors. However, today's global population spends most of the day inside buildings, so a study of the indoor response is necessary. As already mentioned walls of the buildings will act as filters and result in a variation of the response itself. In particular, it is noted that low frequencies tend to penetrate and interact with the structure itself better than high frequencies.
Vibrations inside the building due to sonic boom take the form of rattles. The presence of objects, pictures on the walls and incorrectly fitted doors or windows can lead to rattle generation. Regarding windows, sonic boom response varies significantly depending on the size of the window and how much that are open.
Consequently, the study of home interiors will play an important role in the reduction of the disturbance due to sonic boom.

2

Carlson's Method

Carlson's simplified method is a valid method for supersonic aircraft configurations and spacecraft that operates below an altitude of 76 km. It is able to provide an estimation of sonic boom overpressure and signature duration over the entire exposed area for aircraft in level flight or in a moderate descent or climb profile in a standard atmosphere without wind.
The method has the assumption that the pressure signal is the classical N wave, with a first compression followed by a linear expansion and a second compression which reestablish ambient pressure as already discussed in chapter 1.
These assumptions are valid for the most of the cases, at least for the bow shock and the positive portion of the signature. Moreover, this method manage to provide *N-wave* bow shock pressure rise, time signature duration and also the location of the ground impact having known the position of the aircraft itself.

The first step of the sonic boom pressure calculation is to determine the factors that determine this phenomena and in particular are a function of flight altitude, Mach number or geometrical data such as:

1. pressure amplification factor K_P
2. ray path distance factor K_D
3. signature duration factor K_t

In literature, the reflection factor K_R is generally set at 2 in preliminary studies while normally it varies between 1.8 and 2.1. The last parameter in Carlson's simplified formulation is the shape factor K_S and it's function of the aircraft geometry and there are two possibile strategies for determinate that value.
For aircraft covered by shape factor charts the value of K_S is the value is directly derived or interpolated from the graph. On the other hand, for aircraft that do not have representative graphs of their shape factor, the geometry of the aircraft must be accurately described. In addition to the geometry, for an accurate sonic boom analysis the following operating conditions must be known:

- Mach number
- flight path angle

- Altitude
- Weight
- ray-path azimuth angle
- atmospheric pressure
- sound speed at aircraft altitude

The procedure of the sonic boom calculation by Carlson's simplified method involves three basic steps. The first one include the calculation of aircraft shape factor (see section 2.1) as already mentioned in two possible way:

- from aircraft geometry, having a set of operating conditions and boundary conditions
- from shape factor charts, in the case that specific aircraft is covered by those charts

The second step consist in the calculation of the Mach effective number M_e and effective altitude h_e from the operating conditions and from the aircraft characteristics.
Having defined all factors and constants, the maximum sonic boom pressure could be calculated using the equation 2.1:

$$\Delta p_{max} = K_P \cdot K_R \cdot \sqrt{p_v p_g} \cdot \left(M^2 - 1\right)^{\frac{1}{8}} \cdot h_e^{-\frac{3}{4}} \cdot l^{\frac{3}{4}} \cdot K_s \tag{2.1}$$

Time signature duration could be determined by using the equation 2.2

$$\Delta t = K_t \cdot \frac{3.42}{a_v} \cdot \frac{M}{\left(M^2 - 1\right)^{\frac{3}{8}}} \cdot h_e^{\frac{1}{4}} \cdot l^{\frac{3}{4}} \cdot K_s \tag{2.2}$$

As can be seen from the following equations, the minimization of the shape factor plays a key role in the reduction of the overpressure value and time signature duration.

2.1 Shape factor calculation

In the case that the aircraft has covered by a shape factor charts the calculation of that constant value is very simple having known the operating conditions. Indeed it is sufficient to derive the value directly or interpolate it if the current flight condition is not reported on that graph.
On the other hand, the calculation of the shape factor for aircraft that are not covered by those graphs requires a complex graphical procedure that is function of the cross sectional area and the equivalent area due to lift. An accurate description (but not necessary detailed) of the geometry of the aircraft is required for the calculation, but there is no need to know the lift or weight distribution.
The fist step of the calculation is the definition of the aircraft cross sectional areas along longitudinal axis x. In the case of little angle of attack requires only areas normal to the flight path rather those defined by Mach planes.
Through this methodology the *equivalent area due to volume* $A(x)$ could be derived. In figure 2.1 there is a distribution of equivalent area due to volume for a generic supersonic aircraft:

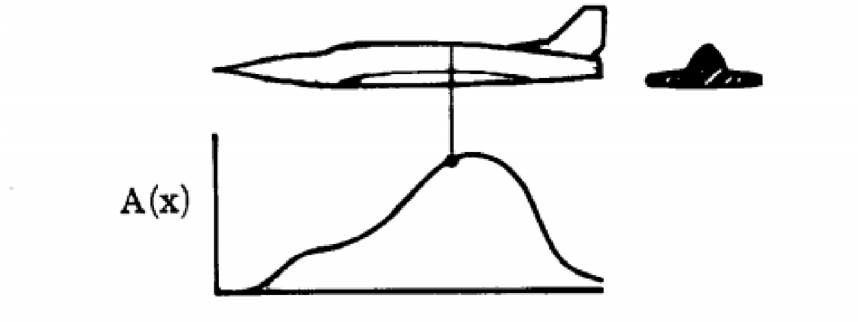

Figure 2.1: Equivalent area due to volume $A(x)$

This semplification in the method has some loss of accurancy for high supersonic speed and for blunt shapes, but they do not affect the final result in an evident manner. If it is known, the area of the stream tube of air entering the engine inlet should be subtracted from the total defined by external contours.
Following the definition of the equivalent area due to volume, the second step for the calculation of the shape factor K_S includes the definition of the equivalent area due to lift. A sufficiently accurate method for the lift distribution is given by the planform area distribution along side longitudinal axis.
An example of equivalent area due to lift could be seen in figure 2.2:

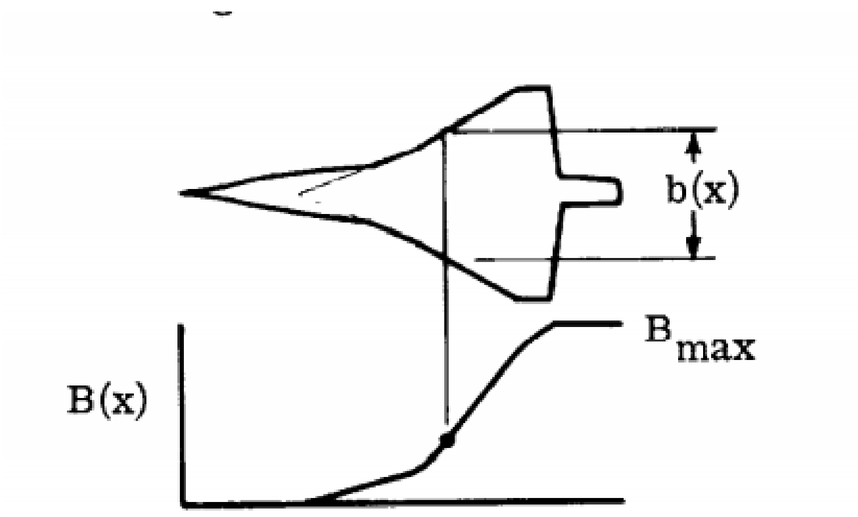

Figure 2.2: Equivalent area due to lift $B(x)$

The complete formulation of equivalent area due to lift is written in equation 2.3:

$$B(x) = \frac{\sqrt{M^2 - 1} \cdot W \cdot \cos\gamma \cdot \cos\theta}{1.4 \cdot p_v \cdot M^2 \cdot S} \cdot \int_0^x b(x)dx \tag{2.3}$$

This formulation is greatly influenced by the operational flight conditions of the aircraft. In particular, there is a dependency with the flight path angle, ray-path azimuth angle, aircraft weight and atmospheric pressure.
Mach number also has a strong influence on its value as it is proportional to $\frac{\sqrt{M^2-1}}{M^2}$: an important increase in Mach number leads to a evident decrease in equivalent area due to lift.

Finally the effect of altitude is shown in the denominator of the equation, as it is proportional to the inverse of the pressure at the operational flight altitude.
The third and penultimate step is the combination of the equivalent area due to volume and the equivalent area due to lift in order to obtain the *total effective area* of the aircraft. An example of this area is represented in figure 2.3:

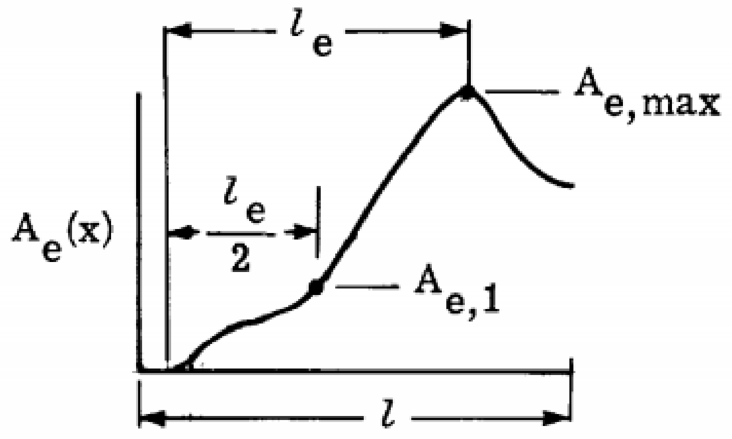

Figure 2.3: Total effective area of the aircraft $A_e(x)$

In figure 2.3 there are all the elements necessary for the simplified calculation of the aircraft shape factor K_S for vehicles that are not covered by dedicated experimental charts.
In particular, $A_{e,max}$ is the maximum effective area with an effective length of the aircraft equal to l_e. $A_{e,1}$ is the total effective area at midpoint of effective length and it's value is necessary for the determination of the shape factor.
In the final step of the calculation, the aircraft shape factor K_S could be calculated by reading the shape factor parameter curve in figure 2.4 with the insertion of the appropriate lengths and areas derived in figure 2.3.

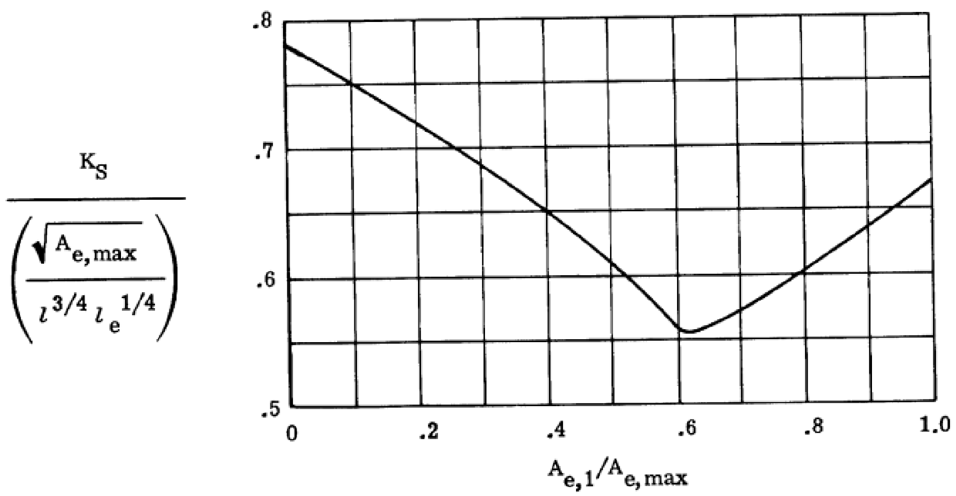

Figure 2.4: Shape factor parameter curve

The value of shape factor K_S has been defined by the evaluation of sonic boom theory for an effective area distribution in parabolic form such as $A_e(x) = k_1 \cdot x + k_2 \cdot x^2$. The value of

the costants k_1 and k_2 are selected in order that the curve passes through $A_{e,1}$ and $A_{e,max}$.
The main parameter that influences the aircraft shape factor is the maximum effective area $A_{e,max}$, while the others have a less dominant role. The value of the shape factor is extremely influential for the calculation of sonic boom pressure and time signature duration. In fact, as can be seen in equations 2.1 and 2.2, both values have a linear dependence with this parameter and it can be reduced by optimisation studies in the conceptual design phase.
It has been found that this simplified method for the evaluation of aircraft shape factor K_S gives value that are within 5/10 % of the actual value based on computer methods.

2.1.1 Shape factor calculation using charts

For a certain number of aircraft, it is not necessary to perform the complex procedure described above as there are dedicated charts based on experimental tests.
In order to use this method, it is necessary to identify the parameter K_L or *lift parameter* which is defined as:

$$K_L = \frac{\sqrt{M^2 - 1} \cdot W \cdot \cos\gamma \cdot \cos\theta}{1.4 \cdot p_v \cdot M^2 \cdot l^2} \tag{2.4}$$

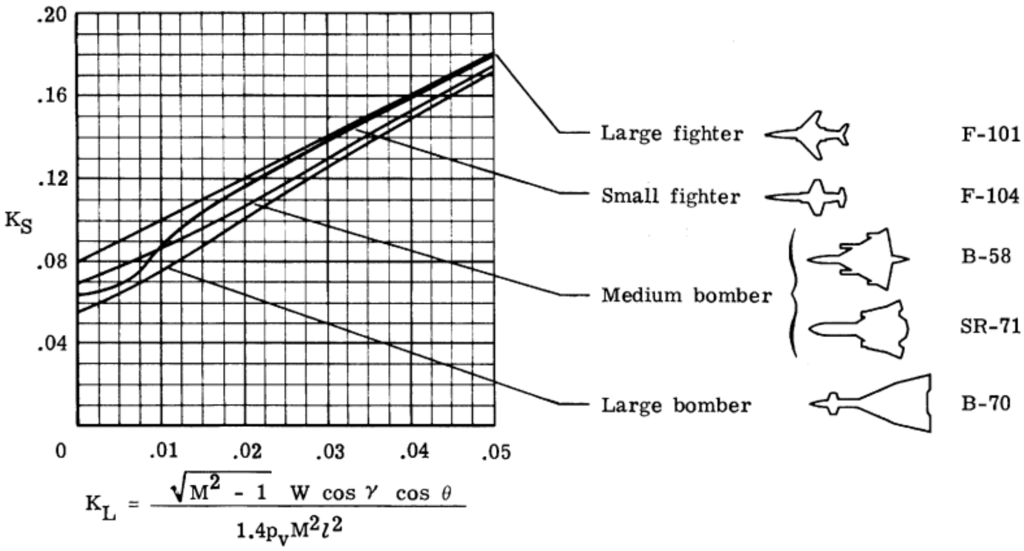

Figure 2.5: Aircraft shape factor as a function of lift parameter K_L

For aircraft not specifically covered by the charts, shape factors may be chosen by selecting a similar configuration. Moreover, larger aircraft has lower shape factor because they are more slender.
It can be seen that the aircraft shape factor K_S is more influenced by the wing planform area than the dimension of the aircraft while highly swept wings tend to have lower value of shape factors.

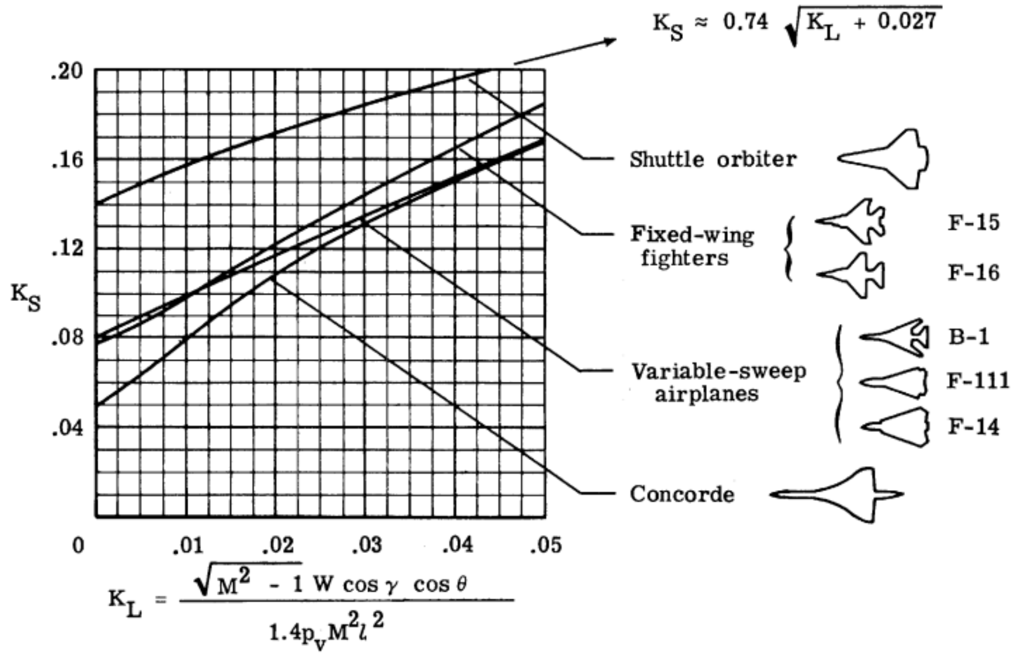

Figure 2.6: Aircraft shape factor of various airplanes

In figure 2.6 there is the representation of aircraft shape factor for different configuration of airplanes as a function of the lift parameter K_L.

2.2 Atmospheric propagation factor

For the evaluation of atmospheric factors it is necessary to use sonic boom propagation computer programs by varying altitude, Mach number, ray path azimuth angle and flight path angle in order to determinate the value of those factors during all the different flight conditions.
The value of these factors is determined using an approximate atmosphere to simplify the model. In fact, in the simplified Carlson's model atmospheric propagation effects are accounted for in the geometric mean of the standard atmospheric pressure of the aircraft altitude and at ground level and equal to $\sqrt{p_v p_g}$.
In order to obtain those values the program makes a first run considering a standard atmosphere and then a second one considering a uniform atmosphere with the intermediate pressure just described. The factors involved are found as the ratio between the value obtained in the first run and the value obtained in the second run of the program.
The notions of effective Mach number and effective altitude are necessary to increase the applicability of atmospheric propagation factors and they are now described. The effective Mach number M_e is the Mach number for level flight with the same ray path angle in flight track plane.
The simplified expression for calculating the effective Mach number is as follows:

$$M_e = \frac{1}{\sin\left(\gamma + \cot^{-1}\sqrt{M^2 - 1}\right)} \tag{2.5}$$

The formulation is a function of the flight path angle γ and the Mach number M. Once the value of the effective Mach number is known, the component of distance between aircraft ground track position and location of the ground impact in direction of aircraft ground track d_x is calculated as:

$$d_x = K_d \left(\frac{h}{\sqrt{M_e^2 - 1}} \right) \tag{2.6}$$

The value of ray path distance factor could be determined once the altitude of the aircraft and operative Mach number are known.

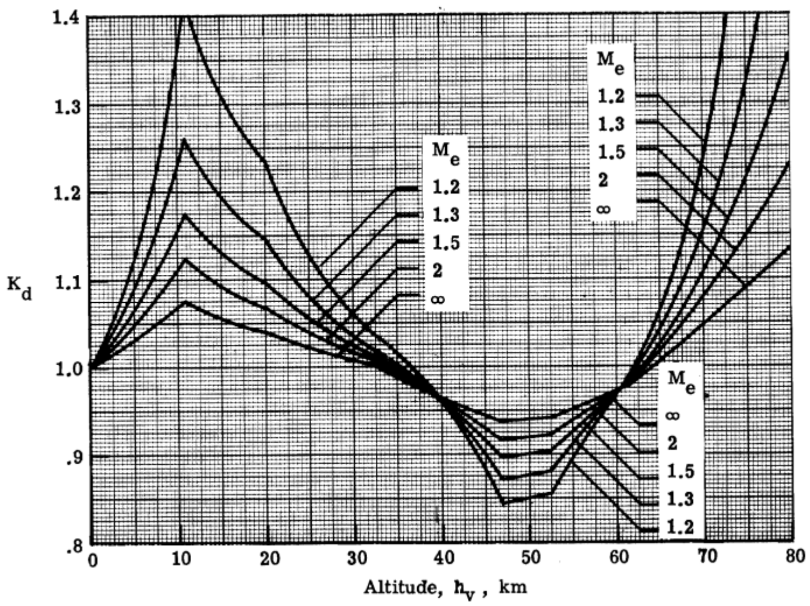

Figure 2.7: Ray path distance factor K_d

On the other hand the effective altitude h_e is the ray path distance measured perpendicular to the aircraft flight path. The simplified formula for the effective altitude is given by:

$$h_e = h \cdot \cos\gamma + d_x \cdot \sin\gamma \tag{2.7}$$

Complete equations

In the previous paragraph were studied the equation for a on-track scenario, but there are also complete equations for a general off-track case.
The equation for the effective Mach number is illustrated in equation 2.8

$$M_e = \sqrt{1 + \frac{\left[\frac{1}{\cos\gamma\sqrt{M^2-1}}\left(1 - \frac{\tan\gamma}{\cos\theta\sqrt{M^2-1}}\right)\right]^2}{\left[\left(\tan\gamma + \frac{1}{\cos\theta\sqrt{M^2-1}}\right)\frac{1}{\cos\gamma\sqrt{M^2-1}}\right]^2 + \left[\frac{\tan\theta}{\sqrt{M^2-1}}(\tan^2\gamma + 1)\right]^2}} \tag{2.8}$$

The distance between aircraft ground track position at the time of sonic boom generation and location of ground impact could be written as:

$$d = K_d \left(\frac{h}{\sqrt{M^2 - 1}} \right) \tag{2.9}$$

The angle between aircraft ground track and ground projection of ray path ϕ is written as:

$$\phi = \tan^{-1} \frac{\tan\theta \cdot \cos\gamma \cdot (1 + \tan^2\gamma)}{\tan\gamma + \frac{1}{\cos\theta\sqrt{M^2-1}}} \tag{2.10}$$

The component of distance d in direction of aircraft ground track and perpendicular to the ground track are respectively:

$$\begin{cases} d_x = d \cdot \cos\phi \\ d_y = d \cdot \sin\phi \end{cases} \tag{2.11}$$

Finally the effective altitude is given by the previous relationships 2.11 and could be written in the complete formulation as:

$$h_e = \sqrt{d_y^2 + (h \cdot \cos\gamma + d_x \cdot \sin\gamma)^2} \tag{2.12}$$

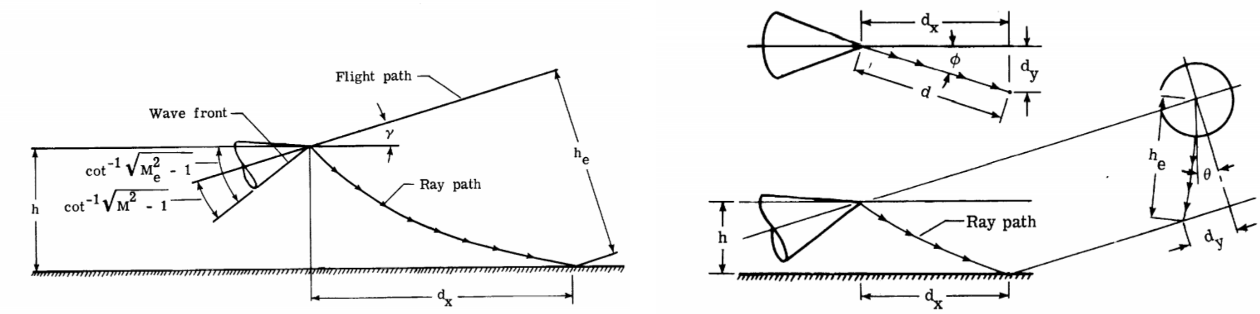

(a) On Track (b) Off Track

Figure 2.8: Propagation geometric parameters

Another feature of the use of the effective Mach number is the reduction of the computational cost of calculating the factors for the specific operating condition.
The example shown in figure 2.9 is valid for an altitude of 20000m for a general supersonic aircraft. These graphs were used to derive the value of the factors of ray path distance factor K_d and pressure amplification factor K_p for the aircraft studied.

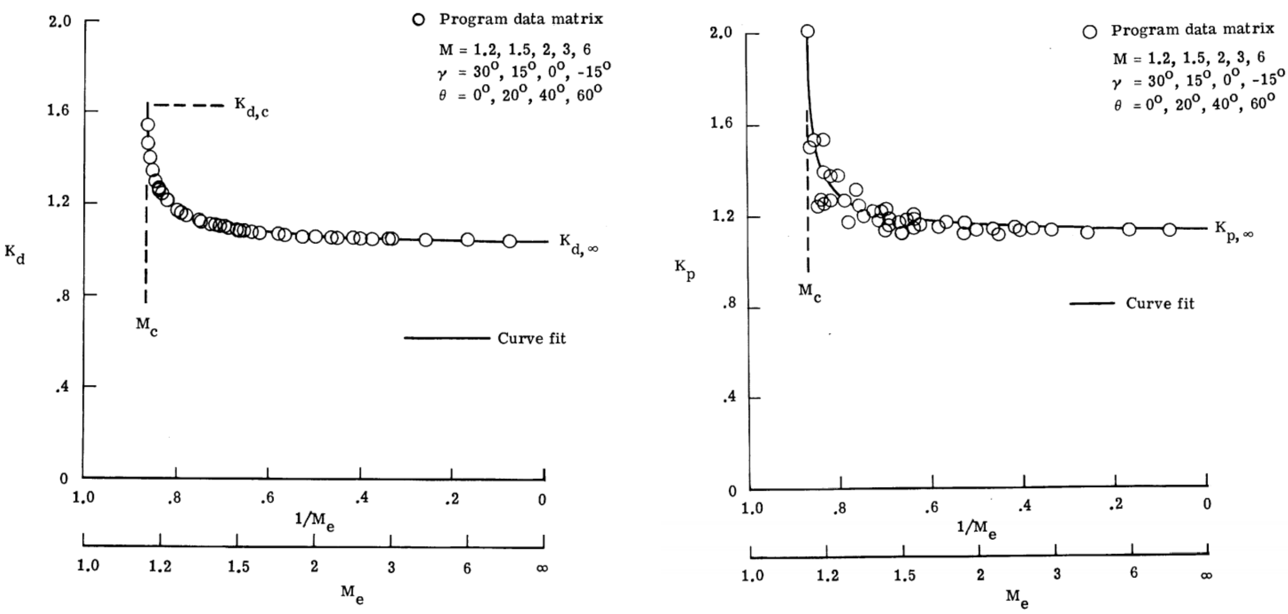

(a) Ray path distance factor (b) Pressure amplification factor

Figure 2.9: Evaluation of K_d & K_p with effective Mach number M_e

2.2.1 Atmospheric factor charts

In this section are illustrated the diagrams that are necessary for the definition of all factors required for the calculation of sonic boom pressure and time duration with the simplified Carlson's method enunciated in equations 2.1 and 2.2.

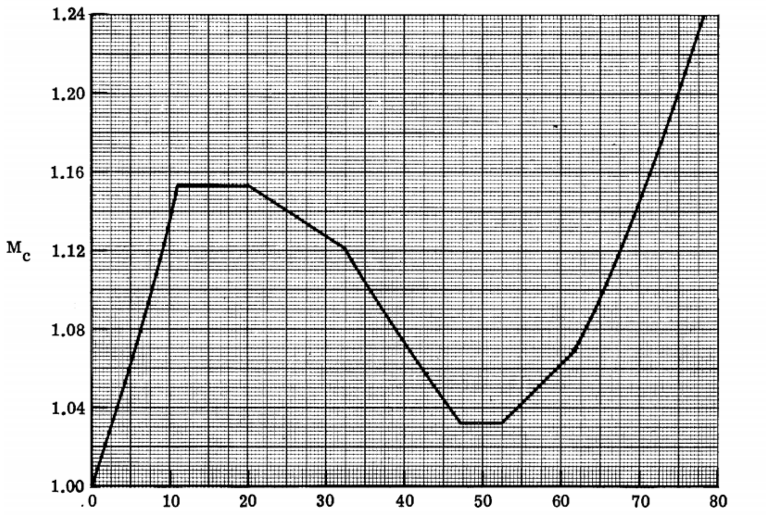

Figure 2.10: Cut off Mach in function of altitude

Figure 2.10 gives the value of cut off Mach number M_c in function of the flight altitude for a standard atmosphere. The physical meaning of the value of the cutoff Mach number has already been described briefly in chapter 1. If the effective Mach number calculated in equation 2.8 is below the value of cut off Mach M_c for a given altitude the signal will not reach the ground. As can be seen in figure 2.10 the cut off Mach number is just above the supersonic value, so these flight conditions are characterised by a high value of drag coefficient C_D as already mentioned in chapter 1. The limiting or cutoff ray-path distance factor could be saw from figure 2.11.

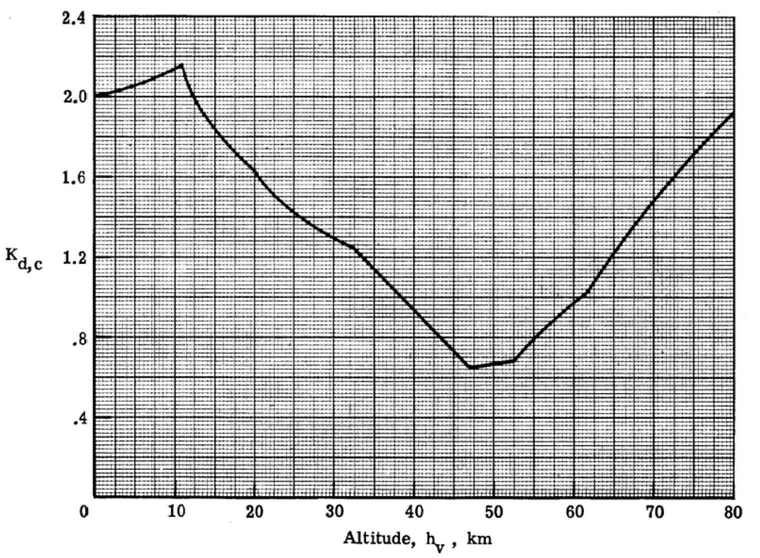

Figure 2.11: Cutoff ray path distance factor

It is also possible to identify the component of distance in the direction perpendicular to the aircraft ground at cutoff of sonic boom ground footprint given by:

$$d_{y,c} = K_{d,c} \cdot \frac{h}{M} \cdot \sqrt{\frac{M^2 - M_c^2}{M_c^2 - 1}} \tag{2.13}$$

The value of the pressure amplification factor as a function of the effective Mach number and the altitude of the aircraft is shown in figure 2.12.

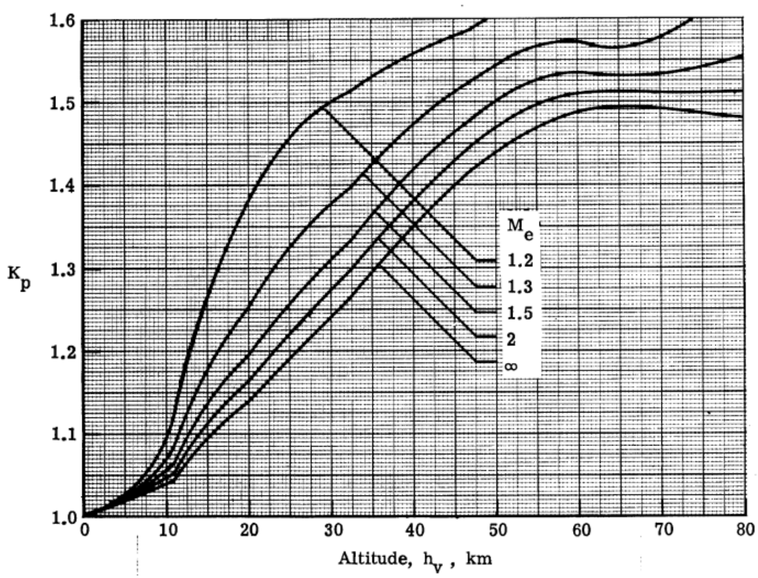

Figure 2.12: Pressure amplification factor K_p

As can be seen from the figure, the value of pressure amplification factor K_p decreases as the effective Mach number increases at the same altitude. Moreover, the correlation is strongly non-linear and a possible interpolation is difficult to evaluate due to the complexity.
The last graph shows the signature duration factor K_t which in combination with the effective altitude h_e consider the presence of an inhomogeneous atmosphere in the equation 2.2 for the time signature duration of the sonic boom.

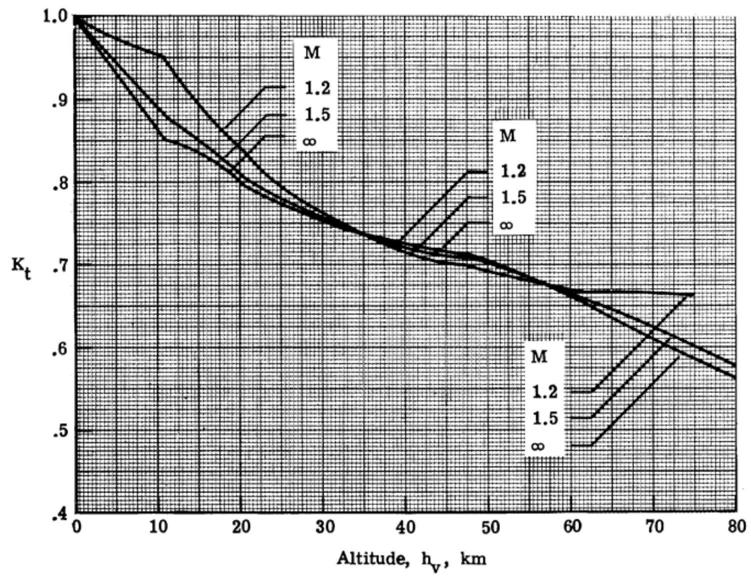

Figure 2.13: Signature duration factor

In addition, this graph also shows that as the Mach number value increases the value of the signature duration factor decreases at the same altitude such as the pressure amplification factor. Moreover, like the previous graphs this one also has a strong non-linearity.
The limitation of these graphs is that they are only able to evaluate atmospheric propagation factors for Mach number values greater than 1.2, without considering the value in cutoff conditions. In order to consider these conditions as well, there are correction coefficients to be applied to the factors just derived.

$$\begin{cases} K_d = K_{d,c} + (K_{d,\infty} - K_{d,c}) \cdot \left(\frac{M_e - M_c}{M_e - 1}\right)^{n_d} \\ K_p = K_{p,\infty} \cdot \left(\frac{M_e - 1}{M_e - M_c}\right)^{n_p} \\ K_t = K_{t,\infty} \cdot \left(\frac{M}{M-1}\right)^{n_t} \end{cases} \tag{2.14}$$

In the equation 2.14 for Mach number equal to the cutoff Mach number M_c the pressure amplification factor K_P has a singularity.

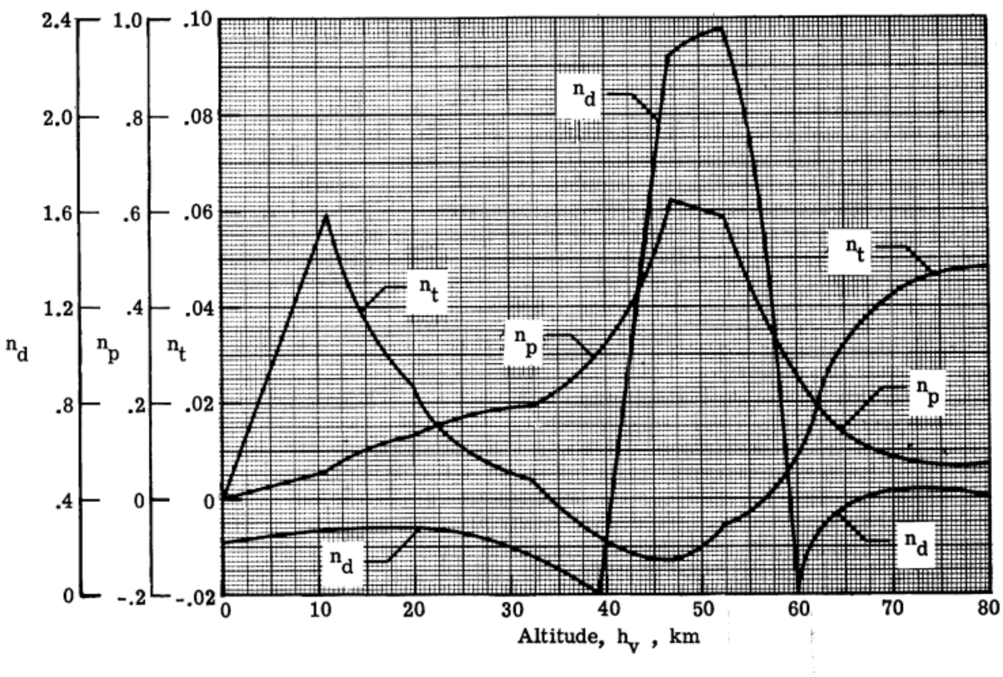

Figure 2.14: Evaluation of corrective factor

For the definition of the corrective factor is necessary to have defined properly the cutoff Mach number M_c and the atmospheric propagation factor from figure 2.7 to figure 2.13. The procedure for deriving these values is very complex due to the strong non-linearity of these graphs themselves.

Reflection factor K_R

At the moment the shock wave reaches the ground, the vertical velocities are blocked and their energy is converted into a pressure increase ΔP.
Theoretically, for weak impacts the overpressure is twice that of the free-air value of the incident wave. Experimental values of the Reflection factor K_R show that it can vary between 1.8 and 2.1. For this thesis work a constant value equal to 2.0 was considered.

2.3 Correlation with flight test

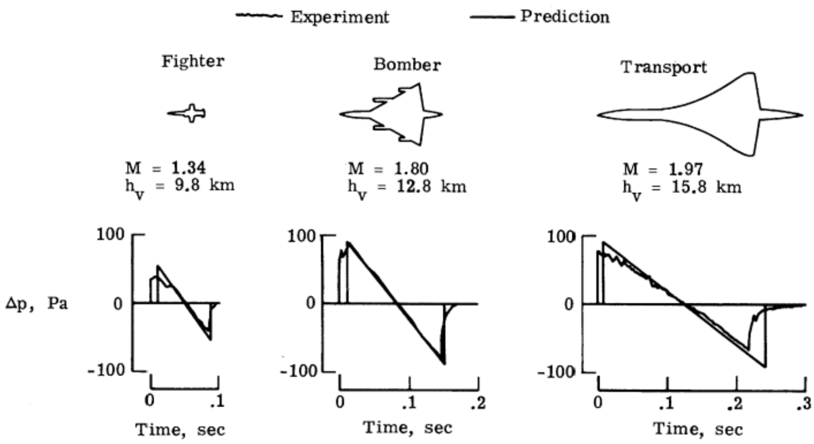

Figure 2.15: Evaluation of prediction method and test data

Figure 2.15 shows a comparison for three different categories of supersonic aircraft between Carlson's simplified method and flight test for bow shock overpressure value.
The values for the bomber and the civil transport aircraft are very similar with minimal discrepancies for the value of the peaks between the predictive method and the flight test. On the other hand, the values for the fighter aircraft are more discordant, although the predictive theory remains conservative rather to the flight test.
In addition, the predictive method agrees with the experimental tests for the variation of sonic boom pressure with altitude h_v. In fact in the case of increase in altitude the value of overpressure decrease clearly.

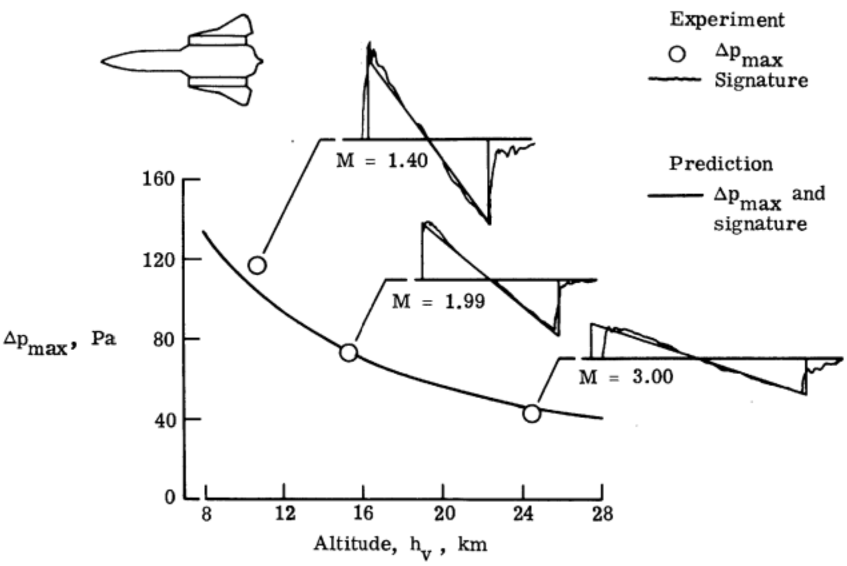

Figure 2.16: Evaluation of prediction method and test data

Figure 2.16 shows that variation in altitude is much more influential than variation in Mach number. In the final chapter of this thesis, this statement will be demonstrated as a consequence

of the results obtained for all the aircraft studied.
As in the previous case, the predictive method is more conservative than the experimental case.

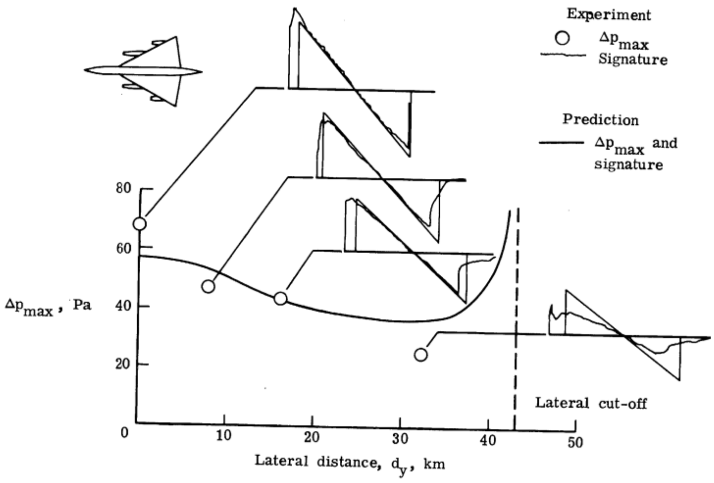

Figure 2.17: Correlation of prediction with flight data for a range of lateral distance for a Bomber

Figure 2.17 show the validity of the method for off track prediction for a bomber aircraft with a Mach number of $M = 2$ and at an altitude of $h_v = 18500$ m.
As the figure show at larger distance there is a signature distorsion for the predictive method that cause random noise beyond the lateral cutoff. In general, variations with lateral distance have small discrepance between flight data test and simplified prediction method.

3

Concorde Sonic boom analysis

3.1 General description of the aicraft

Concorde was the first supersonic civil transport aircraft capable of transporting more than one hundred passengers from the European continent to the American continent in less than four hours at a cruise Mach number equal to 2.02. The aircraft was born from a consortium formed during the 60s between British Aerospace and the french Aèrospatiale and 20 units were produced during the 70s.
Initially, the two Concorde manufacturers had each one developed a project for their own supersonic aircraft and were funded primarily by their respective governments. The decision to join forces to produce a supersonic aircraft was due to the high costs involved in designing and building a technology that was new to the civilian sector.

Figure 3.1: Concorde during take off phase

Concorde made its first flight during 1969, while in 1976 it officially entered in service on the Paris-Dakar-Rio de Janeiro for Air France and London-Bahrain routes for British Airways. After the retirement of its Soviet rival TU-144 in 1998, it remained the only civilian supersonic aircraft until it was retired from service in 2003 due to the high cost.
The airlines that purchased Concorde were only Air France and British Airways, the main reason was also due to the great petrol crisis of 1973, which in relation to the high consumption (approximately 17 liters per passenger every 100 km of flight) of the aircraft led to the cancellation of numerous orders from other companies.

Other issues that limited the production of the aircraft were related to the numerous maintenance hours (about 18 MMH/FH) with such operational costs that made it very unprofitable compared to subsonic aircraft.
The most tragic event for Concorde was the crash near Paris' Charles de Gaulle airport in 2000, which killed the entire crew of the plane and undermined public opinion on the safety of the aircraft. The cause was the collection of debris from a DC-10 that had taken off earlier, which caused a puncture in a fuel tank that, together with other fragments, produced an electric arc that ignited a fire on the left wing of the aircraft.
In 2003, both British Airways and Air France decided to stop operating Concorde due to high operating costs, the reduction in air traffic following the September 11 attacks and the accident occured at one of Air France's Concorde on 25 July 2000.

3.1.1 Dimensions and technical features

Dimensions

The table shows the main dimensions of the aircraft

Production Concorde dimension		
Dimension specification	Value	Unit of measurement
Overall length	61.66	m
Height from ground	12.2	m
Fuselage external width	2.88	m
Fuselage externaal height	3.32	m
Fuselage length	39.32	m
Tail Fin length	10.58	m
Wing span	25.6	m
Wing length (root chord)	27.66	m
Wing area	358.25	m^2

Table 3.1: Concorde dimension

The dimensions present in the table 3.1 have been used for the study of the equivalent area due to volume and equivalent area due to lift of the simplified Carlson's method described in chapter 2.

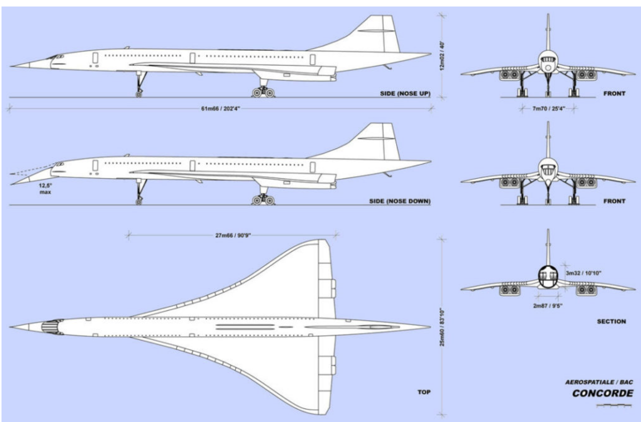

Figure 3.2: Three views of Concorde

Performance

The following table lists the performance characteristics of the aircraft.

Production Concorde performance		
Technical specification	Value	Unit of measurement
Maximum cruise speed	Mach 2.04	
Nominal cruise speed	Mach 2.02	
Maximum range	3900	NM
Take off speed	250	Kt
Operating altitude	60000	ft
Single engine thrust	170	kN
Fuel capacity	95680	kg
Fuel consuption at full power	10500	kgs/hr

Table 3.2: Concorde performance

Weight

The table 3.3 collects information about the different weights of Concorde.

Production Concorde performance		
Weight	Value	Unit of measurement
MTOW	185066	kg
Max Weight without fuel	92080	kg
OEW	78700	kg
Maximum payload	13380	kg
Maximum landing weight	111130	kg
Maximum weight of fuel	95680	kg

Table 3.3: Concorde weight

3.2 Sonic Boom Analysis

Using Carlson's semplified method, sonic boom analysis were made of the bow shock overpressure and time duration for Concorde under certain operating conditions.
Within the study, numerous sensitivity analyses were carried out to determine the influence of various parameters on the sonic boom. As pointed out in chapter 2 the study in question, there are limitations that must be followed in order not to lose accuracy in the final result.
The limitations relate to the fact that only the primary sonic boom with a classic N-wave was analysed. Moreover other limitations of the method include the fact that the effects of flight path curvatures and accelerations of the aircraft are not considered, as well as the fact that it is in a standard atmosphere without wind. These limitations are not so important that the accuracy of the estimates made is compromised.
The sensitivity analyses carried out are as follows:

1. Simultaneous change of flight path and altitude

2. Simultaneous change of aircraft length and Mach number
3. Simultaneous change of Mach number and altitude
4. Simultaneous change of flight path and aircraft length

3.2.1 Evaluation of Primary Sonic-Boom with Mach number and altitude variation

A sensitivity analysis was carried out on the aircraft regarding the evolution of the sonic boom analysis in the case of changes in flight altitude and Mach number.
Regarding Mach number, the parameter has been varied between 1.4 and 2.0 and this last value corresponds to the cruising speed, as previously shown in the table 3.2.
On the other hand, the altitude was varied between 17000m and 20000m, which is approximately equal to the flight altitude of the concorde and this range has been chosen to make comparisons with some other types of aircraft. The following figures 3.3 & 3.4 show the evolution of the equivalent area due to lift, equivalent area due to volume and total effective area in one specific condition.

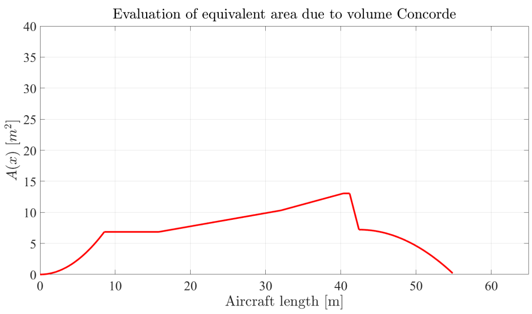

(a) Equivalent area due to volume

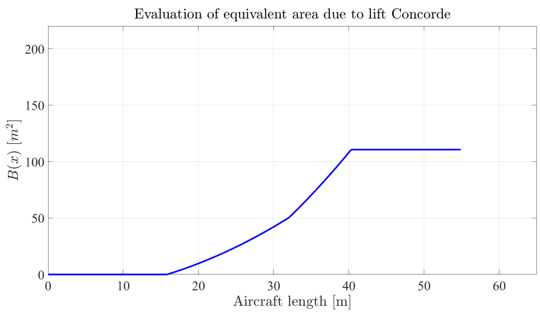

(b) Equivalent area due to lift

Figure 3.3: Evaluation of equivalent area due to volume & lift, M=1.5 & h=17000m

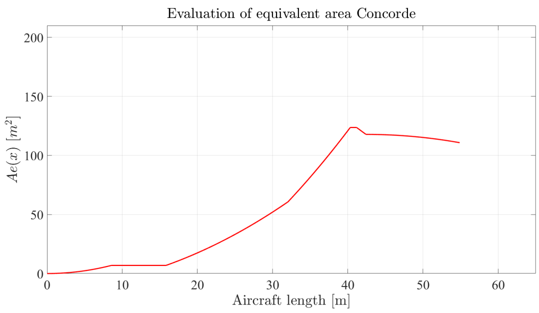

Figure 3.4: Effective area Concorde at M=1.5 & h=17000m

The following table shows the numerical results obtained:

Mach number	A_{e_1} $[m]$	$A_{e_{max}}$ $[m^2]$	Δp $[Pa]$	Δt $[s]$	$A_{e_1}/A_{e_{max}}$	h $[m]$
1.4	21.2	126.87	145.5	0.4941	0.1671	17000
1.5	21.15	126.2	150.0	0.4782	0.1676	17000
1.6	20.85	124.2	152.97	0.4655	0.1680	17000
1.7	20.75	121.49	153.63	0.4513	0.1708	17000
1.8	20.25	118.4	154.70	0.442	0.1710	17000
1.9	20.12	115.23	154.93	0.434	0.1746	17000
2.0	19.65	112	156.06	0.428	0.1754	17000

Table 3.4: Result obtained at 17000m

Mach number	A_{e_1} $[m]$	$A_{e_{max}}$ $[m^2]$	Δp $[Pa]$	Δt $[s]$	$A_{e_1}/A_{e_{max}}$	h $[m]$
1.4	23.13	145.77	139.03	0.5405	0.1587	18000
1.5	23.10	144.97	143.24	0.5229	0.1593	18000
1.6	22.7	142.65	146.08	0.5091	0.1591	18000
1.7	22.5	139.47	147.86	0.497	0.1613	18000
1.8	22.15	135.9	148.8	0.487	0.163	18000
1.9	21.75	132.2	149.4	0.478	0.1645	18000
2.0	21.45	128.4	149.7	0.4701	0.167	18000

Table 3.5: Result obtained at 18000m

Mach number	A_{e_1} $[m]$	$A_{e_{max}}$ $[m^2]$	Δp $[Pa]$	Δt $[s]$	$A_{e_1}/A_{e_{max}}$	h $[m]$
1.4	25.4	167.9	133.02	0.5904	0.1513	19000
1.5	25.2	166.94	137.00	0.571	0.151	19000
1.6	25.03	164.2	139.65	0.5556	0.1524	19000
1.7	24.8	160.47	141.25	0.5425	0.1545	19000
1.8	24.15	156.3	142.40	0.5319	0.1545	19000
1.9	23.9	151.92	142.90	0.5220	0,1572	19000
2.0	23.35	147.5	143.3	0.514	0.1583	19000

Table 3.6: Result obtained at 19000m

Mach number	A_{e_1} $[m]$	$A_{e_{max}}$ $[m^2]$	Δp $[Pa]$	Δt $[s]$	$A_{e_1}/A_{e_{max}}$	h $[m]$
1.4	28.02	193.65	127.28	0.6431	0.1447	20000
1.5	27.8	192.6	131.18	0.622	0.1443	20000
1.6	27.5	189.42	133.72	0.605	0.1452	20000
1.7	27.2	185.1	135.23	0.5913	0.1470	20000
1.8	26.66	180.18	136.40	0.58	0.148	20000
1.9	26.2	175.02	136.84	0.569	0.1497	20000
2.0	25.6	169.9	137.3	0.5606	0.1507	20000

Table 3.7: Result obtained at 20000m

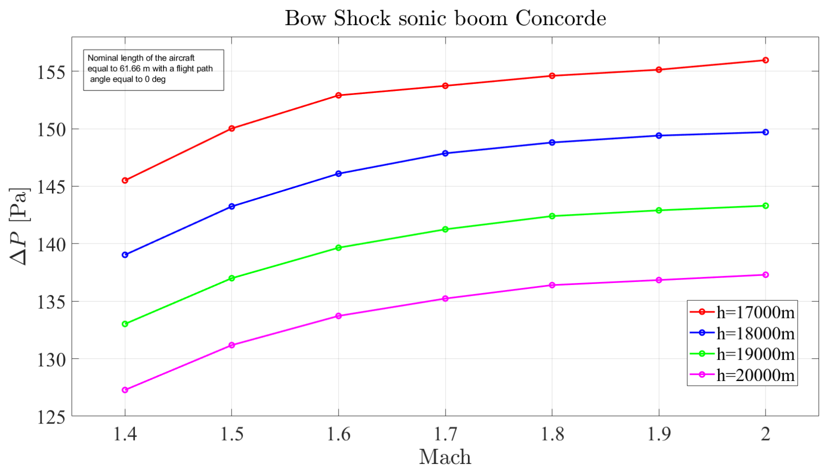

Figure 3.5: Bow Shock overpressure Concorde with Mach number and altitude variation

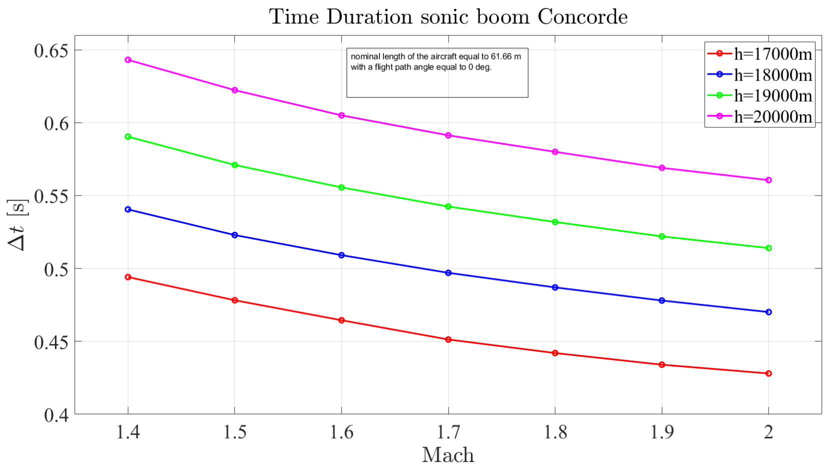

Figure 3.6: Time duration Concorde with Mach number and altitude variation

The bow shock overpressure increases with Mach number and decreases with the growth in altitude. In particular, for low Mach numbers the rate is higher while the contribution given by the increase in altitude is predominant. On the other hand as the altitude increase, the time duration evidently increase, in opposition of the Mach number.

3.2.2 Sonic-Boom with Mach number and aircraft length variation

A second analysis that has been carried out concerns the calculation of bow shock overpressure and time signature duration by varying the Mach number and the length of the aircraft simultaneously.
The Mach number was varied within the range of values proposed above, while the aircraft length was varied between 87 and 100% of the aircraft nominal length (from 52.40 meters to 61.66 m).
The reference altitude is 19200 metres.

Aircraft length $[m]$	$A_{e,1}$ $[m^2]$	$A_{e_{max}}$ $[m^2]$	Δp $[Pa]$	Δt $[s]$	$A_{e_1}/A_{e_{max}}$	l_e $[m]$
52.40	22.8	164.4	132.07	0.5862	0.1387	39.33
53.64	22.95	164.85	132.23	0.5869	0.1392	40.25
54.87	23.5	165.4	132.30	0.5872	0.1420	41.15
55.49	23.65	165.5	132.34	0.5873	0.1429	41.65
56.11	23.8	165.85	132.40	0.5875	0.1435	42.14
57.35	24.05	166.2	132.44	0.5878	0.1447	43.02
58.57	24.5	166.65	132.45	0.5878	0.1470	43.95
60.12	24.65	167.25	132.58	0.5884	0.1479	45.1
61.66	25.5	167.9	132.7	0.5891	0.1517	46.25

Table 3.8: Result obtained with Mach number equal to 1.4

Aircraft length $[m]$	$A_{e,1}$ $[m^2]$	$A_{e_{max}}$ $[m^2]$	Δp $[Pa]$	Δt $[s]$	$A_{e_1}/A_{e_{max}}$	l_e $[m]$
52.40	22.5	160.8	138.40	0.5507	0.1405	39.33
53.64	22.8	161.2	138.8	0.5523	0.1414	40.25
54.87	23.02	161.6	138.86	0.5525	0.1425	41.15
55.49	23.1	161.85	138.96	0.5529	0.1427	41.65
56.11	23.18	162.1	139.05	0.553	0.143	42.14
57.35	23.7	162.55	139.13	0.5535	0.1458	43.02
58.57	24.1	163	139.20	0.5539	0.1477	43.95
60.12	24.8	163.6	139.28	0.554	0.1479	45.1
61.66	25.15	164.2	139.31	0.5543	0.1532	46.25

Table 3.9: Result obtained with Mach number equal to 1.6

Aircraft length $[m]$	$A_{e,1}$ $[m^2]$	$A_{e_{max}}$ $[m^2]$	Δp $[Pa]$	Δt $[s]$	$A_{e_1}/A_{e_{max}}$	l_e $[m]$
52.40	21.75	152.85	141.35	0.528	0.1423	39.33
53.64	21.79	153.3	141.50	0.5285	0.1421	40.25
54.87	22.2	153.72	141.60	0.5290	0.1453	41.15
55.49	22.35	153.95	141.61	0.5290	0.1451	41.65
56.11	22.4	154.2	141.70	0.5291	0.1453	42.14
57.35	22.8	154.7	141.74	0.5293	0.1474	43.02
58.57	23.3	155.1	141.76	0.5295	0.1502	43.95
60.12	23.5	155.7	141.86	0.5297	0.1509	45.1
61.66	24.25	156.3	141.90	0.5301	0.1552	46.25

Table 3.10: Result obtained with Mach number equal to 1.8

Aircraft length $[m]$	$A_{e,1}$ $[m^2]$	$A_{e_{max}}$ $[m^2]$	Δp $[Pa]$	Δt $[s]$	$A_{e_1}/A_{e_{max}}$	l_e $[m]$
52.40	20.8	144	142.15	0.5098	0.1444	39.33
53.64	20.95	144.97	142.32	0.5104	0.145	40.25
54.87	21.05	144.9	142.49	0.511	0.1453	41.15
55.49	21.4	145.2	142.53	0.5112	0.1472	41.65
56.11	21.7	145.37	142.58	0.5114	0.1493	42.14
57.35	22	145.8	142.60	0.5116	0.1509	43.02
58.57	22.44	146.3	142.70	0.5118	0.1531	43.95
60.12	22.6	146.9	142.89	0.5122	0.1538	45.1
61.66	23.15	147.5	142.93	0.5126	0.1569	46.25

Table 3.11: Result obtained with Mach number equal to 2.0

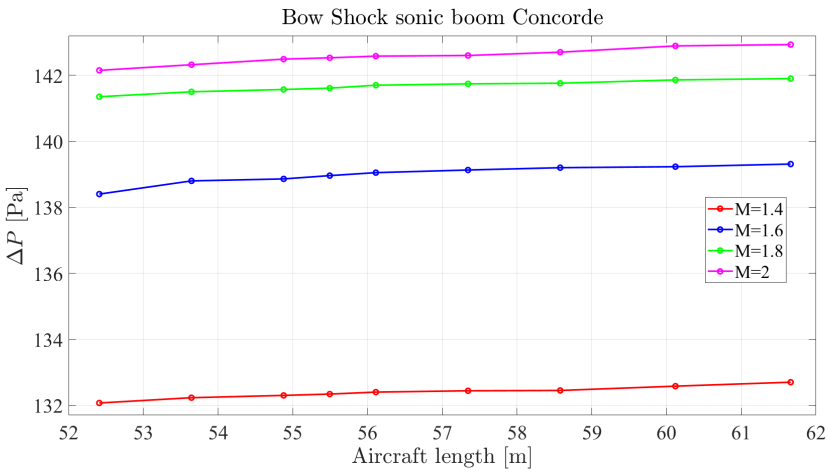

Figure 3.7: Bow Shock overpressure Concorde with Mach number and aircraft length variation

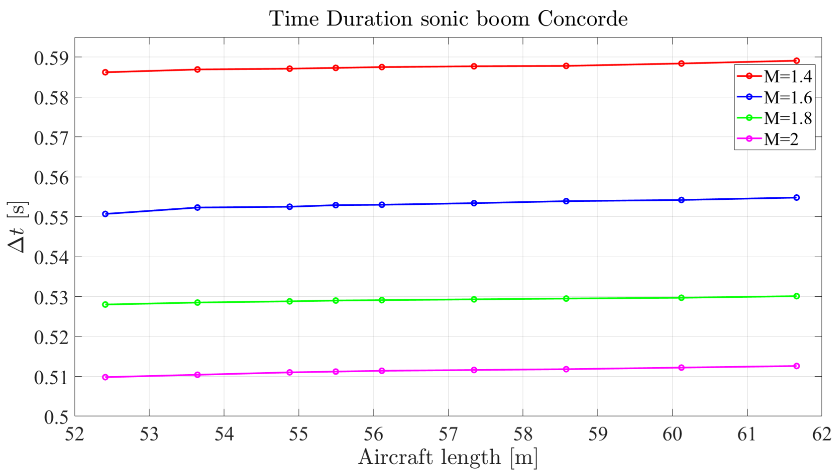

Figure 3.8: Time duration Concorde with Mach number and aircraft length variation

As far as bow shock overpressure is concerned, it increases as the Mach number and the length of the aircraft increase. In particular, however, it can be seen that the increase in overpressure due to the increase in aircraft length is very small compared to that given by the Mach number. For a Mach number equal to 1.4 there is a very reduced bow shock overpressure value and this could be caused by the fact that it is very close to the cut off condition described

in chapter 1 and 2.
The time duration decrease as the Mach number increase as also pointed out above.

3.2.3 Sonic Boom Analysis with flight path and Mach number variation

The analysis was carried out by varying the flight path angle γ and Mach number. As for the Mach number, as in the previous cases the range of variation is between 1.4 and 2.0 while for the flight path angle the variation is between 0 and 15 deg. The calculations shown have been carried out for an altitude of 19200 metres with the nominal length of the aircraft equal to 61.66 meters.

Flight path$[deg]$	Ray path $[deg]$	$A_{e,1}$ $[m^2]$	$A_{e_{max}}$ $[m^2]$	Δp $[Pa]$	Δt $[s]$	$A_{e_1}/A_{e_{max}}$
0	0	25.5	167.9	132.7	0.5891	0.1517
2	2	25.55	167.66	132.44	0.5877	0.1524
4	4	25.51	167.11	132.23	0.5868	0.1525
5	5	25.4	166.7	132.17	0.5866	0.1527
6	6	25.3	166.19	131.8	0.5849	0.1528
8	8	25.26	164.92	131.23	0.5824	0.1532
10	10	24.92	163.25	130.75	0.5802	0.1526
12.5	12.5	24.79	160.72	129.51	0.5748	0.1542
15	15	24.33	157.66	128.38	0.5698	0.1543

Table 3.12: Result obtained with Mach number equal to 1.4

Flight path$[deg]$	Ray path $[deg]$	$A_{e,1}$ $[m^2]$	$A_{e_{max}}$ $[m^2]$	Δp $[Pa]$	Δt $[s]$	$A_{e_1}/A_{e_{max}}$
0	0	25.15	164.2	139.31	0.5543	0.1532
2	2	25.14	164.02	139.04	0.5532	0.1535
4	4	25.10	163.47	138.90	0.5527	0.1537
5	5	24.92	163.07	138.82	0.5524	0.1528
6	6	24.9	162.57	138.44	0.5508	0.1532
8	8	24.8	161.33	137.89	0.5486	0.1537
10	10	24.55	159.73	137.34	0.5465	0.1537
12.5	12.5	24.4	157.24	136.08	0.5415	0.1552
15	15	23.9	154.24	134.88	0.537	0.1550

Table 3.13: Result obtained with Mach number equal to 1.6

Flight path$[deg]$	Ray path $[deg]$	$A_{e,1}$ $[m^2]$	$A_{e_{max}}$ $[m^2]$	Δp $[Pa]$	Δt $[s]$	$A_{e_1}/A_{e_{max}}$
0	0	24.25	156.3	141.9	0.5301	0.1552
2	2	24.15	156.13	141.8	0.5295	0.1547
4	4	24.10	155.6	141.55	0.5286	0.1549
5	5	24.05	155.2	141.43	0.5283	0.1550
6	6	24.02	154.77	141.10	0.5275	0.1552
8	8	23.91	153.57	140.53	0.525	0.1556
10	10	23.75	152.05	139.92	0.5227	0.1562
12.5	12.5	23.53	149.7	138.62	0.5178	0.1572
15	15	23.2	146.9	137.4	0.513	0.1579

Table 3.14: Result obtained with Mach number equal to 1.8

Flight path[deg]	Ray path [deg]	$A_{e,1}$ [m^2]	$A_{e_{max}}$ [m^2]	Δp [Pa]	Δt [s]	$A_{e_1}/A_{e_{max}}$
0	0	23.35	147.5	142.93	0.5126	0.1569
2	2	23.29	147.3	142.68	0.5117	0.1578
4	4	23.22	146.84	142.37	0.5106	0.1581
5	5	23.2	146.5	142.25	0.5102	0.1584
6	6	23.14	146.04	141.92	0.509	0.1585
8	8	23.05	144.93	141.27	0.5067	0.1591
10	10	22.8	143.5	140.71	0.5047	0.1589
12.5	12.5	22.7	141.3	139.5	0.499	0.1604
15	15	22.4	138.65	138.05	0.4952	0.1616

Table 3.15: Result obtained with Mach number equal to 2.0

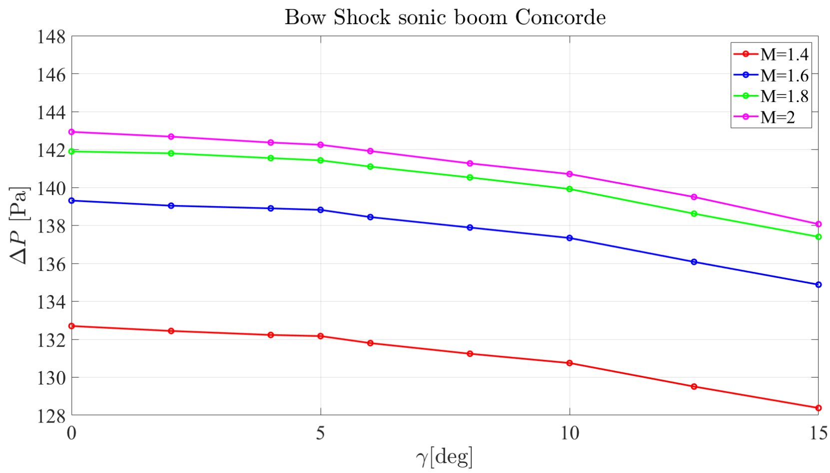

Figure 3.9: Bow Shock overpressure Concorde with Mach number and flight path angle variation

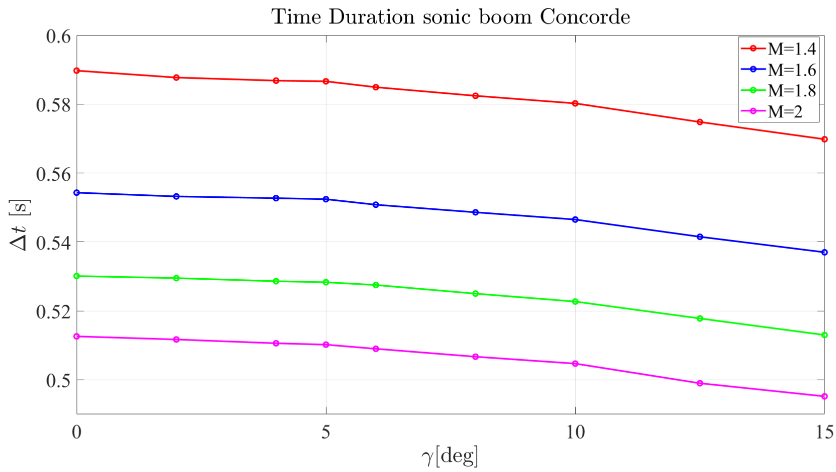

Figure 3.10: Time duration Concorde with Mach number and flight path angle variation

The bow shock overpressure decrease with increasing flight path angle and grows as the Mach number increase. Again, for a Mach number equal to 1.4, the bow shock overpressure is much lower than for the following shocks, possibly due to the reason explained above. On the other hand, time duration increase as the Mach number decrease and falls as the flight path angle grows.

3.2.4 Sonic boom analysis with altitude and flight path angle variation

Sonic boom response was also analyzed by considering the variation of flight path angle and altitude. Altitude variation was kept in the same range as previous tests as well flight path angle variation. The following studies were done considering the nominal length of the aircraft and with a Mach number equal to 2.04.
The following tables show the values obtained during the iterative cycles:

Flight path[deg]	Ray path [deg]	$A_{e,1}$ [m^2]	$A_{e_{max}}$ [m^2]	Δp [Pa]	Δt [s]	$A_{e_1}/A_{e_{max}}$
0	0	19.6	112	157.14	0.4311	0.175
2	2	19.59	111.7	157.03	0.4308	0.1752
4	4	19.52	111.5	156.68	0.4299	0.1753
5	5	19.51	111.26	156.40	0.429	0.1756
6	6	19.48	110.95	156.15	0.4284	0.1757
8	8	19.42	110.12	155.40	0.4263	0.1764
10	10	19.30	109.1	154.46	0.4237	0.1769
12.5	12.5	19.22	107.48	153.09	0.4204	0.1788
15	15	18.95	105.55	151.50	0.4156	0.1795

Table 3.16: Result obtained with an altitude equal to 17000 m

Flight path[deg]	Ray path [deg]	$A_{e,1}$ [m^2]	$A_{e_{max}}$ [m^2]	Δp [Pa]	Δt [s]	$A_{e_1}/A_{e_{max}}$
0	0	21.36	128.37	149.63	0.4701	0.1656
2	2	21.3	128.21	149.49	0.4697	0.1666
4	4	21.27	127.8	149.25	0.4689	0.1667
5	5	21.18	127.5	149.10	0.4684	0.1661
6	6	21.15	127.12	148.89	0.4678	0.1664
8	8	21.1	126.16	148.25	0.466	0.1672
10	10	20.92	124.9	147.52	0.4634	0.1674
12.5	12.5	20.72	123.07	146.38	0.4602	0.1672
15	15	20.5	120.8	144.95	0.4554	0.1697

Table 3.17: Result obtained with an altitude equal to 18000 m

Flight path[deg]	Ray path [deg]	$A_{e,1}$ [m^2]	$A_{e_{max}}$ [m^2]	Δp [Pa]	Δt [s]	$A_{e_1}/A_{e_{max}}$
0	0	23.22	147.5	143.18	0.5135	0.1574
2	2	23.2	147.3	143.08	0.513	0.1575
4	4	23.14	146.84	142.86	0.5124	0.1576
5	5	23.10	146.5	142.68	0.5117	0.1577
6	6	23.06	146.05	142.44	0.5109	0.1579
8	8	22.9	144.94	141.90	0.5089	0.1580
10	10	22.8	143.52	141.17	0.5063	0.1589
12.5	12.5	22.5	141.3	140.04	0.5023	0.1592
15	15	22.32	138.65	138.63	0.4972	0.1610

Table 3.18: Result obtained with an altitude equal to 19000 m

Flight path[deg]	Ray path [deg]	$A_{e,1}$ [m^2]	$A_{e_{max}}$ [m^2]	Δp [Pa]	Δt [s]	$A_{e_1}/A_{e_{max}}$
0	0	23.22	147.5	143.18	0.5135	0.1574
2	2	23.2	147.3	143.08	0.513	0.1575
4	4	23.14	146.84	142.86	0.5124	0.1576
5	5	23.10	146.5	142.68	0.5117	0.1577
6	6	23.06	146.05	142.44	0.5109	0.1579
8	8	22.9	144.94	141.90	0.5089	0.1580
10	10	22.8	143.52	141.17	0.5063	0.1589
12.5	12.5	22.5	141.3	140.04	0.5023	0.1592
15	15	22.32	138.65	138.63	0.4972	0.1610

Table 3.19: Result obtained with an altitude equal to 20000 m

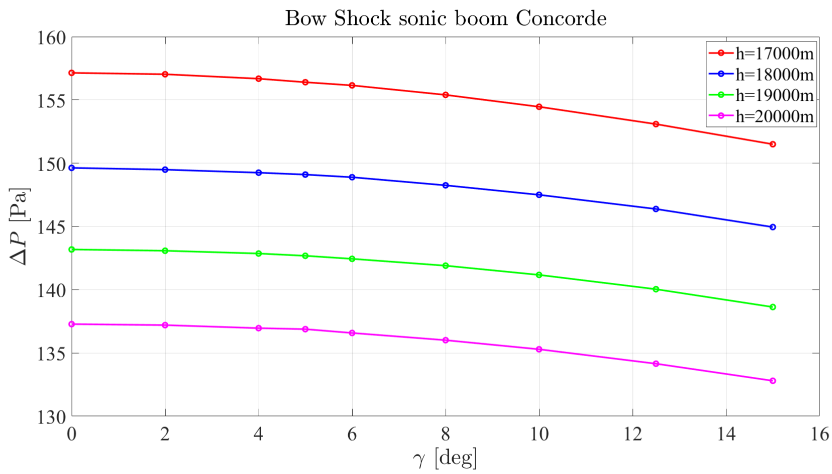

Figure 3.11: Bow Shock Overpressure Concorde with flight path angle and height variation

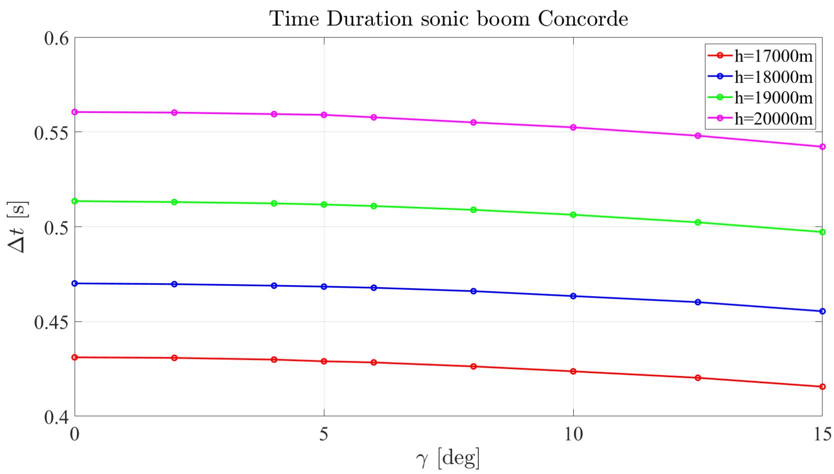

Figure 3.12: Time duration Concorde with flight path angle and height variation

As far as bow shock overpressure is concerned, it clearly decreases with increasing altitude and flight path angle. In particular, as in the previous case, for high flight path angles the rate of decrease of the bow shock overpressure is much greater than for small angles.The time duration rises as the altitude increases and decreases as the flight path angle grows.

4

Stratofly sonic boom analysis

4.1 General description of the aircraft

The Stratofly project is an European project concerning the study of a hypersonic stratospheric aircraft for civil transport. The objective is to study the feasibility and sustainability of a new propulsion technology going to reduce flight time, polluting and acoustic emissions, while respecting all safety requirements imposed by various authorities .
Stratofly would also be the first civilian transport aircraft to fly in the stratosphere which extends up to about 50 km in altitude above ground. The main objectives of the project are related to:

i. reduce intercontinental connection times

ii. use of new technology for hypersonic propulsion

iii. economic feasibility assessment for hypersonic aircraft

iv. reduction of emissions through the use of liquid hydrogen as fuel

v. noise reduction

Figure 4.1: Stratofly concept

One of the major features of the aircraft is the fact that it will be capable of cruising at a Mach number of 8 and at an altitude of over 30 km (about 36 km).

By taking advantage of these features it will be possible to connect the antipodes of the globe in a just a few hours: in fact it will be possible to fly between Australia and Europe in about 3 hours of flight compared to the current 25 hours of subsonic flights.
As far as the propulsion strategy is concerned, Stratofly will integrate 6 air turbo rocket engines able to operate in supersonic regime up to Mach 4.5 and then use a dual mode ramjet for the hypersonic part of the flight up to Mach 8.
Liquid hydrogen (LH_2) will be used as propellant type because of the high specific energy (143 MJ/Kg). This type of propellant does not contain carbon molecules and will lead to a total reduction of CO_2 emissions.

4.2 Sonic Boom Analysis

Also for Stratofly a sonic boom analysis was carried out by calculating the bow shock overpressure and the time signature duration. As in the previous case, the aircraft length, Mach number, flight altitude and flight path angle were varied.

4.2.1 Sonic boom analysis with flight path angle and altitude variation

The first analysis carried out concerns the evaluation of bow shock overpressure and time signature duration by varying the aircraft flight altitude and flight path angle. As far as flight path angle is concerned, the range of values was taken between 0 and 15 deg and this is due to the fact that Carlson's method is correct for flights with moderate climb and descents. On the other hand the altitude will vary between 32000 m and 35000 m.

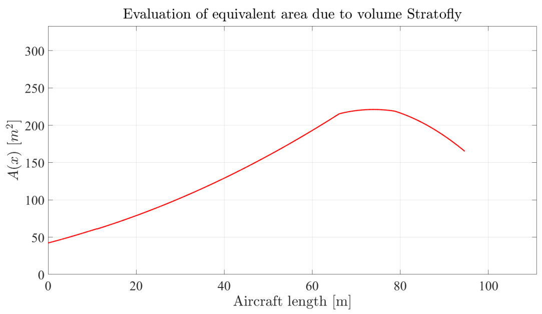

(a) Equivalent area due to volume

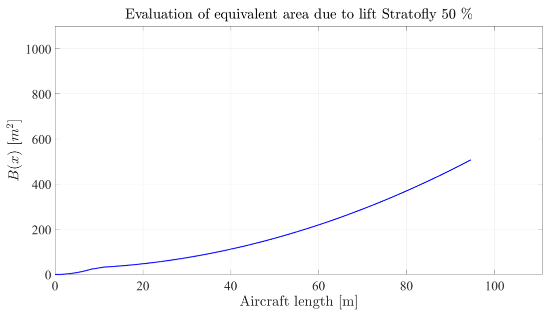

(b) Equivalent area due to lift

Figure 4.2: Evaluation of equivalent area due to volume & lift with flight path angle $\gamma = 15°$, M=7 & h=35000m

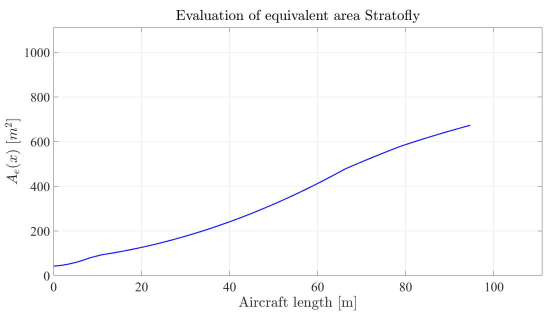

Figure 4.3: Total equivalent area Stratofly with flight path angle $\gamma = 15°$, M=7 & h=35000m

All of these tests were done at a Mach number of 7 and with a flight path angle of 0 deg.

Flight path[deg]	Ray path [deg]	$A_{e,1}$ [m^2]	$A_{e_{max}}$ [m^2]	Δp [Pa]	Δt [s]	$A_{e_1}/A_{e_{max}}$
0	0	252.11	516.84	67.57	0.8440	0.4878
2	2	252.00	516.43	67.55	0.8439	0.488
4	4	251.62	515.15	67.45	0.8426	0.4885
6	6	251.01	513.02	67.30	0.8408	0.4893
8	8	250.15	510.05	67.10	0.838	0.4904
10	10	249.06	506.26	66.82	0.8348	0.492
12.5	12.5	247.37	500.39	66.416	0.8297	0.4944
15	15	245.35	493.3	65.91	0.823	0.4974

Table 4.1: Result obtained with an altitude equal to 32000 m

Flight path[deg]	Ray path [deg]	$A_{e,1}$ [m^2]	$A_{e_{max}}$ [m^2]	Δp [Pa]	Δt [s]	$A_{e_1}/A_{e_{max}}$
0	0	268.18	572.65	64.78	0.8983	0.4683
2	2	268.04	572.17	64.75	0.898	0.4685
4	4	267.63	570.68	64.66	0.896	0.469
6	6	266.9	568.2	64.51	0.8946	0.4697
8	8	265.93	564.75	64.30	0.8917	0.4709
10	10	264.65	560.38	64.03	0.888	0.4723
12.5	12.5	262.7	553.57	63.62	0.882	0.4746
15	15	260.33	545.33	63.14	0.8755	0.4772

Table 4.2: Result obtained with an altitude equal to 33000 m

Flight path[deg]	Ray path [deg]	$A_{e,1}$ [m^2]	$A_{e_{max}}$ [m^2]	Δp [Pa]	Δt [s]	$A_{e_1}/A_{e_{max}}$
0	0	286.7	636.6	62.40	0.9589	0.4504
2	2	286.47	635.89	62.37	0.9584	0.4504
4	4	285.97	634.17	62.28	0.957	0.4509
6	6	285.18	631.31	62.12	0.9545	0.4517
8	8	283.94	627.35	61.92	0.9513	0.4526
10	10	282.47	622.25	61.66	0.947	0.4539
12.5	12.5	280.22	614.4	61.24	0.941	0.4561
15	15	277.47	604.9	60.75	0.9334	0.4587

Table 4.3: Result obtained with an altitude equal to 34000 m

Flight path[deg]	Ray path [deg]	$A_{e,1}$ [m^2]	$A_{e_{max}}$ [m^2]	Δp [Pa]	Δt [s]	$A_{e_1}/A_{e_{max}}$
0	0	307.57	709.3	60.47	1.0277	0.4336
2	2	307.3	708.63	60.44	1.0273	0.4336
4	4	306.8	706.65	60.35	1.0257	0.4341
6	6	305.83	703.37	60.20	1.0231	0.4348
8	8	304.50	698.77	59.99	1.0196	0.4358
10	10	302.9	692.9	59.72	1.015	0.4372
12.5	12.5	300.2	683.82	59.31	1.008	0.439
15	15	297.05	672.9	58.81	0.9996	0.4414

Table 4.4: Result obtained with an altitude equal to 35000 m

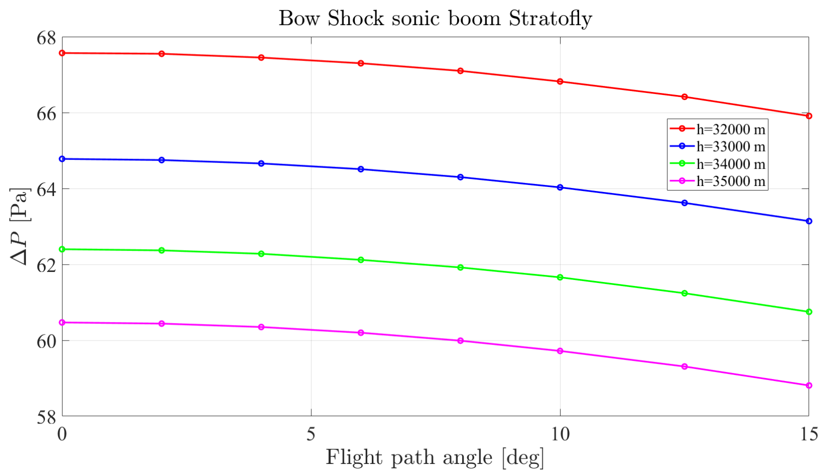

Figure 4.4: Bow Shock Stratofly at Mach 7 with variation flight path angle and altitude

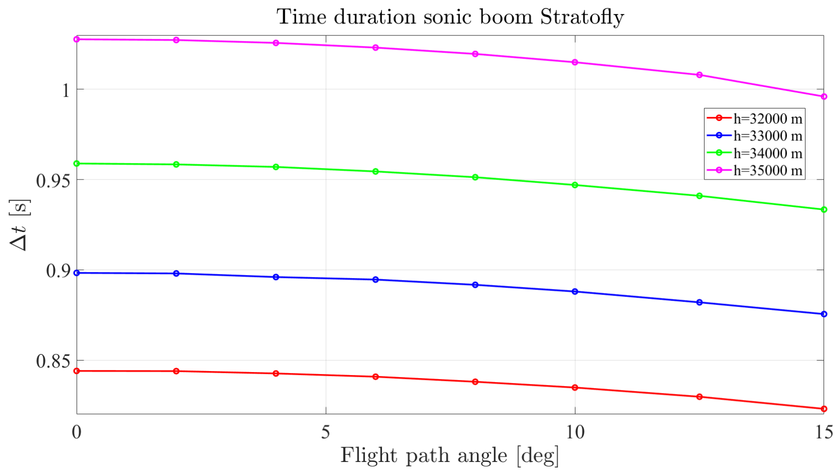

Figure 4.5: Time duration Stratofly at Mach 7 with variation flight path angle and altitude

Regarding bow shock overpressure, there is a clear decrease as altitude and flight path angle increase, although the most important contribution is given by altitude variation.
On the other hand the time duration increases as the altitude rises and the opposite happens when the flight path angle increases.

4.2.2 Sonic boom analysis with aircraft length and altitude variation

A sensitivity analysis was done regarding the simultaneous change in aircraft length and flight altitude.
The flight altitude was varied between 31000 meters and 34000 meters while the aircraft length was varied between 87 to 100% of the nominal length (between 82.3 meters and 94.6).
The following tables show the results obtained for a Mach number equal to 7 and a flight path angle equal to 0 deg.

Aircraft length $[m]$	$A_{e,1}$ $[m^2]$	$A_{e_{max}}$ $[m^2]$	Δp $[Pa]$	Δt $[s]$	$A_{e_1}/A_{e_{max}}$
82.32	190	389.2	66.87	0.7515	0.4882
84.21	197.5	401.3	67.39	0.757	0.4922
86.10	204.5	413	67.89	0.762	0.495
87.99	212	425.2	68.40	0.768	0.4986
89.89	219.6	437.3	68.76	0.77	0.502
92.25	229	453	69.33	0.779	0.5046
94.62	238	469	69.93	0.785	0.5075

Table 4.5: Result obtained with an altitude equal to 31000 m

Aircraft length $[m]$	$A_{e,1}$ $[m^2]$	$A_{e_{max}}$ $[m^2]$	Δp $[Pa]$	Δt $[s]$	$A_{e_1}/A_{e_{max}}$
82.32	202.2	431.4	64.27	0.8029	0.4687
84.21	210.1	444.2	64.68	0.808	0.4730
86.10	218	457.1	65.20	0.814	0.4767
87.99	225	470.2	65.71	0.820	0.4783
89.89	233	483.2	66.17	0.826	0.4818
92.25	241.7	500.2	66.87	0.835	0.4830
94.62	252.1	516.8	67.57	0.843	0.4878

Table 4.6: Result obtained with an altitude equal to 32000 m

Aircraft length $[m]$	$A_{e,1}$ $[m^2]$	$A_{e_{max}}$ $[m^2]$	Δp $[Pa]$	Δt $[s]$	$A_{e_1}/A_{e_{max}}$
82.32	216.3	480.14	61.73	0.856	0.4505
84.21	223.7	494	62.22	0.863	0.4527
86.10	232.5	508	62.6	0.868	0.4577
87.99	240	522.2	63.16	0.876	0.4595
89.89	248.3	536.5	63.59	0.882	0.463
92.25	258.4	554.4	64.26	0.891	0.466
94.62	268.3	572.6	64.95	0.901	0.469

Table 4.7: Result obtained with an altitude equal to 33000 m

Aircraft length $[m]$	$A_{e,1}$ $[m^2]$	$A_{e_{max}}$ $[m^2]$	Δp $[Pa]$	Δt $[s]$	$A_{e_1}/A_{e_{max}}$
82.32	232.55	535.7	59.75	0.918	0.434
84.21	240.9	550.7	60.16	0.924	0.437
86.10	248.7	566.3	60.65	0.932	0.439
87.99	257.3	581.7	60.96	0.937	0.442
89.89	265.8	597.3	61.3	0.942	0.445
92.25	275.7	616.6	61.87	0.950	0.447
94.62	286.7	636.5	62.41	0.958	0.4504

Table 4.8: Result obtained with an altitude equal to 34000 m

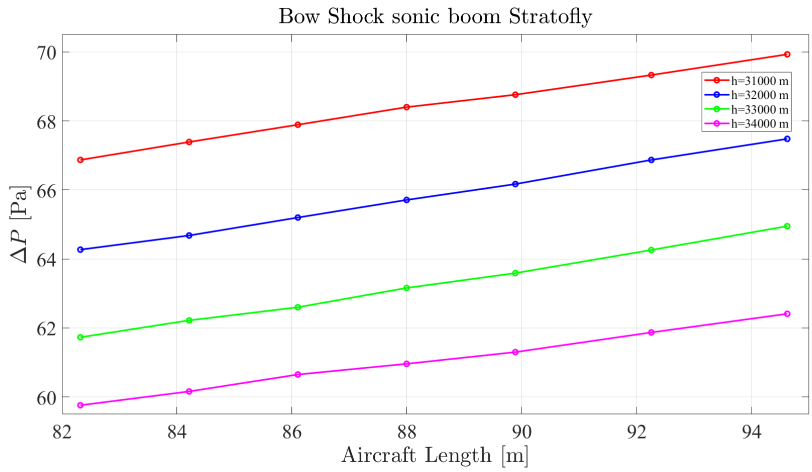

Figure 4.6: Bow Shock Stratofly with variation in aircraft length and altitude

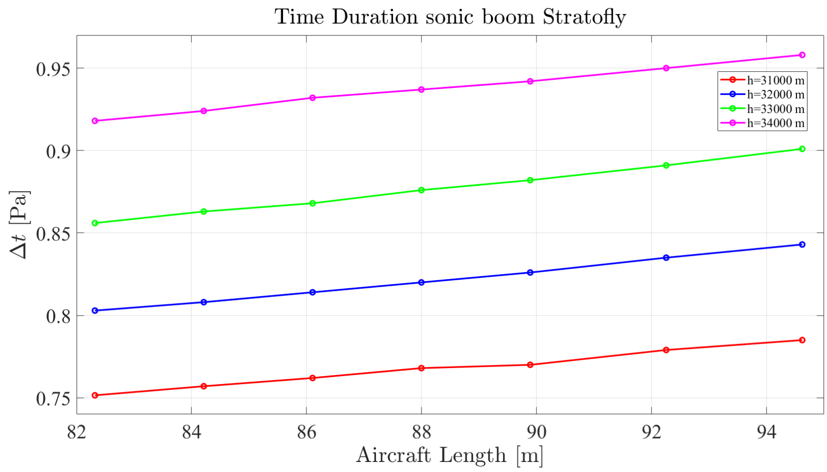

Figure 4.7: Time duration Stratofly with variation in aircraft length and altitude

In this case the bow shock overpressure increase as the length of the aircraft grows and decreases as the flight altitude rises in accordance with Carlson's method.
As far as time duration is concerned, it increases as both flight altitude and aircraft length increase.

4.2.3 Sonic boom analysis with Mach number and altitude variation

The analysis related to bow shock overpressure and time duration has been done by varying the Mach number of the aircraft and the flight altitude. For Mach number the variation is between 5 to 7.5 while for altitude the variation between 30000m and 35000m was studied. For this study, the aircraft was considered to be in level flight with its nominal length of approximately 94.6 meters.

Aircraft altitude $[m]$	$A_{e,1}$ $[m^2]$	$A_{e_{max}}$ $[m^2]$	Δp $[Pa]$	Δt $[s]$	$A_{e_1}/A_{e_{max}}$
30000	255	527.2	76.96	0.7847	0.4841
31000	272	585.4	73.75	0.837	0.4646
32000	291.2	652.5	71.52	0.902	0.4463
33000	313.5	729.6	69.21	0.9697	0.4295
34000	339	818.4	66.95	1.039	0.4142
35000	368	918.9	65.5	1.125	0.4005

Table 4.9: Result obtained with a Mach number equal to 5

Aircraft altitude $[m]$	$A_{e,1}$ $[m^2]$	$A_{e_{max}}$ $[m^2]$	Δp $[Pa]$	Δt $[s]$	$A_{e_1}/A_{e_{max}}$
30000	246	495.5	76.23	0.7745	0.4965
31000	261	549.3	72.96	0.828	0.4752
32000	278.9	610	70.90	0.8916	0.4572
33000	299.3	680.6	68.52	0.9566	0.4398
34000	322.6	761.5	66.30	1.026	0.4236
35000	349.2	853.8	64.42	1.103	0.409

Table 4.10: Result obtained with a Mach number equal to 5.5

Aircraft altitude $[m]$	$A_{e,1}$ $[m^2]$	$A_{e_{max}}$ $[m^2]$	Δp $[Pa]$	Δt $[s]$	$A_{e_1}/A_{e_{max}}$
30000	238.2	468.9	75.47	0.7647	0.508
31000	252.4	518	72.26	0.815	0.4873
32000	268.5	575.8	70.39	0.883	0.4679
33000	287.5	638.9	67.68	0.942	0.45
34000	308.7	713.2	65.31	1.017	0.4328
35000	333.3	798.4	63.41	1.082	0.4175

Table 4.11: Result obtained with a Mach number equal to 6

Aircraft altitude $[m]$	$A_{e,1}$ $[m^2]$	$A_{e_{max}}$ $[m^2]$	Δp $[Pa]$	Δt $[s]$	$A_{e_1}/A_{e_{max}}$
30000	231.6	446	75.14	0.759	0.5193
31000	244.8	491.6	71.86	0.809	0.498
32000	259.7	543.3	69.08	0.865	0.478
33000	277.1	603.4	66.72	0.927	0.459
34000	296.4	671.4	64.49	0.992	0.4415
35000	319.5	750.7	62.57	1.07	0.4256

Table 4.12: Result obtained with a Mach number equal to 6.5

Aircraft altitude $[m]$	$A_{e,1}$ $[m^2]$	$A_{e_{max}}$ $[m^2]$	Δp $[Pa]$	Δt $[s]$	$A_{e_1}/A_{e_{max}}$
30000	222.6	426.5	74.88	0.756	0.5299
31000	238.3	468.7	71.05	0.799	0.508
32000	252.2	517	67.57	0.855	0.4878
33000	267.9	572.7	64.78	0.917	0.4678
34000	286.7	636.7	62.40	0.982	0.4503
35000	307.6	709.8	60.47	1.05	0.4334

Table 4.13: Result obtained with a Mach number equal to 7

Aircraft altitude $[m]$	$A_{e,1}$ $[m^2]$	$A_{e_{max}}$ $[m^2]$	Δp $[Pa]$	Δt $[s]$	$A_{e_1}/A_{e_{max}}$
30000	221.7	409.31	73.20	0.738	0.540
31000	232.59	448.89	70.02	0.7905	0.518
32000	245.55	493.6	67.05	0.8441	0.4973
33000	260.65	546.15	64.41	0.9046	0.4773
34000	277.8	605.95	62.05	0.9692	0.4585
35000	297.5	674.3	60.22	1.036	0.4412

Table 4.14: Result obtained with a Mach number equal to 7.5

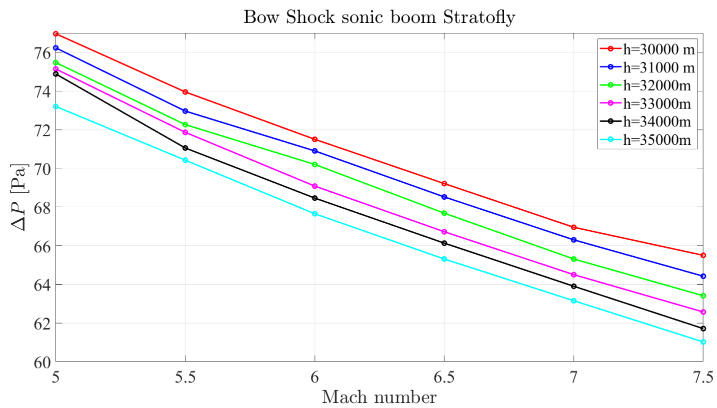

Figure 4.8: Bow Shock Stratofly at an altitude of 35000 m with Mach number equal to 5

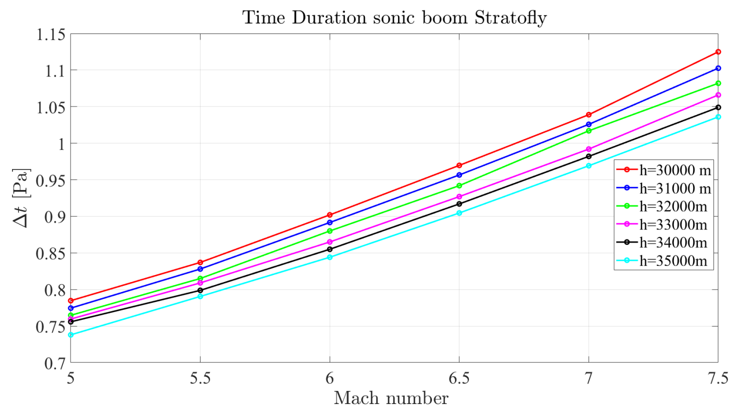

Figure 4.9: Time duration Stratofly at an altitude of 35000 m with Mach number equal to 5

In this case the bow shock overpressure is surprisingly decreasing as the Mach number increases, which could be due to the increasing area ratio $A_{e,1}/A_{e,max}$ that lead to a reduction of

the value of shape factor K_S.
The time duration, on the other hand, decreases correctly as the Mach number increases according to Carlson's method.

4.2.4 Sonic boom analysis with Mach number and aircraft length variation

The final sensitivity analysis developed for Concorde is related to the study of bow shock overpressure and time duration by varying the Mach number and the length of the aircraft. The length of the aircraft was varied between 82.3 m and 94.6 m, which is the nominal length of the aircraft. The variation for Mach number is between 5 and 7.5.
The results are obtained for an altitude of 34000 m in steady condition.

Aircraft length $[m]$	$A_{e,1}$ $[m^2]$	$A_{e_{max}}$ $[m^2]$	Δp $[Pa]$	Δt $[s]$	$A_{e_1}/A_{e_{max}}$
82.32	278.4	694.2	64.68	1.00	0.401
84.21	288	713	65.09	1.01	0.404
86.10	298.6	731.7	65.72	1.02	0.4075
87.99	305.1	751.2	65.9	1.028	0.406
89.9	316	769.7	66.11	1.028	0.4107
92.25	326.8	794	66.77	1.035	0.4115
94.62	339	818.4	66.89	1.038	0.4142

Table 4.15: Result obtained with an Mach number equal to 5

Aircraft length $[m]$	$A_{e,1}$ $[m^2]$	$A_{e_{max}}$ $[m^2]$	Δp $[Pa]$	Δt $[s]$	$A_{e_1}/A_{e_{max}}$
82.32	264	644.2	63.5	0.98	0.4101
84.21	273	662	64.05	0.99	0.4124
86.10	281.7	679.7	64.2	0.992	0.4144
87.99	290.3	697.6	64.27	0.994	0.415
89.90	300.2	715.6	64.52	0.998	0.4195
92.25	311.8	738.2	65.01	1.0054	0.4222
94.62	322.5	761.1	65.5	1.01	0.4235

Table 4.16: Result obtained with an Mach number equal to 5.5

Aircraft length $[m]$	$A_{e,1}$ $[m^2]$	$A_{e_{max}}$ $[m^2]$	Δp $[Pa]$	Δt $[s]$	$A_{e_1}/A_{e_{max}}$
82.32	251.4	602.5	62.01	0.957	0.4172
84.21	260.9	619.2	62.28	0.96	0.4214
86.10	271.5	635.7	62.54	0.965	0.4268
87.99	277.7	652.7	63.11	0.973	0.4255
89.90	286.9	669.7	63.44	0.978	0.4284
92.25	298	691	63.96	0.986	0.4310
94.62	308.7	713.2	64.50	0.995	0.4328

Table 4.17: Result obtained with an Mach number equal to 6

Aircraft length $[m]$	$A_{e,1}$ $[m^2]$	$A_{e_{max}}$ $[m^2]$	Δp $[Pa]$	Δt $[s]$	$A_{e_1}/A_{e_{max}}$
82.32	241.9	566.7	61.01	0.939	0.4268
84.21	250.7	582.4	61.28	0.943	0.4305
86.10	258.7	598.4	61.66	0.949	0.432
87.99	266.4	614.5	62.05	0.955	0.4335
89.90	275.5	630.72	62.37	0.96	0.437
92.25	286.1	651.2	62.85	0.969	0.4393
94.62	296.8	671.7	63.40	0.975	0.4422

Table 4.18: Result obtained with an Mach number equal to 6.5

Aircraft length $[m]$	$A_{e,1}$ $[m^2]$	$A_{e_{max}}$ $[m^2]$	Δp $[Pa]$	Δt $[s]$	$A_{e_1}/A_{e_{max}}$
82.32	232.6	535.7	60.05	0.923	0.4342
84.21	241.0	550.8	60.38	0.928	0.4376
86.10	248.5	566.1	60.88	0.935	0.439
87.99	257.5	581.5	61.23	0.94	0.4428
89.90	265.7	597.2	61.6	0.946	0.4446
92.25	276.1	616.7	62.13	0.954	0.4477
94.62	286.8	636.5	62.40	0.962	0.45

Table 4.19: Result obtained with an Mach number equal to 7

Aircraft length $[m]$	$A_{e,1}$ $[m^2]$	$A_{e_{max}}$ $[m^2]$	Δp $[Pa]$	Δt $[s]$	$A_{e_1}/A_{e_{max}}$
82.32	226.2	508.87	57.21	0.878	0.442
84.21	232.8	523.39	57.96	0.889	0.445
86.10	240.7	538.05	58.67	0.900	0.447
87.99	248.6	552.84	59.36	0.911	0.4497
89.90	257.4	567.77	59.98	0.92	0.453
92.25	267.1	586.59	60.77	0.932	0.455
94.62	227.7	605.6	61.75	0.947	0.458

Table 4.20: Result obtained with an Mach number equal to 7.5

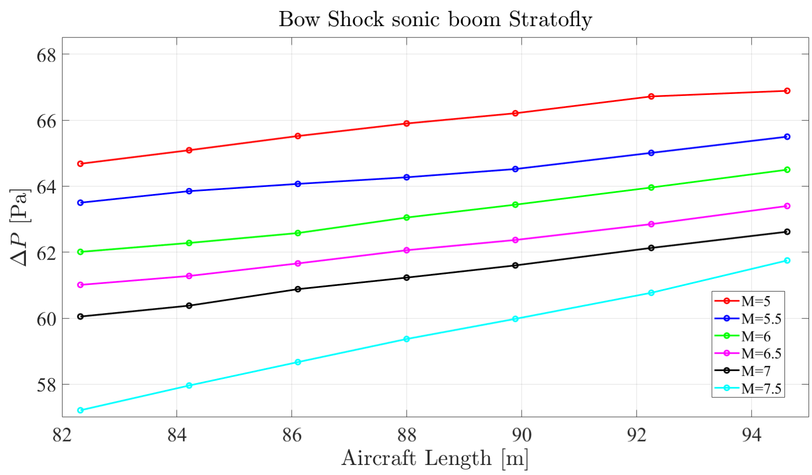

Figure 4.10: Bow Shock Stratofly at an altitude of 34000 m with Mach and length variation

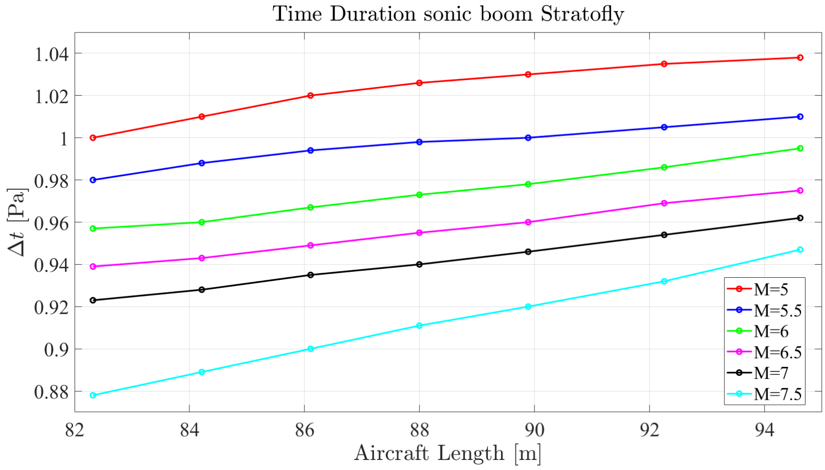

Figure 4.11: Time duration Stratofly at an altitude of 34000 m with Mach and length variation

As in the previous case, the bow shock overpressure value is lower as the Mach number increases, which may be due to the same reason as explained above. Instead, it correctly increases according to Carlson's method as the length of the aircraft increases.
As far as time duration is concerned, it decreases quite clearly as the Mach number increases and it rises approximately linearly as the length of the aircraft grows.

5

GreenHawk3 sonic boom analysis

5.1 General description of the aircraft

GreenHawk3 is a conceptual design project developed by 11 students of the Master of Science in Aerospace Engineering course at Politecnico di Torino during the period between September 2020 and January 2021.
The aim of the project was to develop a concept for a supersonic aircraft that would meet the following requirements:

i. Range between 5000 to 9000 km

ii. Cruise Mach number equal to 3

iii. Use of biofuel as a propeller

iv. 20 passengers in business jet layout

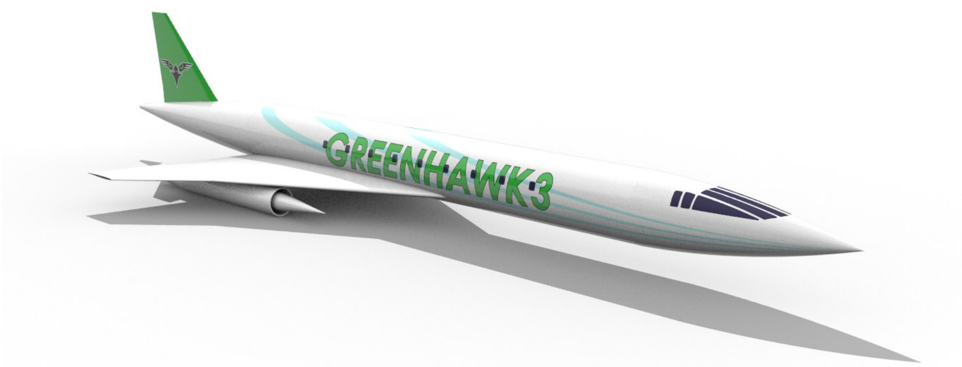

Figure 5.1: GreenHawk3 Concept

During the initial design phases of the aircraft, no recommendations were made regarding the sonic boom phenomena as it was not among the constraints and requirements imposed.
Regarding range, due to the impossibility of supersonic flights over the land, it was decided to bring the range towards the upper end. Through a simulation of the mission profile carried out using ASTOS software, it was noted that the actual range of the aircraft is approximately 8200 km with 20000 kg of fuel.
Regarding Mach number, with cruise Mach number equal to 3 as the requirement a trade-off analysis had to be made as concerns the use of a turbojet engine or a turbo-ramjet configuration with turbines integrated with ramjets. As a result of the trade-off analysis, it was decided to use a configuration with a pair of turbojet engines without an afterburner.
One of the most innovative aspects of the project concerns the choice of propellant: no kerosene is used, but instead biofuel. As a type of biofuel it was decided to use *HEFA*(Hydrotreated Esters and Fatty Acids) which is already commercially available and has similar characteristics to the typical Jet A-1. Hefa biofuel has the advantage of being a drop in fuel that don't require changes in aircraft and fuel infrastructure and are applicable across all aircraft segments.
With the 20-passenger requirement, a configuration with a fuselage 10% wider than others civil business jets has been studied in order to increase comfort on board, with the typical 1-1 configuration.

GreenHawk3 main features		
Dimension specification	Value	Unit of measurement
Overall length	42	m
MTOW	38256	kg
First sweep angle	64	deg
Second sweep angle	51	deg
Wing surface	131	m^2
Root Chord	12.28	m
Slenderness ratio	0.20	/
Taper ratio	0.14	/
Fuel capacity	20000	kg
OEW	15376	kg

Table 5.1: GreenHawk3 features

5.2 Sonic boom analysis

As with previous aircraft, sonic boom analysis of bow shock overpressure and time signature duration were carried out for the GreenHawk3. The parameters that were varied are the same as those used in the previous tests for the other aircraft.
Regarding the variation in Mach number and altitude, the variation values that were noted using ASTOS software used for the mission profile.

5.2.1 Sonic boom analysis with Mach number and aircraft length variation

The first analysis that has been made relates to the simultaneous variation of Mach number and aircraft length.

For the Mach number as previously pointed out, it was varied within the values obtained by ASTOS software during the cruise. Moreover the length of the aircraft was varied between 87 and 100% of the nominal length as in the previous studies.
The evaluations were made for an altitude of 20000 metres and with a flight path angle equal to 0 deg.

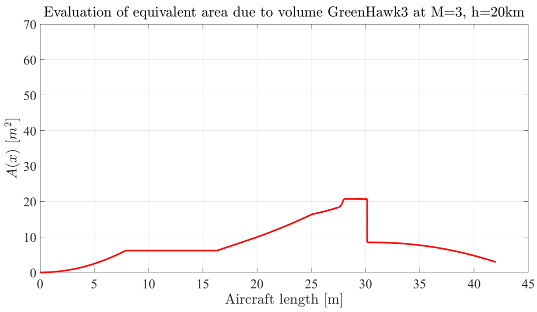

(a) Equivalent area due to volume

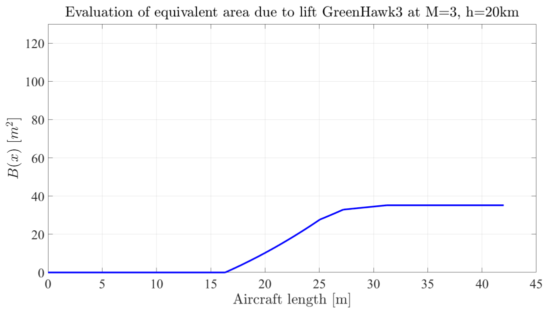

(b) Equivalent area due to lift

Figure 5.2: Evaluation of equivalent area due to volume & lift with a Mach number equal to 3, a flight path angle equal to 15 deg and at 20000 m of altitude

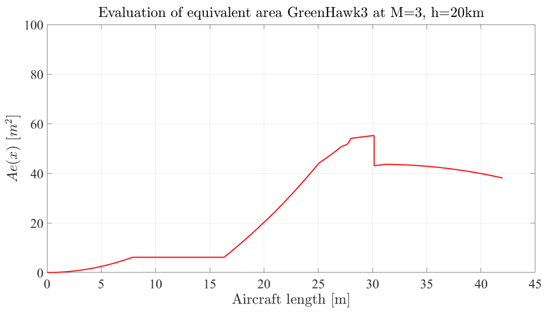

Figure 5.3: Evaluation of equivalent area with a Mach number equal to 3, a flight path angle equal to 15 deg and at 20000 m of altitude

The following tables summarise the numerical values obtained :

Mach number	$A_{e,1}$ $[m^2]$	$A_{e_{max}}$ $[m^2]$	Δp $[Pa]$	Δt $[s]$	$A_{e_1}/A_{e_{max}}$
2.4	4.45	58.38	100.09	0.391	0.0762
2.5	4.45	57.03	100.02	0.3876	0.078
2.6	4.45	55.74	99.97	0.385	0.0798
2.7	4.45	54.53	99.77	0.3815	0.0816
2.8	4.45	53.36	99.61	0.380	0.0834
3	4.45	51.22	99.26	0.3739	0.0869

Table 5.2: Result obtained with an aircraft length equal to 35.70 m

Mach number	$A_{e,1}$ $[m^2]$	$A_{e_{max}}$ $[m^2]$	Δp $[Pa]$	Δt $[s]$	$A_{e_1}/A_{e_{max}}$
2.4	4.66	59.8	100.66	0.3932	0.0778
2.5	4.66	58.49	100.64	0.39	0.0797
2.6	4.66	57.18	100.47	0.3865	0.0815
2.7	4.66	55.93	100.33	0.3836	0.0833
2.8	4.66	54.75	100.18	0.381	0.0851
3	4.66	52.55	99.83	0.376	0.0887

Table 5.3: Result obtained with an aircraft length equal to 36.54 m

Mach number	$A_{e,1}$ $[m^2]$	$A_{e_{max}}$ $[m^2]$	Δp $[Pa]$	Δt $[s]$	$A_{e_1}/A_{e_{max}}$
2.4	4.877	61.38	101.26	0.3956	0.0795
2.5	4.877	59.97	101.12	0.392	0.0813
2.6	4.877	58.63	101.02	0.3887	0.0832
2.7	4.877	57.36	100.89	0.3857	0.085
2.8	4.877	56.15	100.74	0.383	0.0869
3	4.877	53.92	100.40	0.3782	0.0904

Table 5.4: Result obtained with an aircraft length equal to 37.38 m

Mach number	$A_{e,1}$ $[m^2]$	$A_{e_{max}}$ $[m^2]$	Δp $[Pa]$	Δt $[s]$	$A_{e_1}/A_{e_{max}}$
2.4	5.1	62.9	101.77	0.3976	0.0811
2.5	5.1	61.46	101.70	0.394	0.083
2.6	5.1	60.06	101.57	0.391	0.0849
2.7	4.877	57.36	100.89	0.3857	0.085
2.8	4.877	56.15	100.74	0.383	0.0869
3	4.877	53.92	100.40	0.3782	0.0904

Table 5.5: Result obtained with an aircraft length equal to 38.22 m

Mach number	$A_{e,1}$ $[m^2]$	$A_{e_{max}}$ $[m^2]$	Δp $[Pa]$	Δt $[s]$	$A_{e_1}/A_{e_{max}}$
2.4	5.33	64.4	102.24	0.399	0.0828
2.5	5.33	62.96	102.21	0.396	0.0847
2.6	5.33	61.56	102.11	0.393	0.0866
2.7	5.33	60.23	101.97	0.3900	0.0885
2.8	5.33	58.96	101.83	0.3872	0.0904
3	5.33	56.63	99.53	0.3784	0.0941

Table 5.6: Result obtained with an aircraft length equal to 39.06 m

Mach number	$A_{e,1}$ $[m^2]$	$A_{e_{max}}$ $[m^2]$	Δp $[Pa]$	Δt $[s]$	$A_{e_1}/A_{e_{max}}$
2.4	5.56	65.96	102.74	0.4014	0.0858
2.5	5.56	64.46	102.68	0.398	0.0878
2.6	5.56	63.03	102.58	0.3947	0.0898
2.7	5.56	61.67	102.39	0.3915	0.0918
2.8	5.56	60.37	102.24	0.3887	0.0938
3	5.56	58.01	101.86	0.3837	0.0976

Table 5.7: Result obtained with an aircraft length equal to 39.90 m

Mach number	$A_{e,1}$ $[m^2]$	$A_{e_{max}}$ $[m^2]$	Δp $[Pa]$	Δt $[s]$	$A_{e_1}/A_{e_{max}}$
2.4	5.855	67.89	103.49	0.404	0.0862
2.5	5.855	66.34	103.43	0.4008	0.0882
2.6	5.855	64.88	103.34	0.3976	0.0902
2.7	5.855	63.49	103.22	0.3946	0.0922
2.8	5.855	62.17	103.01	0.3917	0.0941
3	5.855	59.77	102.66	0.387	0.0979

Table 5.8: Result obtained with an aircraft length equal to 40.95 m

Mach number	$A_{e,1}$ $[m^2]$	$A_{e_{max}}$ $[m^2]$	Δp $[Pa]$	Δt $[s]$	$A_{e_1}/A_{e_{max}}$
2.4	6.16	69.78	104.11	0.4067	0.0883
2.5	6.16	68.20	104.05	0.4032	0.0903
2.6	6.16	66.71	103.97	0.400	0.0923
2.7	6.16	65.27	103.77	0.397	0.0944
2.8	6.16	63.93	103.58	0.394	0.0964
3	6.16	61.43	103.13	0.3885	0.1003

Table 5.9: Result obtained with an aircraft length equal to 42 m

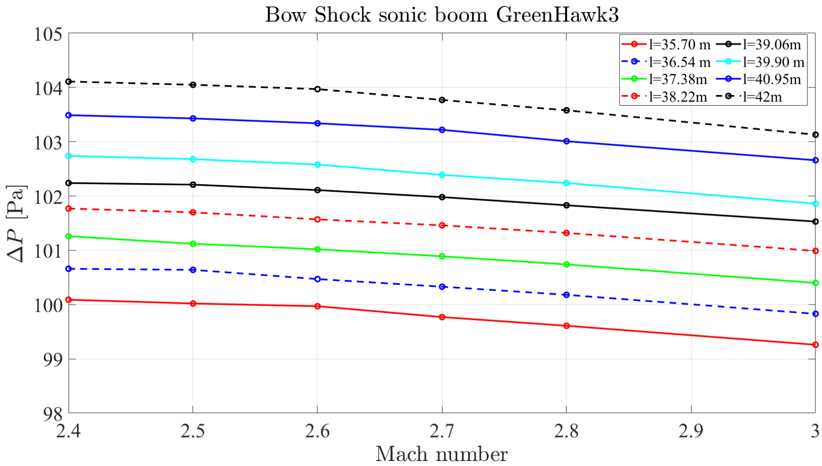

Figure 5.4: Bow Shock Overpressure GreenHawk3 with Mach number and aircraft length variation

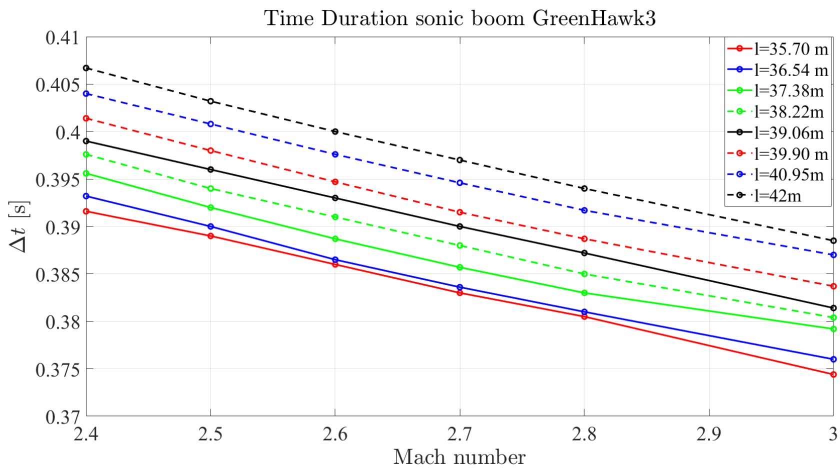

Figure 5.5: Time duration GreenHawk3 with Mach number and aircraft length variation

As can be seen from figure 5.4 as the Mach number increase the value of bow shock overpressure remains more or less constant with a small reduction, while it clearly increase as the length of the aircraft grows. On the other hand, the time duration decreases clearly as the Mach number increases, while it has the opposite behaviour as the length of the aircraft increases.

5.2.2 Sonic boom analysis with flight path angle and altitude

The sonic boom analysis was also evaluated by varying the aircraft altitude and flight path angle. As far as the altitude is concerned, the variation is between 16000m and 20000m while the flight path angle has been varied between 0 and 15 deg, as in the previous tests.
The results are relative to a Mach number of 3 and with the nominal length of the aircraft of 42 meters. The following tables describe the values obtained :

Flight path angle	Ray path angle	$A_{e,1}$ $[m^2]$	$A_{e_{max}}$ $[m^2]$	Δp $[Pa]$	Δt $[s]$	$A_{e_1}/A_{e_{max}}$
0	0	6.158	42.23	136.21	0.2985	0.1458
2	2	6.158	42.21	136.18	0.2984	0.1459
4	4	6.158	42.13	135.99	0.298	0.1462
6	6	6.158	42.00	135.76	0.2975	0.1466
8	8	6.158	41.82	135.42	0.2968	0.1473
10	10	6.158	41.59	134.94	0.2957	0.1481
12.5	12.5	6.158	41.28	134.31	0.2944	0.1494
15	15	6.158	40.78	133.48	0.2926	0.1510

Table 5.10: Result obtained with an altitude of 16000m

Flight path angle	Ray path angle	$A_{e,1}$ $[m^2]$	$A_{e_{max}}$ $[m^2]$	Δp $[Pa]$	Δt $[s]$	$A_{e_1}/A_{e_{max}}$
0	0	6.158	45.89	126.12	0.3177	0.1342
2	2	6.158	45.86	126.09	0.3176	0.1343
4	4	6.158	45.77	125.93	0.3172	0.1345
6	6	6.158	45.62	125.67	0.3165	0.135
8	8	6.158	45.4	125.32	0.3156	0.1356
10	10	6.158	45.14	124.92	0.3146	0.1364
12.5	12.5	6.158	44.72	124.31	0.313	0.1377
15	15	6.158	44.20	123.53	0.311	0.1393

Table 5.11: Result obtained with an altitude of 17000m

Flight path angle	Ray path angle	$A_{e,1}$ $[m^2]$	$A_{e_{max}}$ $[m^2]$	Δp $[Pa]$	Δt $[s]$	$A_{e_1}/A_{e_{max}}$
0	0	6.158	50.175	117.61	0.3392	0.1227
2	2	6.158	50.14	117.57	0.3391	0.1228
4	4	6.158	50.03	117.43	0.3387	0.1231
6	6	6.158	49.85	117.18	0.338	0.1235
8	8	6.158	49.6	116.84	0.337	0.1242
10	10	6.158	49.28	116.40	0.3357	0.125
12.5	12.5	6.158	48.8	115.77	0.3339	0.1262
15	15	6.158	48.20	114.97	0.3316	0.1278

Table 5.12: Result obtained with an altitude of 18000m

Flight path angle	Ray path angle	$A_{e,1}$ $[m^2]$	$A_{e_{max}}$ $[m^2]$	Δp $[Pa]$	Δt $[s]$	$A_{e_1}/A_{e_{max}}$
0	0	6.158	55.17	109.93	0.362	0.1116
2	2	6.158	55.14	109.9	0.3619	0.1117
4	4	6.158	55.01	109.76	0.3614	0.1119
6	6	6.158	54.8	109.53	0.3606	0.1124
8	8	6.158	54.5	109.19	0.3596	0.113
10	10	6.158	54.14	108.79	0.3582	0.1137
12.5	12.5	6.158	53.57	108.16	0.356	0.115
15	15	6.158	52.87	107.39	0.3536	0.1165

Table 5.13: Result obtained with an altitude of 19000m

Flight path angle	Ray path angle	$A_{e,1}$ $[m^2]$	$A_{e_{max}}$ $[m^2]$	Δp $[Pa]$	Δt $[s]$	$A_{e_1}/A_{e_{max}}$
0	0	6.158	61.03	103.13	0.387	0.1009
2	2	6.158	60.98	103.10	0.3869	0.1010
4	4	6.158	60.83	103.03	0.3864	0.1012
6	6	6.158	60.59	102.85	0.3606	0.1124
8	8	6.158	60.25	102.54	0.3844	0.1022
10	10	6.158	59.82	102.13	0.3828	0.1029
12.5	12.5	6.158	59.17	101.52	0.3805	0.1041
15	15	6.158	58.33	100.71	0.3775	0.1056

Table 5.14: Result obtained with an altitude of 20000 m

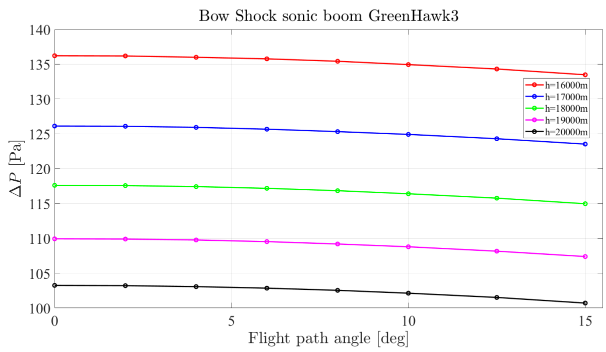

Figure 5.6: Bow Shock Overpressure GreenHawk3 with flight path angle and altitude variation

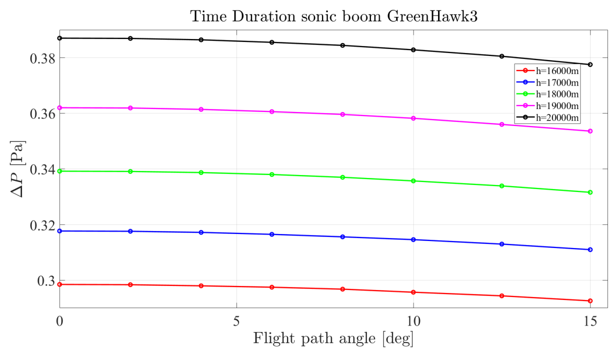

Figure 5.7: Time duration GreenHawk3 with flight path angle and altitude variation

As can be seen from the figure 5.6, as the altitude and flight path angle increase, there is a marked reduction in bow shock overpressure, in accordance with Carlson's theory.
The time duration, on the other hand, decreases as the flight path angle increases, while the opposite occurs as the flight altitude grows.

5.2.3 Sonic boom analysis with Mach and altitude variation

An analysis of the sonic boom was then performed by varying the flight altitude and the operative Mach number. As for the Mach number, as in the previous cases, it was varied between 2.4 and 3.0, the same for the altitude, which was varied between 16000m and 20000m. The following analysis was carried out considering the nominal length of the aircraft and with a flight path angle of 0 deg.

Mach number	$A_{e,1}$ $[m^2]$	$A_{e_{max}}$ $[m^2]$	Δp $[Pa]$	Δt $[s]$	$A_{e_1}/A_{e_{max}}$
2.4	6.158	46.66	135.00	0.3069	0.132
2.5	6.158	45.825	135.31	0.3051	0.1344
2.6	6.158	45.05	135.57	0.3035	0.1367
2.7	6.158	44.27	135.79	0.302	0.1391
2.8	6.158	43.56	135.93	0.3007	0.1414
3	6.158	42.23	136.21	0.2985	0.1458

Table 5.15: Result obtained with an altitude of 16000 m

Mach number	$A_{e,1}$ $[m^2]$	$A_{e_{max}}$ $[m^2]$	Δp $[Pa]$	Δt $[s]$	$A_{e_1}/A_{e_{max}}$
2.4	6.158	51.07	125.77	0.3288	0.1206
2.5	6.158	50.09	125.86	0.3261	0.1229
2.6	6.158	49.17	125.98	0.3241	0.1252
2.7	6.158	48.29	126.06	0.3223	0.1275
2.8	6.158	47.45	126.11	0.3206	0.1298
3	6.158	45.9	126.14	0.3177	0.1342

Table 5.16: Result obtained with an altitude of 17000 m

Mach number	$A_{e,1}$ $[m^2]$	$A_{e_{max}}$ $[m^2]$	Δp $[Pa]$	Δt $[s]$	$A_{e_1}/A_{e_{max}}$
2.4	6.158	56.22	117.30	0.351	0.1095
2.5	6.158	55.08	117.37	0.348	0.1118
2.6	6.158	54.00	117.45	0.346	0.114
2.7	6.158	52.97	117.48	0.344	0.1163
2.8	6.158	51.99	117.59	0.342	0.1184
3	6.158	50.17	117.60	0.340	0.1227

Table 5.17: Result obtained with an altitude of 18000 m

Mach number	$A_{e,1}$ $[m^2]$	$A_{e_{max}}$ $[m^2]$	Δp $[Pa]$	Δt $[s]$	$A_{e_1}/A_{e_{max}}$
2.4	6.158	62.27	09.97	0.3756	0.0989
2.5	6.158	60.92	110.01	0.3726	0.1011
2.6	6.158	59.65	110.03	0.37	0.1032
2.7	6.158	58.44	110.05	0.369	0.1054
2.8	6.158	57.4	110.15	0.3661	0.1073
3	6.158	55.18	110.17	0.364	0.1116

Table 5.18: Result obtained with an altitude of 19000 m

Mach number	$A_{e,1}$ $[m^2]$	$A_{e_{max}}$ $[m^2]$	Δp $[Pa]$	Δt $[s]$	$A_{e_1}/A_{e_{max}}$
2.4	6.158	69.31	102.99	0.4027	0.0888
2.5	6.158	67.75	103.01	0.3995	0.0909
2.6	6.158	66.26	103.04	0.3966	0.0929
2.7	6.158	64.95	103.06	0.394	0.0948
2.8	6.158	63.65	103.08	0.392	0.0967
3	6.158	61.25	103.13	0.389	0.1005

Table 5.19: Result obtained with an altitude of 20000 m

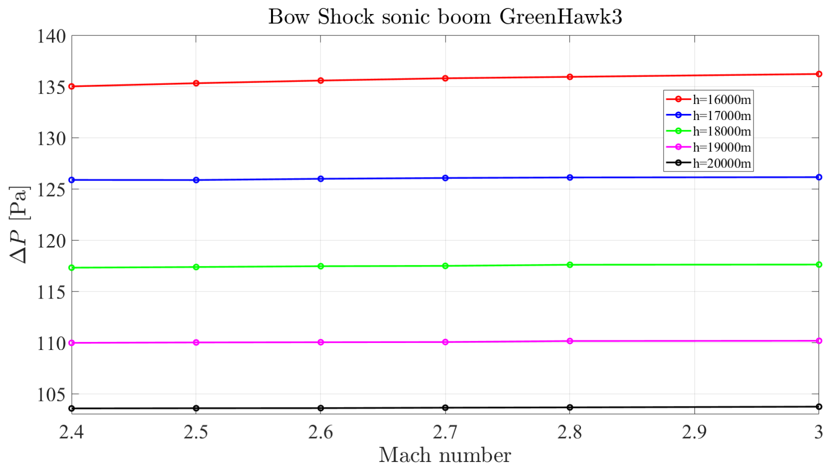

Figure 5.8: Bow Shock Overpressure GreenHawk3 with Mach and altitude variation

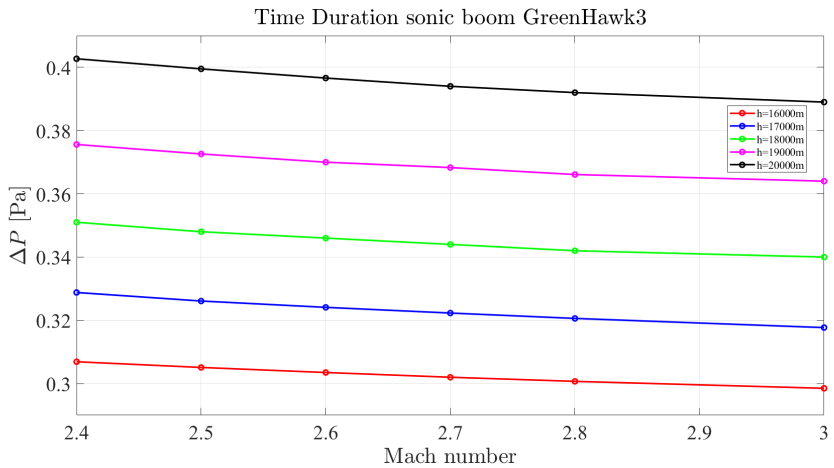

Figure 5.9: Time duration GreenHawk3 with Mach and altitude variation

As can be seen from the figure 5.8 there is a slight increase in bow shock overpressure as the Mach number increases, as opposed to what happens with increasing altitude.
As far as time duration is concerned, it increases with increasing in flight altitude and decreases as Mach number rises, in accordance with Carlson's theory.

5.2.4 Sonic boom analysis with aircraft length and altitude variation

A sonic boom analysis was carried out by varying simultaneously the altitude and length of the aircraft. The altitude was varied in a range between 16000m and 20000m while the length of the aircraft was varied between 35.70m and 42m, which correspond to a variation between 87 and 100 % of the nominal length.
The following tests were carried out for a flight condition with a Mach number of 3 and a flight path angle of 0 deg. The following tables show the results obtained:

Aircraft length $[m]$	$A_{e,1}$ $[m^2]$	$A_{e_{max}}$ $[m^2]$	Δp $[Pa]$	Δt $[s]$	$A_{e_1}/A_{e_{max}}$
35.70	4.449	34.78	129.97	0.2849	0.1279
36.54	4.66	35.64	130.80	0.2867	0.1305
37.38	4.88	36.74	131.54	0.2883	0.1327
38.22	5.099	37.73	132.40	0.2902	0.1351
39.06	5.325	38.75	133.18	0.2919	0.1376
39.90	5.558	39.73	134.00	0.2937	0.1399
40.95	5.86	41.01	135.08	0.296	0.1429
42.00	6.158	42.23	136.02	0.298	0.1458

Table 5.20: Result obtained with an altitude of 16000 m

Aircraft length $[m]$	$A_{e,1}$ $[m^2]$	$A_{e_{max}}$ $[m^2]$	Δp $[Pa]$	Δt $[s]$	$A_{e_1}/A_{e_{max}}$
35.70	4.449	37.91	120.37	0.3032	0.1174
36.54	4.66	38.96	121.19	0.3052	0.1196
37.38	4.88	40.04	122.01	0.3073	0.1219
38.22	5.099	41.02	122.72	0.3091	0.1243
39.06	5.325	42.14	123.56	0.3113	0.1264
39.90	5.558	43.21	124.32	0.313	0.1286
40.95	5.86	44.57	125.27	0.3155	0.1315
42.00	6.158	45.89	126.03	0.3175	0.1342

Table 5.21: Result obtained with an altitude of 17000 m

Aircraft length $[m]$	$A_{e,1}$ $[m^2]$	$A_{e_{max}}$ $[m^2]$	Δp $[Pa]$	Δt $[s]$	$A_{e_1}/A_{e_{max}}$
35.70	4.449	41.58	112.11	0.3234	0.107
36.54	4.66	42.71	112.85	0.3255	0.1091
37.38	4.88	43.8	113.53	0.3275	0.1114
38.22	5.099	44.99	114.31	0.3297	0.1133
39.06	5.325	46.133	114.93	0.332	0.1155
39.90	5.558	47.28	115.76	0.334	0.1176
40.95	5.86	48.75	116.71	0.3366	0.1202
42.00	6.158	50.17	117.52	0.339	0.1227

Table 5.22: Result obtained with an altitude of 18000 m

Aircraft length $[m]$	$A_{e,1}$ $[m^2]$	$A_{e_{max}}$ $[m^2]$	Δp $[Pa]$	Δt $[s]$	$A_{e_1}/A_{e_{max}}$
35.70	4.449	45.85	104.88	0.3453	0.0971
36.54	4.66	47.09	105.61	0.3478	0.0990
37.38	4.88	48.32	106.32	0.35	0.101
38.22	5.099	49.55	106.99	0.3523	0.1029
39.06	5.325	50.8	107.57	0.3542	0.1048
39.90	5.558	52.07	108.22	0.356	0.1067
40.95	5.86	53.63	108.97	0.3588	0.1093
42.00	6.158	55.18	109.75	0.3614	0.116

Table 5.23: Result obtained with an altitude of 19000 m

Aircraft length $[m]$	$A_{e,1}$ $[m^2]$	$A_{e_{max}}$ $[m^2]$	Δp $[Pa]$	Δt $[s]$	$A_{e_1}/A_{e_{max}}$
35.70	4.449	50.87	99.27	0.372	0.0876
36.54	4.66	52.2	99.84	0.3743	0.0892
37.38	4.88	53.55	100.42	0.3765	0.0911
38.22	5.099	54.9	101.00	0.3786	0.0929
39.06	5.325	56.25	101.52	0.3806	0.0947
39.90	5.558	57.62	102.10	0.3877	0.0965
40.95	5.86	59.34	102.72	0.3850	0.0988
42.00	6.158	61.43	103.13	0.3855	0.1003

Table 5.24: Result obtained with an altitude of 20000 m

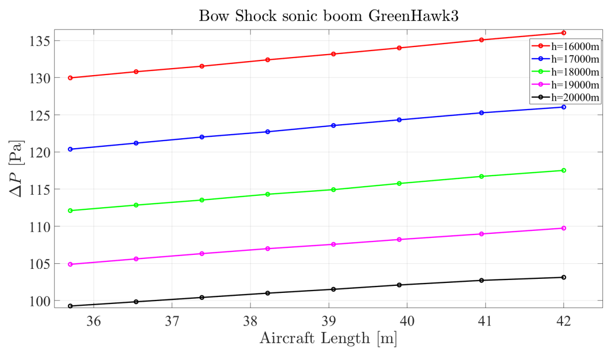

Figure 5.10: Bow Shock GreenHawk3 with altitude and length variation

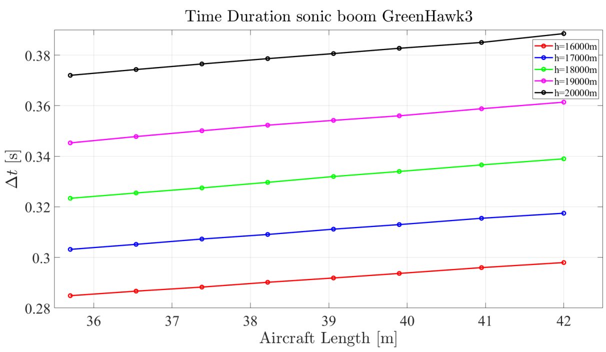

Figure 5.11: Time duration GreenHawk3 with altitude and length variation

As far as bow shock overpressure is concerned, it increases linearly as the length of the aircraft grows, while it clearly decreases as the flight altitude increase as can be seen in the figure 5.10.
Regarding time duration it increases with both flight altitude and aircraft length increase.

6

Shorter Stratofly sonic boom analysis

The configuration of the Stratofly aircraft studied earlier in chapter 4 will be resumed.
In the previous chapter, sonic boom analysis was carried out for a configuration 94.6 m long and capable of flying at cruise Mach number equal to 8. Instead, this chapter will deal with a reduced version of the aircraft by studying a configuration with a length of 70% of the previous one and equal to 66.25 meters and reduced performance.
For this configuration, a typical mission at an altitude of about 30,000m and a Mach number of 5 was taken as reference, while the previous one had a reference altitude of 36,000m and a Mach number equal to 8.

Figure 6.1: Stratofly shorter configuration

The following aircraft would have the same objectives and characteristics as described in the previous chapter, also the type of propellant used is the same as in the previous case.
As for the various dimensional quantities, they have all been scaled proportionally by the same amount

6.1 Sonic boom analysis

Various type of sonic boom analysis regarding bow shock overpressure and time signature duration were carried out.
During these analysis, the length of the aircraft was not varied, maintaining it at 70% of the original and consequently equal to 66.25 m. The analysis that has been made concerns:

i. simultaneous change in Mach number and altitude

ii. simultaneous variation of Mach number and flight path angle

iii. simultaneous variation of altitude and flight path angle

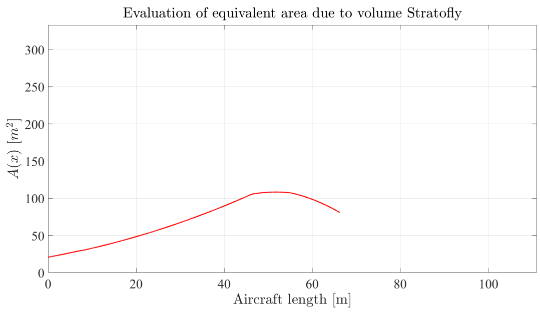

(a) Equivalent area due to volume

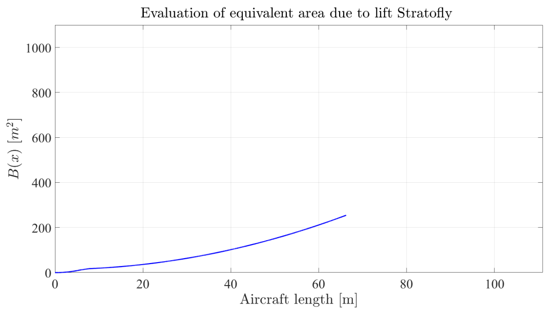

(b) Equivalent area due to lift

Figure 6.2: Evaluation of equivalent area due to volume & lift

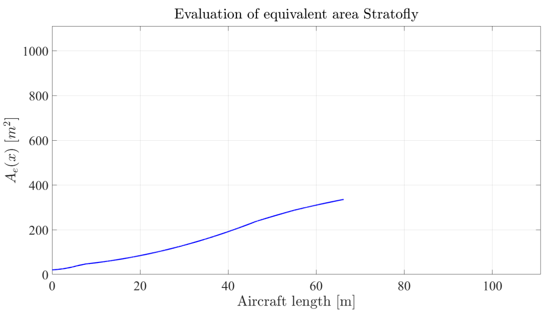

Figure 6.3: Effective area Short Stratofly with aircraft length equal to 66.3 m, h=30000m,M=5

6.1.1 Sonic boom analysis with Mach number and flight path angle variation

A first analysis that has been carried out relates to the sonic boom analysis by varying simultaneously the Mach number and the flight path angle. The Mach number was varied between 4 and 5 with a 0.2 step while the flight path angle was varied between 0 and 15 with a 2 degree step. Analysis was performed at an altitude of 30500 m and a length of 66.3 m.

flight path angle[deg]	ray path [deg]	$A_{e,1}$ $[m^2]$	$A_{e_{max}}$ $[m^2]$	Δp $[Pa]$	Δt $[s]$	$A_{e_1}/A_{e_{max}}$
0	0	165.5	395.46	71.50	0.7377	0.4185
2	2	165.4	395.08	71.46	0.7373	0.4186
4	4	165.1	393.93	71.317	0.7360	0.4192
6	6	164.5	392.03	71.10	0.7335	0.4196
8	8	167.35	389.37	70.85	0.731	0.4197
10	10	162.75	385.97	70.42	0.7265	0.4217
12.5	12.5	161.2	380.72	69.82	0.7204	0.4234
15	15	159.45	374.39	69.08	0.7129	0.426

Table 6.1: Result obtained with a Mach number equal to 4.0

flight path angle[deg]	ray path [deg]	$A_{e,1}$ $[m^2]$	$A_{e_{max}}$ $[m^2]$	Δp $[Pa]$	Δt $[s]$	$A_{e_1}/A_{e_{max}}$
0	0	161.47	381.42	70.80	0.7282	0.4234
2	2	161.37	381.04	70.77	0.7279	0.4235
4	4	161.00	379.65	70.62	0.7264	0.4237
6	6	160.49	378.12	70.387	0.7239	0.424
8	8	159.72	375.59	70.06	0.7206	0.4253
10	10	158.79	372.35	69.65	0.7165	0.426
12.5	12.5	157.3	367.33	69.05	0.710	0.4282
15	15	155.56	361.27	68.37	0.7032	0.4306

Table 6.2: Result obtained with a Mach number equal to 4.2

flight path angle[deg]	ray path [deg]	$A_{e,1}$ $[m^2]$	$A_{e_{max}}$ $[m^2]$	Δp $[Pa]$	Δt $[s]$	$A_{e_1}/A_{e_{max}}$
0	0	157.66	368.52	70.02	0.7183	0.4278
2	2	157.56	368.16	69.98	0.7179	0.428
4	4	157.26	367.12	69.85	0.7165	0.4283
6	6	156.73	365.37	69.63	0.7143	0.429
8	8	156.1	362.94	69.30	0.7109	0.4301
10	10	155.15	359.85	68.92	0.707	0.4312
12.5	12.5	153.7	355.05	68.35	0.701	0.4329
15	15	152.05	349.25	67.63	0.694	0.4354

Table 6.3: Result obtained with a Mach number equal to 4.4

flight path angle[deg]	ray path [deg]	$A_{e,1}$ $[m^2]$	$A_{e_{max}}$ $[m^2]$	Δp $[Pa]$	Δt $[s]$	$A_{e_1}/A_{e_{max}}$
0	0	154.2	356.64	69.32	0.7094	0.4324
2	2	154.16	356.31	69.28	0.709	0.4326
4	4	153.81	355.30	69.17	0.7079	9,4329
6	6	153.35	353.65	68.96	0.7058	0.4336
8	8	152.67	351.30	68.65	0.7026	0.4346
10	10	151.77	348.33	68.29	0.6989	0.4357
12.5	12.5	150.49	343.725	67.72	0.6931	0.4378
15	15	148.87	338.17	67.05	0.6862	0.4402

Table 6.4: Result obtained with a Mach number equal to 4.6

flight path angle[deg]	ray path [deg]	$A_{e,1}$ $[m^2]$	$A_{e_{max}}$ $[m^2]$	Δp $[Pa]$	Δt $[s]$	$A_{e_1}/A_{e_{max}}$
0	0	151.11	345.69	68.70	0.7017	0.4371
2	2	150.92	345.36	68.667	0.7013	0.437
4	4	150.7	344.4	68.56	0.7002	0.4374
6	6	150.2	342.79	68.34	0.698	0.4382
8	8	149.47	340.56	68.03	0.6949	0.4389
10	10	148.67	337.7	67.63	0.6908	0.4402
12.5	12.5	147.45	333.29	67.11	0.6855	0.4424
15	15	145.9	327.95	66.47	0.6788	0.445

Table 6.5: Result obtained with a Mach number equal to 4.8

flight path angle[deg]	ray path [deg]	$A_{e,1}$ $[m^2]$	$A_{e_{max}}$ $[m^2]$	Δp $[Pa]$	Δt $[s]$	$A_{e_1}/A_{e_{max}}$
0	0	148.05	335.55	67.53	0.6898	0.4412
2	2	147.96	335.24	67.50	0.6895	0.4414
4	4	147.68	334.31	67.40	0.6884	0.4417
6	6	147.24	332.78	67.19	0.6863	0.4425
8	8	146.6	330.63	66.90	0.6833	0.4434
10	10	145.81	327.9	66.54	0.6796	0.4447
12.5	12.5	144.58	323.62	66.01	0.6743	0.4468
15	15	143.07	318.5	65.40	0.668	0.4492

Table 6.6: Result obtained with a Mach number equal to 5.0.

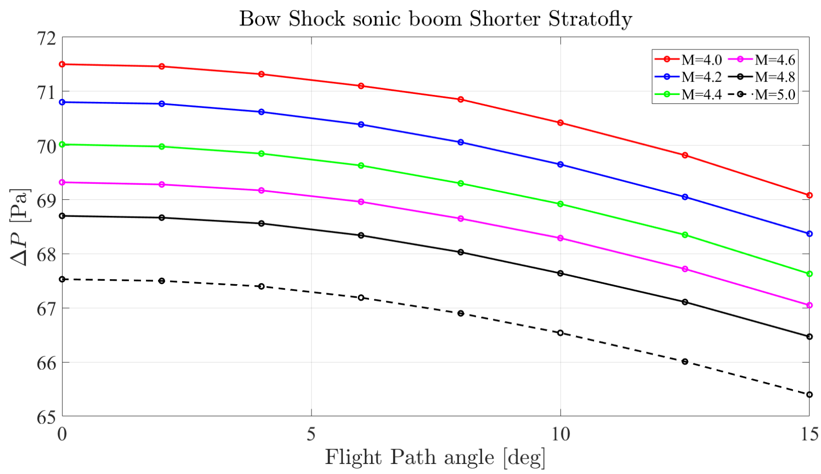

Figure 6.4: Bow Shock Short Stratofly with Mach number and flight path angle variation

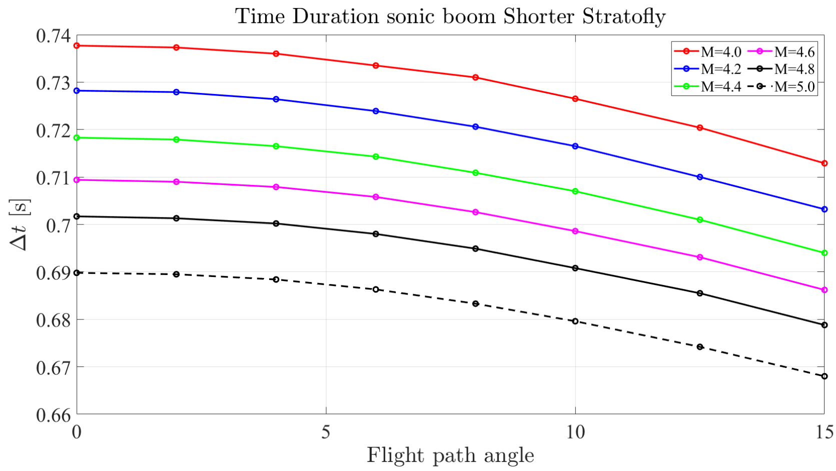

Figure 6.5: Time duration Short Stratofly with Mach number and flight path angle variation

As can be seen from the figure 6.4, the bow shock overpressure changes slightly as the Mach number increase, while it decreases more noticeably as the flight path angle rises. Regarding time signature duration, in accordance with Carlson's theory it decreases as both the Mach number and the flight path angle increase.

6.1.2 Sonic boom analysis with flight path angle and altitude variation

As a second test, the sonic boom analysis was studied in relation to the simultaneous variation of flight altitude and flight path angle.
Concerning flight altitude, the range of variation is between 26000m and 30000m, while the flight path angle range is between 0 and 15 degrees. The following analysis were carried out for a Mach number of 5 and an aircraft length of 66.3 m.

flight path angle[deg]	ray path [deg]	$A_{e,1}$ $[m^2]$	$A_{e_{max}}$ $[m^2]$	Δp $[Pa]$	Δt $[s]$	$A_{e_1}/A_{e_{max}}$
0	0	114.46	220.19	78.98	0.516	0.5198
2	2	114.40	220.02	78.95	0.5159	0.5200
4	4	114.22	219.515	78.82	0.5151	0.5203
6	6	113.97	218.67	78.5	0.5135	0.5212
8	8	113.63	217.49	78.17	0.5108	0.5225
10	10	113.19	215.99	77.77	0.508	0.524
12.5	12.5	112.5	213.66	77.14	0.504	0.5265
15	15	111.7	210.86	76.45	0.4996	0.5297

Table 6.7: Result obtained with an altitude of 26000 m

flight path angle[deg]	ray path [deg]	$A_{e,1}$ $[m^2]$	$A_{e_{max}}$ $[m^2]$	Δp $[Pa]$	Δt $[s]$	$A_{e_1}/A_{e_{max}}$
0	0	121.08	243.04	76.63	0.5611	0.4982
2	2	121.02	242.85	76.60	0.5609	0.4984
4	4	120.85	242.25	76.45	0.56	0.4989
6	6	120.565	241.27	76.16	0.5588	0.4997
8	8	120.16	239.9	75.82	0.552	0.5009
10	10	119.65	238.15	75.43	0.550	0.5024
12.5	12.5	118.85	235.44	74.81	0.5478	0.5048
15	15	117.91	232.19	74.11	0.5426	0.5079

Table 6.8: Result obtained with an altitude of 27000 m

flight path angle[deg]	ray path [deg]	$A_{e,1}$ $[m^2]$	$A_{e_{max}}$ $[m^2]$	Δp $[Pa]$	Δt $[s]$	$A_{e_1}/A_{e_{max}}$
0	0	128.78	269.52	74.12	0.6069	0.4778
2	2	128.73	269.27	74.066	0.6065	0.4781
4	4	128.53	268.585	73.94	0.605	0.4786
6	6	128.2	267.45	73.71	0.6036	0.4793
8	8	127.73	265.85	73.40	0.601	0.4805
10	10	127.19	263.81	72.99	0.5978	0.4819
12.5	12.5	126.23	260.67	72.42	0.593	0.4843
15	15	125.14	256.88	71.77	0.5878	0.4871

Table 6.9: Result obtained with an altitude of 28000 m

flight path angle[deg]	ray path [deg]	$A_{e,1}$ $[m^2]$	$A_{e_{max}}$ $[m^2]$	Δp $[Pa]$	Δt $[s]$	$A_{e_1}/A_{e_{max}}$
0	0	137.72	300.14	71.67	0.6554	0.4589
2	2	137.65	299.86	71.64	0.6551	0.459
4	4	137.44	299.06	71.49	0.6537	0.4596
6	6	137.05	297.73	71.27	0.6517	0.4603
8	8	136.48	245.88	70.96	0.6489	0.4613
10	10	135.8	293.52	70.54	0.6451	0.4627
12.5	12.5	134.72	289.86	69.98	0.64	0.4648
15	15	133.45	285.45	69.34	0.6362	0.4675

Table 6.10: Result obtained with an altitude of 29000 m

flight path angle[deg]	ray path [deg]	$A_{e,1}$ $[m^2]$	$A_{e_{max}}$ $[m^2]$	Δp $[Pa]$	Δt $[s]$	$A_{e_1}/A_{e_{max}}$
0	0	148.05	335.55	69.41	0.7077	0.4412
2	2	147.96	335.24	69.38	0.7074	0.4414
4	4	147.68	334.31	69.22	0.7058	0.4417
6	6	147.24	332.78	68.987	0.7033	0.4425
8	8	146.6	330.63	68.68	0.700	0.4434
10	10	145.81	327.9	68.40	0.697	0.4447
12.5	12.5	144.58	323.62	67.75	0.6907	0.4468
15	15	143.07	318.5	67.10	0.684	0.4492

Table 6.11: Result obtained with an altitude of 30000 m

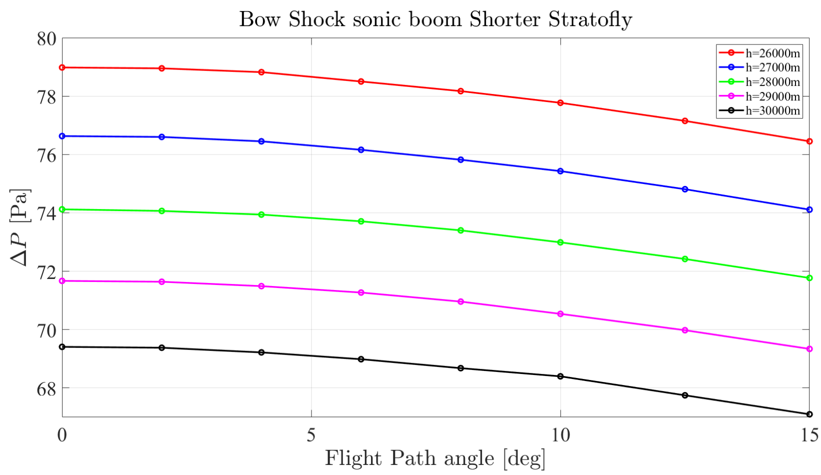

Figure 6.6: Bow Shock overpressure Shorter Stratofly

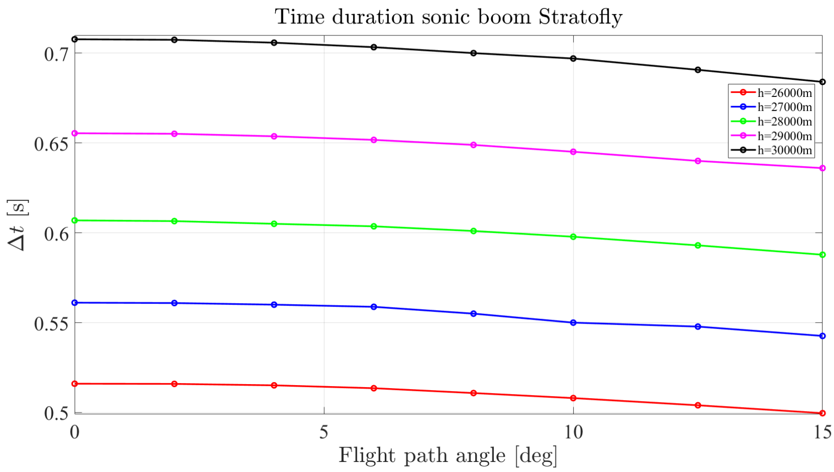

Figure 6.7: Time duration Shorter Stratofly

As can be seen from the figure 6.6, the bow shock overpressure decreases with increasing altitude and flight path angle. Concerning time signature duration, it decreases as the flight path angle grows and increases with flight altitude.

6.1.3 Sonic boom analysis with Mach number and altitude variation

A final sonic boom analysis of bow shock overpressure and time signature duration was performed by varying the Mach number and flight altitude. Mach number was varied between 4.0 and 5.0, while flight altitude was varied between 25500m and 29500m.
These analysis were conducted for an overall aircraft length of 66.3 meters and a flight path angle equal to 0 deg.

Mach number	$A_{e,1}$ $[m^2]$	$A_{e_{max}}$ $[m^2]$	Δp $[Pa]$	Δt $[s]$	$A_{e_1}/A_{e_{max}}$
4.0	124	252.96	82.35	0.5446	0.4902
4.2	121.75	245.27	81.88	0.5392	0.4964
4.4	119.695	238.22	81.43	0.5354	0.5025
4.6	117.8	231.73	80.99	0.5313	0.5084
4.8	116.05	225.74	80.51	0.5271	0.5141
5.0	114.4	220.19	80.10	0.5235	0.5196

Table 6.12: Result obtained with an altitude of 25500m

Mach number	$A_{e,1}$ $[m^2]$	$A_{e_{max}}$ $[m^2]$	Δp $[Pa]$	Δt $[s]$	$A_{e_1}/A_{e_{max}}$
4.0	132.23	281.18	78.98	0.5852	0.4703
4.2	129.62	272.24	78.48	0.5797	0.4761
4.4	127.23	264.03	78.02	0.5748	0.4819
4.6	125.02	256.47	77.57	0.5702	0.4875
4.8	122.97	249.49	77.19	0.5662	0.4929
5.0	121.10	243.04	76.76	0.562	0.4983

Table 6.13: Result obtained with an altitude of 26500m

Mach number	$A_{e,1}$ $[m^2]$	$A_{e_{max}}$ $[m^2]$	Δp $[Pa]$	Δt $[s]$	$A_{e_1}/A_{e_{max}}$
4.0	141.76	313.87	76.01	0.63	0.4516
4.2	138.73	303.47	75.49	0.6236	0.4571
4.4	135.93	293.92	74.96	0.6177	0.4625
4.6	133.38	285.13	74.46	0.612	0.4678
4.8	131.01	277.01	74.10	0.608	0.4729
5.0	128.8	269.5	73.68	0.6034	0.4779

Table 6.14: Result obtained with an altitude of 27500m

Mach number	$A_{e,1}$ $[m^2]$	$A_{e_{max}}$ $[m^2]$	Δp $[Pa]$	Δt $[s]$	$A_{e_1}/A_{e_{max}}$
4.0	152.8	351.7	73.39	0.6791	0.4343
4.2	149.26	339.61	72.86	0.6722	0.4395
4.4	146.04	328.51	72.34	0.6656	0.4446
4.6	143.05	318.29	71.87	0.6598	0.4494
4.8	140.3	308.86	71.37	0.6538	0.4543
5.0	137.75	300.13	70.91	0.6485	0.459

Table 6.15: Result obtained with an altitude of 28500m

Mach number	$A_{e,1}$ $[m^2]$	$A_{e_{max}}$ $[m^2]$	Δp $[Pa]$	Δt $[s]$	$A_{e_1}/A_{e_{max}}$
4.0	165.55	395.46	71.05	0.7331	0.4186
4.2	161.44	381.41	70.51	0.7252	0.4233
4.4	157.68	368.51	69.96	0.7177	0.4279
4.6	154.23	356.64	69.47	0.711	0.4325
4.8	151.03	345.7	68.94	0.704	0.4369
5.0	148.07	335.55	68.51	0.6985	0.4413

Table 6.16: Result obtained with an altitude of 29500m

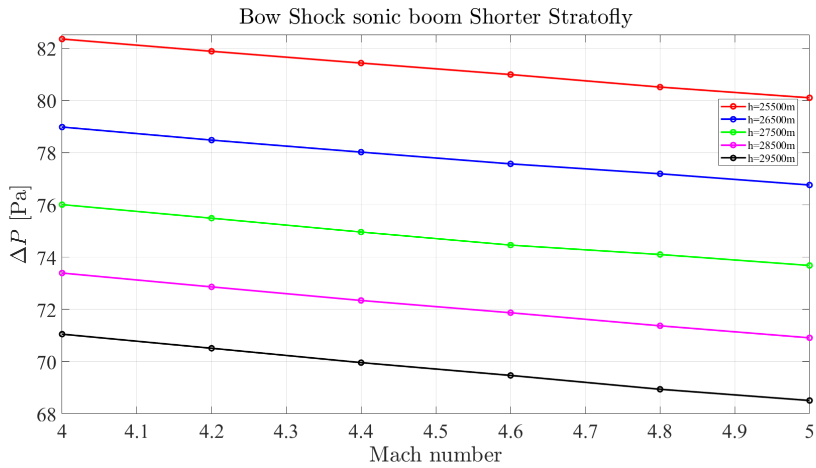

Figure 6.8: Bow Shock overpressure Short Stratofly with Mach number and altitude variation

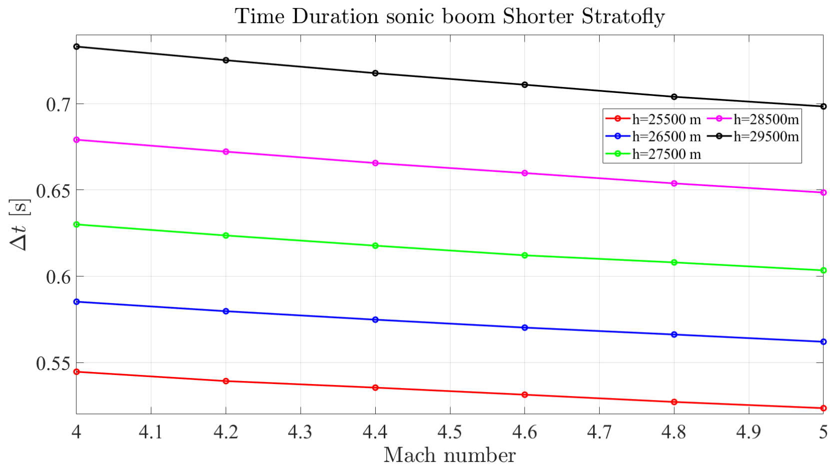

Figure 6.9: Time duration Short Stratofly with Mach number and altitude variation

As can be seen from the figure, as the Mach number increases, there is a slight reduction in bow shock overpressure in opposition to Carlson's theory, while as the altitude grows, the reduction is much more evident.
Concerning time signature duration, it decreases with increasing Mach number, as opposed to what happens with increasing aircraft altitude.

7

GreenHawk3 with forward positioning of wings

7.1 Introduction to the method

Analyzing the results obtained in chapter 5 regarding GreenHawk3 it was decided to study the evaluation of the bow shock overpressure and time signature duration by varying the configuration of the aircraft. As previously mentioned, the conceptual design of the aircraft did not take into account any sonic boom constraints. Consequently, the resulting configuration maximizes performance from the point of view of:

i. Range

ii. Cruise Mach number

iii. Use of a turbojet instead of a turboramjet as a power source

iv. Increased cabin space to enhance cabin comfort

Analyzing the values obtained in chapter 5, it can be seen that the value of total effective area at the half of effective aircraft length is less variable than the maximum effective area.

Figure 7.1: GreenHawk3 Conceptual Design

A first plausible explanation is due to the fact that the positioning of the wings is very backward and consequently the ratio between these two areas tends to be very low taking as reference figure 2.3. The main reason for which in conceptual design it was decided to move the wing so far backwards is mainly due to reasons of excursion of the center of gravity of the aircraft. So analyzing the figure 2.4 a very low value of the ratio will lead to a higher value of shape factor K_S, so a an attempt is made to modify the location of the wings was made to reduce this value. The formulation for Carlson's method for deriving bow shock overpressure and time duration values for a primary sonic boom are again exposed:

$$\Delta p_{max} = K_P \cdot K_R \cdot \sqrt{p_v \cdot p_g} \cdot \left(M^2 - 1\right)^{\frac{1}{8}} \cdot h_e^{-\frac{3}{4}} \cdot l^{\frac{3}{4}} \cdot K_s \tag{7.1}$$

Time signature duration could be determined:

$$\Delta t = K_t \cdot \frac{3.42}{a_v} \cdot \frac{M}{\left(M^2 - 1\right)^{\frac{3}{8}}} \cdot h_e^{\frac{1}{4}} \cdot l^{\frac{3}{4}} \cdot K_s \tag{7.2}$$

As can be seen from these two equations there is a direct correlation between the values of bow shock overpressure and time signature duration with the value of shape factor K_S.
This chapter will assess how the overpressure and time signature when moving the wings forward of 2 meters without considering the possible problems of positioning the centre of gravity.

7.2 Sonic boom analysis

The section on benefits compared to the classical configuration will be discussed in the final conclusions chapter of this thesis.

7.2.1 Sonic boom analysis with aircraft length and altitude variation

The first analysis carried out concerns the study of the bow shock overpressure and the time duration of this new version of the GreenHawk3 concept design by varying the flight altitude and aircraft length.The variations made are the same as those applied in the previous chapter, in particular the length of the aircraft was varied between 87 and 100% of the nominal length. Flight altitudes have been varied between 16000 m and 20000 m such as GreenHawk3.

Aircraft effective Length$[m]$	$A_{e,1}$ $[m^2]$	$A_{e_{max}}$ $[m^2]$	Δp $[Pa]$	Δt $[s]$	$A_{e_1}/A_{e_{max}}$
26.22	4.66	35.405	132.29	0.2899	0.1316
26.83	4.88	36.17	132.73	0.2909	0.1349
27.43	5.1	36.97	133.32	0.2922	0.1379
28.03	5.325	37.747	133.60	0.2928	0.1411
28.64	5.556	38.53	134.06	0.2938	0.1443
29.40	5.855	39.52	134.48	0.2947	0.1482
30.15	6.158	40.47	135.04	0.296	0.1522

Table 7.1: Result obtained with an altitude of 16000m

Aircraft effective Length$[m]$	$A_{e,1}$ $[m^2]$	$A_{e_{max}}$ $[m^2]$	Δp $[Pa]$	Δt $[s]$	$A_{e_1}/A_{e_{max}}$
26.22	4.66	38.55	122.42	0.3083	0.1209
26.83	4.88	39.36	122.907	0.3097	0.1240
27.43	5.1	40.175	123.37	0.3107	0.1269
28.03	5.325	40.99	123.75	0.3117	0.1299
28.64	5.556	41.81	124.11	0.3126	0.1330
29.40	5.855	42.85	124.56	0.3137	0.1366
30.15	6.158	43.84	124.92	0.3146	0.1405

Table 7.2: Result obtained with an altitude of 17000m

Aircraft effective Length$[m]$	$A_{e,1}$ $[m^2]$	$A_{e_{max}}$ $[m^2]$	Δp $[Pa]$	Δt $[s]$	$A_{e_1}/A_{e_{max}}$
26.22	4.66	42.24	113.99	0.3288	0.1103
26.83	4.88	43.08	114.37	0.3299	0.1133
27.43	5.1	43.94	114.67	0.3308	0.1161
28.03	5.325	44.8	115.07	0.3319	0.1189
28.64	5.556	45.87	115.61	0.333	0.1211
29.40	5.855	46.73	115.88	0.3342	0.1253
30.15	6.158	47.767	116.24	0.3353	0.1289

Table 7.3: Result obtained with an altitude of 18000m

Aircraft effective Length$[m]$	$A_{e,1}$ $[m^2]$	$A_{e_{max}}$ $[m^2]$	Δp $[Pa]$	Δt $[s]$	$A_{e_1}/A_{e_{max}}$
26.22	4.66	46.53	106.67	0.3512	0.1002
26.83	4.88	47.43	106.94	0.3521	0.1028
27.43	5.1	48.33	107.26	0.3532	0.1055
28.03	5.325	49.24	107.56	0.3542	0.1081
28.64	5.556	50.14	107.88	0.3552	0.1104
29.40	5.855	51.28	108.23	0.3564	0.1142
30.15	6.158	52.36	108.54	0.3574	0.1176

Table 7.4: Result obtained with an altitude of 19000m

Aircraft effective Length$[m]$	$A_{e,1}$ $[m^2]$	$A_{e_{max}}$ $[m^2]$	Δp $[Pa]$	Δt $[s]$	$A_{e_1}/A_{e_{max}}$
26.22	4.66	51.55	100.29	0.376	0.0904
26.83	4.88	52.52	100.53	0.3769	0.0929
27.43	5.1	53.47	100.78	0.3778	0.0954
28.03	5.325	54.41	101.04	0.3788	0.0978
28.64	5.556	55.4	101.23	0.3799	0.1003
29.40	5.855	56.58	101.57	0.3807	0.1035
30.15	6.158	57.73	101.80	0.3811	0.1067

Table 7.5: Result obtained with an altitude of 20000m

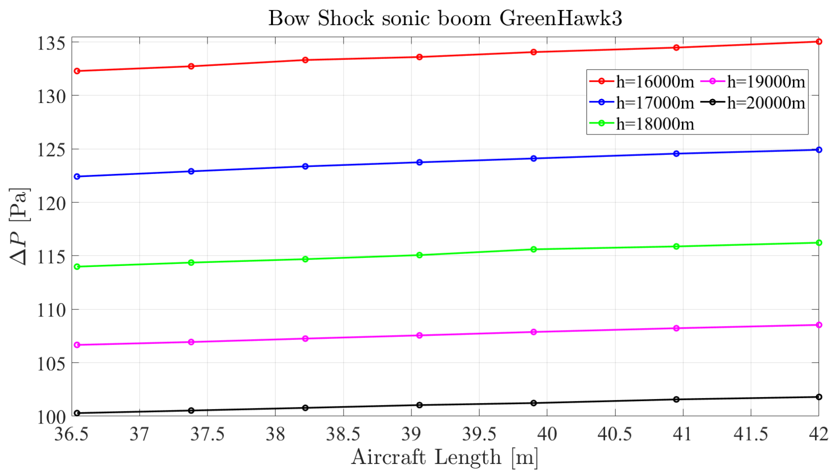

Figure 7.2: Bow Shock overpressure with altitude and aircraft length variation

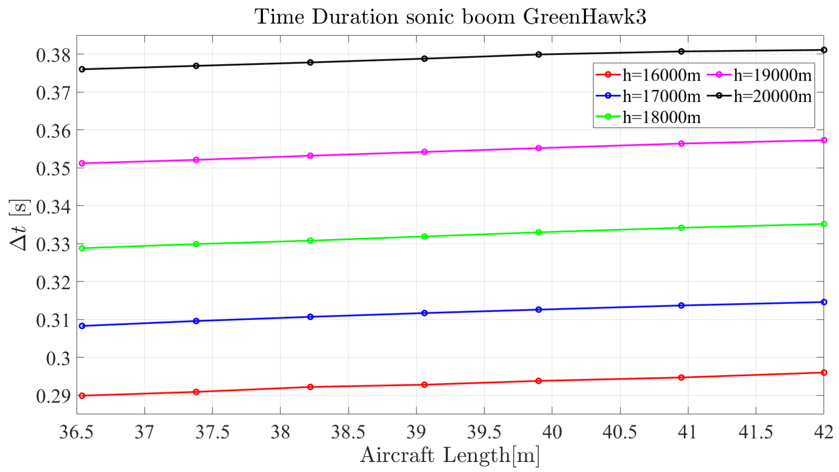

Figure 7.3: Time duration with altitude and aircraft length variation

Regarding bow shock overpressure, as the length of the aircraft increases, it grows more or less in a linear relationship and decreases significantly as the altitude increases. Concerning time signature duration, the value increase at the aircraft flight at higher value of altitude while the same trend is visible in case of increase in aircraft length.

7.2.2 Sonic boom analysis with altitude and flight path angle variation

Another analysis was then carried out by varying the flight altitude and flight path angle. As far as altitude is concerned, the extremes studied are the same as in the previous case (between 16000m and 20000m) while the variation for flight path angle is between 0 and 15 degrees.

Flight path angle	Ray path angle	$A_{e,1}$ $[m^2]$	$A_{e_{max}}$ $[m^2]$	Δp $[Pa]$	Δt $[s]$	$A_{e_1}/A_{e_{max}}$
0	0	6.158	40.47	135.04	0.2960	0.1522
2	2	6.158	40.45	135.00	0.2959	0.1522
4	4	6.158	40.38	134.85	0.2955	0.1525
6	6	6.158	40.26	134.60	0.2950	0.1530
8	8	6.158	40.09	134.26	0.0.2943	0.1536
10	10	6.158	39.88	133.85	0.2933	0.1544
12.5	12.5	6.158	39.55	133.85	0.2919	0.1557
15	15	6.158	39.15	132.44	0.2903	0.1573

Table 7.6: Result obtained with an altitude of 16000m

Flight path angle	Ray path angle	$A_{e,1}$ $[m^2]$	$A_{e_{max}}$ $[m^2]$	Δp $[Pa]$	Δt $[s]$	$A_{e_1}/A_{e_{max}}$
0	0	6.158	43.84	124.92	0.3146	0.1405
2	2	6.158	43.81	124.88	0.3145	0.1406
4	4	6.158	43.725	124.75	0.3142	0.1408
6	6	6.158	43.53	124.54	0.3137	0.1413
8	8	6.158	43.39	124.20	0.3128	0.1419
10	10	6.158	43.14	123.80	0.3118	0.1427
12.5	12.5	6.158	42.75	123.17	0.3102	0.1440
15	15	6.158	42.29	122.40	0.3083	0.1456

Table 7.7: Result obtained with an altitude of 17000m

Flight path angle	Ray path angle	$A_{e,1}$ $[m^2]$	$A_{e_{max}}$ $[m^2]$	Δp $[Pa]$	Δt $[s]$	$A_{e_1}/A_{e_{max}}$
0	0	6.158	47.767	116.23	0.3353	0.1289
2	2	6.158	47.735	116.20	0.335	0.1290
4	4	6.158	47.634	116.06	0.3347	0.1293
6	6	6.158	47.47	115.84	0.3341	0.1297
8	8	6.158	47.24	115.52	0.3332	0.1304
10	10	6.158	46.95	115.11	0.332	0.1312
12.5	12.5	6.158	46.50	114.50	0.3302	0.1324
15	15	6.158	45.95	113.70	0.3279	0.1340

Table 7.8: Result obtained with an altitude of 18000m

Flight path angle	Ray path angle	$A_{e,1}$ $[m^2]$	$A_{e_{max}}$ $[m^2]$	Δp $[Pa]$	Δt $[s]$	$A_{e_1}/A_{e_{max}}$
0	0	6.158	52.362	108.54	0.3574	0.1176
2	2	6.158	52.323	108.51	0.3573	0.1177
4	4	6.158	52.21	108.37	0.3568	0.1179
6	6	6.158	52.016	108.14	0.3561	0.1184
8	8	6.158	51.75	107.82	0.355	0.119
10	10	6.158	51.41	107.41	0.3537	0.1198
12.5	12.5	6.158	50.88	106.80	0.3517	0.1210
15	15	6.158	50.24	106.08	0.3493	0.1226

Table 7.9: Result obtained with an altitude of 19000m

Flight path angle	Ray path angle	$A_{e,1}$ $[m^2]$	$A_{e_{max}}$ $[m^2]$	Δp $[Pa]$	Δt $[s]$	$A_{e_1}/A_{e_{max}}$
0	0	6.158	57.736	101.80	0.3811	0.1067
2	2	6.158	57.69	101.76	0.3810	0.1068
4	4	6.158	57.55	101.63	0.381	0.107
6	6	6.158	57.33	101.44	0.3802	0.1074
8	8	6.158	57.02	101.12	0.3791	0.108
10	10	6.158	56.62	100.73	0.3776	0.1088
12.5	12.5	6.158	56.00	100.14	0.3754	0.11
15	15	6.158	55.25	99.44	0.3727	0.1115

Table 7.10: Result obtained with an altitude of 20000m

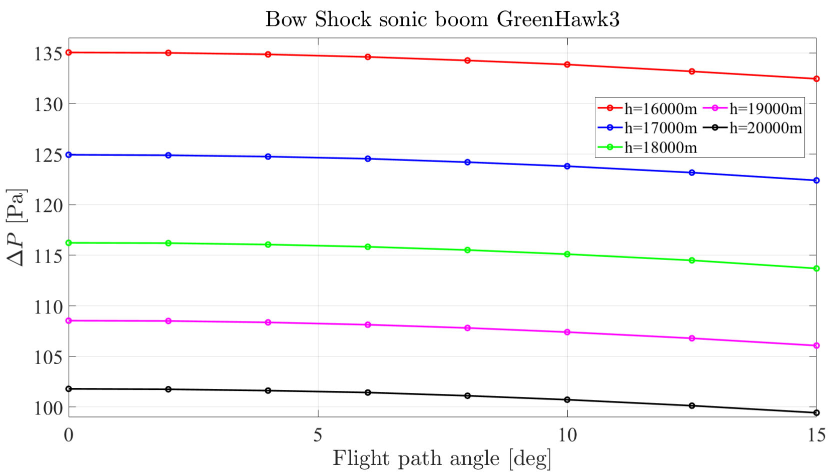

Figure 7.4: Bow Shock overpressure with altitude and flight path angle variation

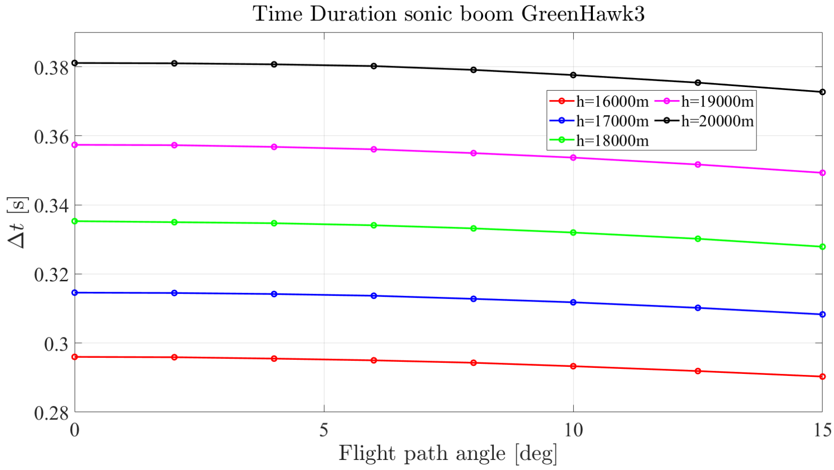

Figure 7.5: Time duration with altitude and flight path angle variation

As far as bow shock overpressure is concerned, a similar trend is observed for all flight altitudes, with a decrease as altitude and flight path angle increases. In particular, the decrease rate increases as the flight path angle increases and this could be an inaccuracy of the method, which is accurate for moderate descents and climbs.
Regarding time duration an increase in flight altitude increase the time signature duration, while there is an opposite trend for the growth of flight path angle.

7.2.3 Sonic Boom analysis with Mach number and altitude variation

An analysis was then carried out by varying the Mach number and flight altitude. As for the Mach number the variation is, as in the previous cases, in the range between 2.4 and 3.0 while the altitude range is between 16000m and 20000m. The nominal length of the aircraft was taken into account and with a flight path angle of 0 deg.

Mach number	$A_{e,1}$ $[m^2]$	$A_{e_{max}}$ $[m^2]$	Δp $[Pa]$	Δt $[s]$	$A_{e_1}/A_{e_{max}}$
2.4	6.158	44.54	133.71	0.3039	0.1383
2.5	6.158	43.77	124.02	0.3021	0.1407
2.6	6.158	43.04	134.26	0.3005	0.1431
2.7	6.158	42.35	134.51	0.2992	0.1454
2.8	6.158	41.69	134.72	0.2980	0.1477
2.9	6.158	41.07	134.92	0.297	0.1499
3.0	6.158	40.47	135.04	0.2960	0.1522

Table 7.11: Result obtained with an altitude of 16000m

Mach number	$A_{e,1}$ $[m^2]$	$A_{e_{max}}$ $[m^2]$	Δp $[Pa]$	Δt $[s]$	$A_{e_1}/A_{e_{max}}$
2.4	6.158	48.59	124.13	0.3242	0.1267
2.5	6.158	47.69	124.37	0.3222	0.1291
2.6	6.158	46.83	124.55	0.3204	0.1315
2.7	6.158	46.03	124.64	0.3186	0.1338
2.8	6.158	45.26	124.75	0.3171	0.1361
2.9	6.158	44.53	124.83	0.3158	0.1383
3.0	6.158	43.84	124.92	0.3146	0.1405

Table 7.12: Result obtained with an altitude of 17000m

Mach number	$A_{e,1}$ $[m^2]$	$A_{e_{max}}$ $[m^2]$	Δp $[Pa]$	Δt $[s]$	$A_{e_1}/A_{e_{max}}$
2.4	6.158	53.32	115.65	0.346	0.1155
2.5	6.158	52.28	115.80	0.3436	0.1178
2.6	6.158	51.278	115.91	0.3415	0.1201
2.7	6.158	50.33	116.02	0.3397	0.1224
2.8	6.158	49.43	116.08	0.338	0.1246
2.9	6.158	48.57	116.18	0.3363	0.1268
3.0	6.158	47.767	116.23	0.3353	0.1289

Table 7.13: Result obtained with an altitude of 18000m

Mach number	$A_{e,1}$ $[m^2]$	$A_{e_{max}}$ $[m^2]$	Δp $[Pa]$	Δt $[s]$	$A_{e_1}/A_{e_{max}}$
2.4	6.158	58.87	108.16	0.3698	0.1046
2.5	6.158	57.63	108.21	0.3667	0.1079
2.6	6.158	56.42	108.36	0.3643	0.1091
2.7	6.158	55.37	108.44	0.3625	0.1113
2.8	6.158	54.31	108.51	0.3607	0.1134
2.9	6.158	53.31	108.53	0.3590	0.1155
3.0	6.158	52.36	108.54	0.3574	0.1176

Table 7.14: Result obtained with an altitude of 19000m

Mach number	$A_{e,1}$ $[m^2]$	$A_{e_{max}}$ $[m^2]$	Δp $[Pa]$	Δt $[s]$	$A_{e_1}/A_{e_{max}}$
2.4	6.158	65.34	102.20	0.397	0.0942
2.5	6.158	63.9	102.12	0.3937	0.0964
2.6	6.158	62.54	102.07	0.3908	0.0985
2.7	6.158	61.25	102.02	0.3882	0.1005
2.8	6.158	60.01	101.94	0.3857	0.1026
2.9	6.158	58.84	101.89	0.3836	0.1047
3.0	6.158	57.74	101.80	0.3811	0.1067

Table 7.15: Result obtained with an altitude of 20000m

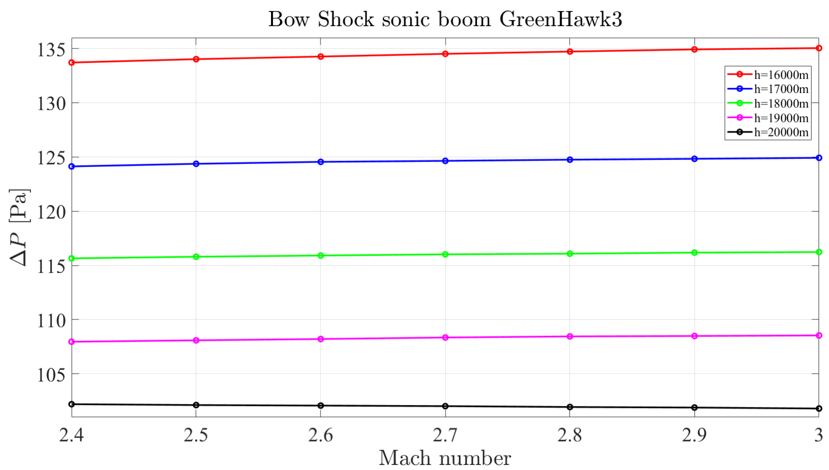

Figure 7.6: Bow Shock overpressure with altitude and Mach number variation

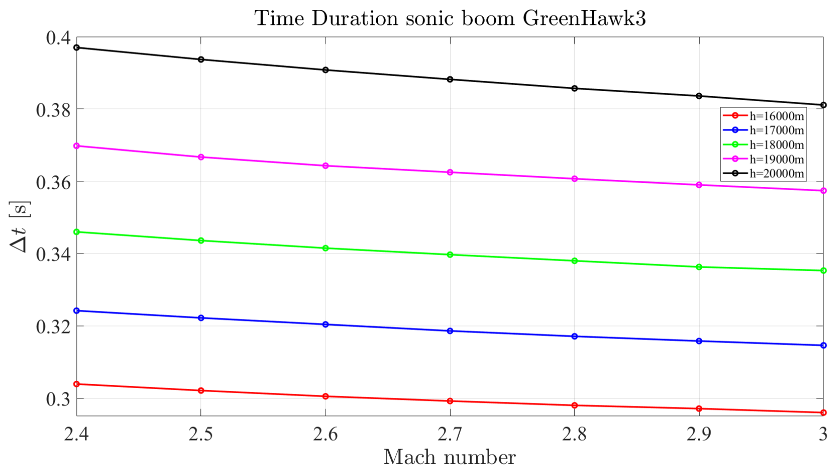

Figure 7.7: Time duration with altitude and Mach number variation

The observed behaviour in figure 7.6 is discordant, in fact for altitudes lower than 19000 m the bow shock overpressure increases according to Carlson's formulation even if with a decreasing rate. On the other hand, at an altitude of 20000 m there is a very slight decrease as the Mach number increases and this could be caused by the decreasing ratio of $A_{e,1}/A_{e,max}$. It should be noted that between the altitudes of 16000 and 19000m the growth rate was not constant but decreased as the altitude increased. Regarding the time duration, there is a coherent trend for all altitudes with a decrease as the Mach number increase.

7.2.4 Sonic boom variation with Mach and aircraft length variation

A sonic boom analysis was carried out by varying the aircraft length and Mach number.The Mach number has been varied between 2.4 and 3.0, while the length of the aircraft has been varied between 36.5 and 42 metres while flight conditions were studied at an altitude of 20000 metres and a flight path angle of 0 degree.

Aircraft effective Length$[m]$	$A_{e,1}$ $[m^2]$	$A_{e_{max}}$ $[m^2]$	Δp $[Pa]$	Δt $[s]$	$A_{e_1}/A_{e_{max}}$
26.22	4.66	58.67	100.75	0.3917	0.0794
26.83	4.88	59.7	100.96	0.3925	0.0817
27.43	5.1	60.75	101.19	0.3934	0.084
28.03	5.325	61.77	101.41	0.3942	0.0862
28.64	5.556	62.8	101.60	0.395	0.0885
29.40	5.855	64.095	101.85	0.396	0.0914
30.15	6.158	65.35	102.13	0.3968	0.0942

Table 7.16: Result obtained with a Mach number equal to 2.4

Aircraft effective Length$[m]$	$A_{e,1}$ $[m^2]$	$A_{e_{max}}$ $[m^2]$	Δp $[Pa]$	Δt $[s]$	$A_{e_1}/A_{e_{max}}$
26.22	4.66	57.33	100.73	0.3884	0.0813
26.83	4.88	58.35	100.947	0.3893	0.0876
27.43	5.1	59.37	101.17	0.3901	0.0859
28.03	5.325	60.39	101.38	0.3909	0.0882
28.64	5.556	61.40	101.58	0.3917	0.0905
29.40	5.855	62.68	101.84	0.3927	0.0934
30.15	6.158	63.95	102.11	0.3938	0.0963

Table 7.17: Result obtained with a Mach number equal to 2.5

Aircraft effective Length$[m]$	$A_{e,1}$ $[m^2]$	$A_{e_{max}}$ $[m^2]$	Δp $[Pa]$	Δt $[s]$	$A_{e_1}/A_{e_{max}}$
26.22	4.66	56.06	100.64	0.3855	0.0831
26.83	4.88	57.06	100.91	0.3863	0.0855
27.43	5.1	58.07	101.14	0.3872	0.0878
28.03	5.325	59.07	101.35	0.3880	0.0901
28.64	5.556	60.08	101.57	0.3889	0.0925
29.40	5.855	61.33	101.82	0.3898	0.0954
30.15	6.158	62.54	102.04	0.3907	0.0985

Table 7.18: Result obtained with a Mach number equal to 2.6

Aircraft effective Length$[m]$	$A_{e,1}$ $[m^2]$	$A_{e_{max}}$ $[m^2]$	Δp $[Pa]$	Δt $[s]$	$A_{e_1}/A_{e_{max}}$
26.22	4.66	54.85	100.62	0.3828	0.0850
26.83	4.88	55.83	100.82	0.3836	0.0874
27.43	5.1	56.83	101.07	0.3845	0.0897
28.03	5.325	57.82	101.29	0.3854	0.0921
28.64	5.556	58.82	101.51	0.3862	0.0945
29.40	5.855	60.05	101.79	0.3873	0.0975
30.15	6.158	61.24	102.01	0.3882	0.1006

Table 7.19: Result obtained with a Mach number equal to 2.7

Aircraft effective Length$[m]$	$A_{e,1}$ $[m^2]$	$A_{e_{max}}$ $[m^2]$	Δp $[Pa]$	Δt $[s]$	$A_{e_1}/A_{e_{max}}$
26.22	4.66	53.695	100.51	0.3803	0.0868
26.83	4.88	54.67	100.75	0.3812	0.0893
27.43	5.1	55.65	101.01	0.3822	0.0893
28.03	5.325	56.63	101.23	0.383	0.094
28.64	5.556	57.62	101.47	0.384	0.0964
29.40	5.855	58.83	101.74	0.3849	0.0995
30.15	6.158	60.01	101.97	0.3858	0.1026

Table 7.20: Result obtained with a Mach number equal to 2.8

Aircraft effective Length$[m]$	$A_{e,1}$ $[m^2]$	$A_{e_{max}}$ $[m^2]$	Δp $[Pa]$	Δt $[s]$	$A_{e_1}/A_{e_{max}}$
26.22	4.66	52.59	100.42	0.3783	0.0866
26.83	4.88	53.56	100.66	0.379	0.0911
27.43	5.1	54.55	100.91	0.3799	0.0935
28.03	5.325	55.5	101.19	0.381	0.0958
28.64	5.556	56.47	101.38	0.3817	0.0984
29.40	5.855	57.68	101.65	0.3827	0.1015
30.15	6.158	58.84	101.90	0.3837	0.1047

Table 7.21: Result obtained with a Mach number equal to 2.9

Aircraft effective Length$[m]$	$A_{e,1}$ $[m^2]$	$A_{e_{max}}$ $[m^2]$	Δp $[Pa]$	Δt $[s]$	$A_{e_1}/A_{e_{max}}$
26.22	4.66	51.55	100.29	0.376	0.0904
26.83	4.88	52.52	100.53	0.3769	0.0929
27.43	5.1	53.47	100.78	0.3778	0.0954
28.03	5.325	54.4	101.04	0.3788	0.0978
28.64	5.556	55.4	101.23	0.3794	0.1003
29.40	5.855	56.58	101.57	0.3807	0.1035
30.15	6.158	57.736	101.80	0.3811	0.1067

Table 7.22: Result obtained with a Mach number equal to 3.0

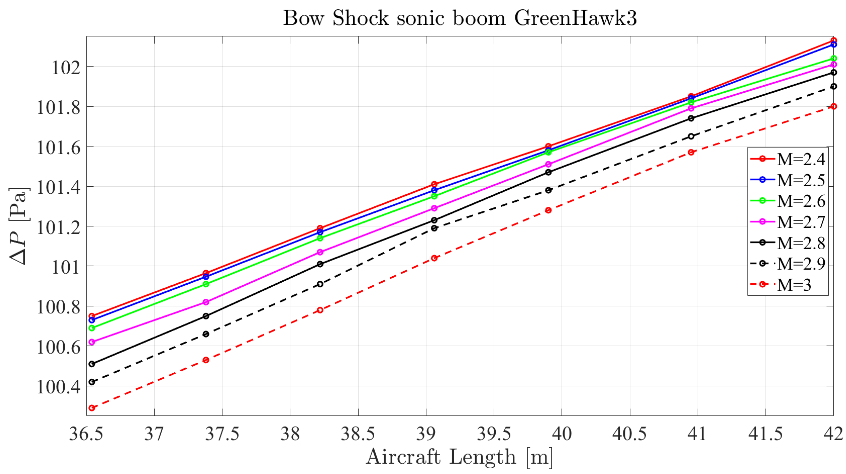

Figure 7.8: Bow Shock overpressure with Mach number and aircraft length variation

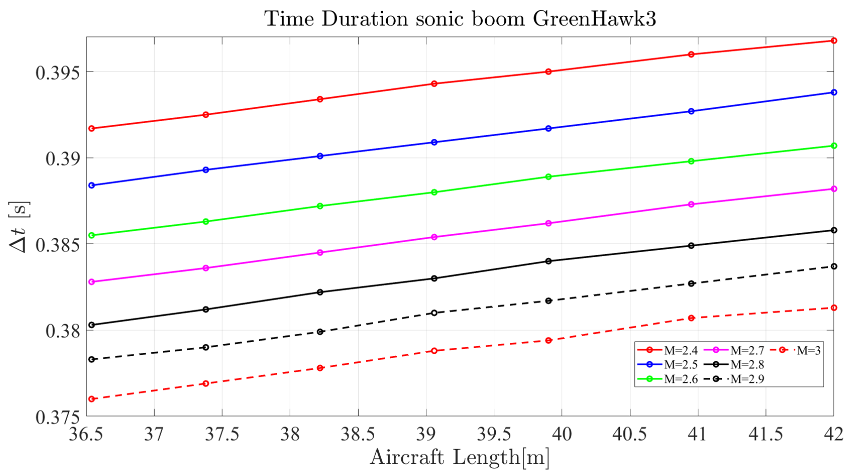

Figure 7.9: Bow Shock overpressure with Mach number and aircraft length variation

As far as bow shock overpressure is concerned, as the Mach number increases, this value slightly decrease(less than 2 percentage points), while it rises slightly as the length of the aircraft increases.
The time duration clearly decreases as the Mach number increases according to Carlson's method.

7.2.5 Sonic boom analysis with Mach number and flight path angle variation

A sonic boom analysis was also carried out by varying the Mach number and flight path angle. As in the previous situation, the flight path angle was varied between 0 and 15 deg, while the Mach number was varied between 2.4 and 3.0.
These analysis were conducted at 20000 metres with the nominal length of the aircraft being 42 metres.

Flight path angle	Ray path angle	$A_{e,1}$ $[m^2]$	$A_{e_{max}}$ $[m^2]$	Δp $[Pa]$	Δt $[s]$	$A_{e_1}/A_{e_{max}}$
0	0	6.158	65.35	102.13	0.3968	0.0942
2	2	6.158	65.28	102.01	0.3966	0.0943
4	4	6.158	65.12	101.88	0.3961	0.0946
6	6	6.158	64.85	101.63	0.3951	0.095
8	8	6.158	64.47	101.32	0.3939	0.0955
10	10	6.158	63.99	100.90	0.3923	0.0962
12.5	12.5	6.158	63.25	100.26	0.3898	0.0974
15	15	6.158	62.35	99.50	0.3868	0.0988

Table 7.23: Result obtained with a Mach number equal to 2.4

Flight path angle	Ray path angle	$A_{e,1}$ $[m^2]$	$A_{e_{max}}$ $[m^2]$	Δp $[Pa]$	Δt $[s]$	$A_{e_1}/A_{e_{max}}$
0	0	6.158	63.95	102.11	0.3938	0.0963
2	2	6.158	63.85	102.03	0.3934	0.0964
4	4	6.158	63.695	101.89	0.3929	0.0967
6	6	6.158	63.45	101.70	0.3922	0.097
8	8	6.158	63.07	101.34	0.3908	0.0976
10	10	6.158	62.6	100.92	0.3892	0.0984
12.5	12.5	6.158	61.88	100.29	0.3867	0.0995
15	15	6.158	61.01	99.54	0.3838	0.1009

Table 7.24: Result obtained with a Mach number equal to 2.5

Flight path angle	Ray path angle	$A_{e,1}$ $[m^2]$	$A_{e_{max}}$ $[m^2]$	Δp $[Pa]$	Δt $[s]$	$A_{e_1}/A_{e_{max}}$
0	0	6.158	62.54	102.04	0.3907	0.0985
2	2	6.158	62.49	101.99	0.3905	0.0985
4	4	6.158	62.34	101.85	0.3900	0.0988
6	6	6.158	62.08	101.63	0.3891	0.0992
8	8	6.158	61.73	101.33	0.3879	0.0998
10	10	6.158	61.28	100.94	0.3864	0.1005
12.5	12.5	6.158	60.58	100.77	0.3839	0.1017
15	15	6.158	59.74	99.52	0.3811	0.1031

Table 7.25: Result obtained with a Mach number equal to 2.6

Flight path angle	Ray path angle	$A_{e,1}$ $[m^2]$	$A_{e_{max}}$ $[m^2]$	Δp $[Pa]$	Δt $[s]$	$A_{e_1}/A_{e_{max}}$
0	0	6.158	61.24	102.01	0.3882	0.1006
2	2	6.158	61.19	101.97	0.3880	0.1006
4	4	6.158	61.05	101.84	0.3875	0.1009
6	6	6.158	60.80	101.61	0.3866	0.1013
8	8	6.158	60.46	101.30	0.3854	0.1019
10	10	6.158	60.02	100.90	0.384	0.1026
12.5	12.5	6.158	59.34	100.27	0.3815	0.1038
15	15	6.158	58.53	99.47	0.378	0.1052

Table 7.26: Result obtained with a Mach number equal to 2.7

Flight path angle	Ray path angle	$A_{e,1}$ $[m^2]$	$A_{e_{max}}$ $[m^2]$	Δp $[Pa]$	Δt $[s]$	$A_{e_1}/A_{e_{max}}$
0	0	6.158	60.01	101.97	0.3858	0.1026
2	2	6.158	59.97	101.92	0.3856	0.1027
4	4	6.158	59.82	101.78	0.3851	0.1029
6	6	6.158	59.58	101.55	0.3842	0.1034
8	8	6.158	59.25	101.24	0.3831	0.1039
10	10	6.158	58.83	100.84	0.3816	0.1047
12.5	12.5	6.158	58.17	100.22	0.3792	0.1059
15	15	6.158	57.38	99.46	0.3765	0.1073

Table 7.27: Result obtained with a Mach number equal to 2.8

Flight path angle	Ray path angle	$A_{e,1}$ $[m^2]$	$A_{e_{max}}$ $[m^2]$	Δp $[Pa]$	Δt $[s]$	$A_{e_1}/A_{e_{max}}$
0	0	6.158	58.84	101.90	0.3837	0.1047
2	2	6.158	58.8	101.85	0.3835	0.1047
4	4	6.158	58.65	101.71	0.3830	0.1050
6	6	6.158	58.43	101.50	0.3821	0.1054
8	8	6.158	58.10	101.17	0.3809	0.1060
10	10	6.158	57.69	100.78	0.3795	0.1067
12.5	12.5	6.158	57.06	100.17	0.3771	0.1079
15	15	6.158	56.29	99.42	0.3744	0.1094

Table 7.28: Result obtained with a Mach number equal to 2.9

Flight path angle	Ray path angle	$A_{e,1}$ $[m^2]$	$A_{e_{max}}$ $[m^2]$	Δp $[Pa]$	Δt $[s]$	$A_{e_1}/A_{e_{max}}$
0	0	6.158	57.73	101.80	0.3815	0.1067
2	2	6.158	57.69	101.76	0.3811	0.1067
4	4	6.158	57.55	101.63	0.381	0.107
6	6	6.158	57.33	101.41	0.3801	0.1074
8	8	6.158	57.02	101.10	0.379	0.108
10	10	6.158	56.62	100.72	0.3776	0.1088
12.5	12.5	6.158	56.01	100.11	0.3753	0.11
15	15	6.158	55.26	99.37	0.3725	0.1114

Table 7.29: Result obtained with a Mach number equal to 3.0

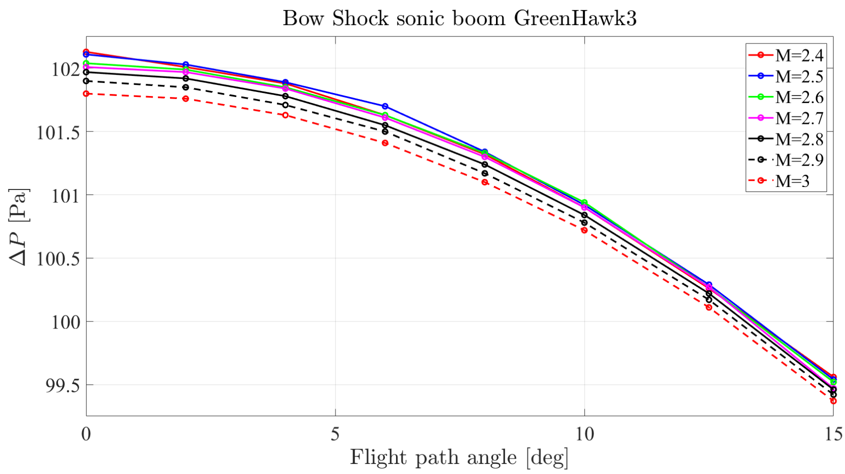

Figure 7.10: Bow Shock overpressure with Mach and flight path variation

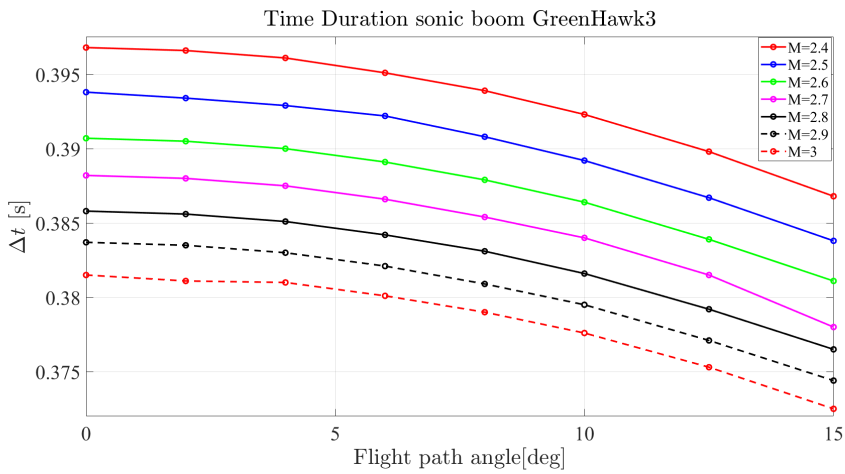

Figure 7.11: Time duration with Mach and flight path angle variation

Concerning bow shock overpressure, as the Mach number increases it slightly decreases, while as the flight path angle increases there is a clear decrease.
Regarding the time duration, as the flight path angle and Mach number increase, there is a clear decrease.
The comparison with the nominal aircraft, as already mentioned, will be presented in the final chapter on conclusions.

8

Sonic boom evaluation with Canard

8.1 General description

The GreenHawk3 aircraft was taken and the influence of a canard was studied in terms of sonic boom analysis. The value of bow shock overpressure and time duration were calculated in order to assess whether the presence of a canard leads to advantages for both. The following test were made:

i. Simultaneous change in altitude and Mach number

ii. Simultaneous change in altitude and aircraft length

iii. Simultaneous change in Mach number and aircraft length

iv. Simultaneous change of altitude and flight path angle

v. Simultaneous variation of Mach number and flight path angle

The values obtained with the presence of the canard and those obtained with the nominal version will then be compared in order to have an evaluation of the possible advantages of this configuration.
It was decided to use the size of the EFA2000 canard as this is one of the examples of a supersonic canard.

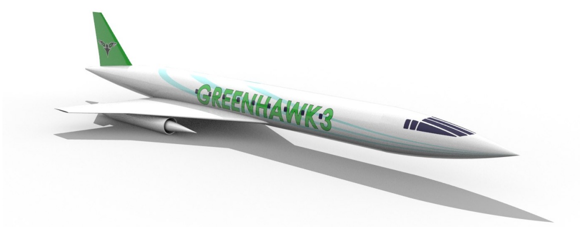

Figure 8.1: Aircraft in which the canard will be studied

8.2 Sonic boom analysis

8.2.1 Sonic boom analysis by varying Mach number and altitude

The first analysis that was carried out related to the evaluation of the sonic boom by simultaneously varying the Mach number and the flight altitude.The flight altitude has been varied between 16000m and 20000m and the Mach number has been varied between 2.4 and 3.0. These values, like those studied in the chapter on the conceptual design of the GreenHawk3 are derived from the values found in the mission profile carried out with the ASTOS software.The results obtained are presented first in numerical form as tables and then by a graphical representation.

Mach number	$A_{e,1}$ $[m^2]$	$A_{e_{max}}$ $[m^2]$	Δp $[Pa]$	Δt $[s]$	$A_{e_1}/A_{e_{max}}$
2.4	7.467	47.97	135.25	0.3074	0.1557
2.5	7.43	47.10	135.52	0.3055	0.1577
2.6	7.38	46.25	135.74	0.3038	0.1596
2.7	7.34	45.47	135.97	0.3024	0.1614
2.8	7.31	44.71	136.11	0.3011	0.1635
2.9	7.28	44.01	136.21	0.3002	0.1655
3.0	7.25	43.32	136.42	0.2990	0.1672

Table 8.1: Result obtained at 16000 m of altitude

Mach number	$A_{e,1}$ $[m^2]$	$A_{e_{max}}$ $[m^2]$	Δp $[Pa]$	Δt $[s]$	$A_{e_1}/A_{e_{max}}$
2.4	7.69	52.6	125.52	0.3279	0.1461
2.5	7.64	51.58	125.65	0.3256	0.1516
2.6	7.59	50.06	125.77	0.3240	0.1520
2.7	7.55	49.67	125.90	0.3225	0.1538
2.8	7.506	48.79	126.03	0.321	0.1557
2.9	7.466	47.96	126.17	0.3194	0.1564
3.0	7.43	47.17	126.29	0.3181	0.1575

Table 8.2: Result obtained at 17000 m of altitude

Mach number	$A_{e,1}$ $[m^2]$	$A_{e_{max}}$ $[m^2]$	Δp $[Pa]$	Δt $[s]$	$A_{e_1}/A_{e_{max}}$
2.4	8	58	117.08	0.3511	0.1379
2.5	7.93	56.82	117.24	0.3486	0.1396
2.6	7.86	55.68	117.36	0.3464	0.1412
2.7	7.8	54.59	117.42	0.3443	0.1429
2.8	7.735	53.56	117.48	0.3423	0.1444
2.9	7.688	52.58	117.59	0.3404	0.1462
3.0	7.63	56.66	117.62	0.339	0.1477

Table 8.3: Result obtained at 18000 m of altitude

Mach number	$A_{e,1}$ $[m^2]$	$A_{e_{max}}$ $[m^2]$	Δp $[Pa]$	Δt $[s]$	$A_{e_1}/A_{e_{max}}$
2.4	8.25	64.35	110.44	0.3768	0.1282
2.5	8.20	62.96	110.38	0.3736	0.1303
2.6	8.13	61.61	110.34	0.3711	0.1320
2.7	8.06	60.35	110.33	0.3687	0.1335
2.8	8	59.14	110.26	0.3665	0.1353
2.9	7.95	58	110.15	0.3643	0.1374
3.0	7.9	56.93	110.12	0.3626	0.1388

Table 8.4: Result obtained at 19000 m of altitude

Mach number	$A_{e,1}$ $[m^2]$	$A_{e_{max}}$ $[m^2]$	Δp $[Pa]$	Δt $[s]$	$A_{e_1}/A_{e_{max}}$
2.4	8.61	71.77	104.20	0.4051	0.12
2.5	8.53	70.12	104.16	0.4017	0.1216
2.6	8.45	68.56	104.09	0.3985	0.1232
2.7	8.38	67.08	104.00	0.3957	0.1249
2.8	8.316	65.67	103.89	0.3931	0.1266
2.9	8.25	64.33	103.79	0.3908	0.1282
3.0	8.18	63.06	103.72	0.3888	0.1297

Table 8.5: Result obtained at 20000 m of altitude

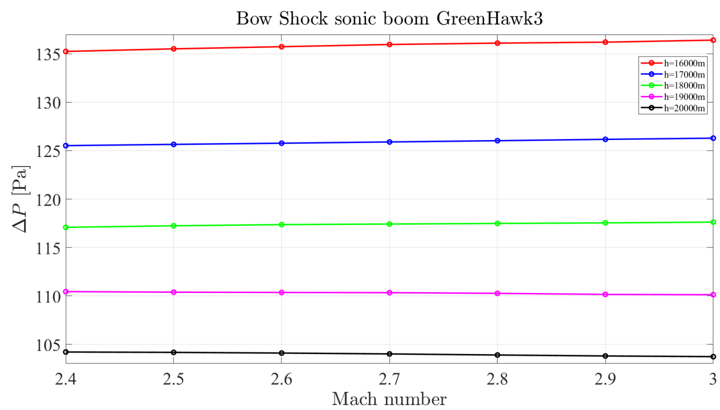

Figure 8.2: Bow Shock overpressure with Mach number and altitude variation

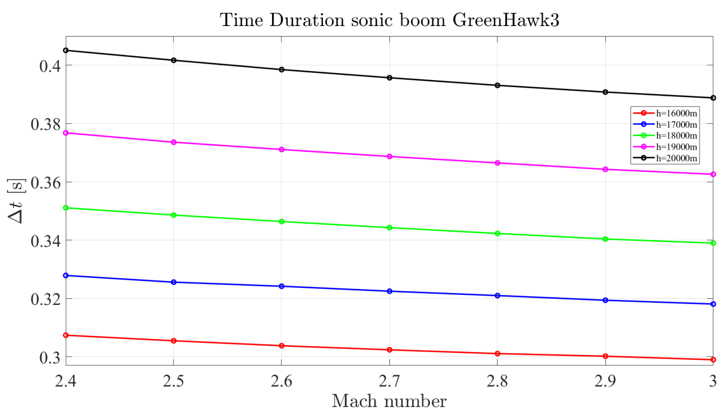

Figure 8.3: Time duration with Mach number and altitude variation

As can be seen from the figure 8.2 the bow shock overpressure increases for low altitudes as the Mach number increases, while for altitudes of 19000 and 20000 m the values are slightly decreasing. The same trend was visible for others configuration of GreenHawk3.
Concerning time signature duration it decreases with increasing Mach number, and the opposite with increasing altitude.

8.2.2 Sonic boom analysis by varying flight path angle and altitude

Another analysis was then carried out by varying the flight altitude and flight path angle. As in the previous case, the same lower and upper extremes were kept in order to make a comparison with the previously studied aircraft.
Consequently, the flight altitude will vary between 16000 m and 20000 m while the flight path angle will vary between 0 and 15 deg, the Mach number was equal to 3.0 with the nominal length of the aircraft.

Flight path angle [deg]	$A_{e,1}$ $[m^2]$	$A_{e_{max}}$ $[m^2]$	Δp $[Pa]$	Δt $[s]$	$A_{e_1}/A_{e_{max}}$
0	7.25	43.32	136.42	0.299	0.1672
2	7.24	43.28	136.26	0.2986	0.1675
4	7.24	43.21	136.15	0.2984	0.1676
6	7.23	43.07	135.93	0.2979	0.1678
8	7.22	42.88	135.57	0.2971	0.1684
10	7.21	42.64	135.14	0.2962	0.1691
12.5	7.195	42.26	134.46	0.2947	0.1703
15	7.17	41.806	133.66	0.2929	0.1715

Table 8.6: Result obtained at 16000 m of altitude

Flight path angle [deg]	$A_{e,1}$ $[m^2]$	$A_{e_{max}}$ $[m^2]$	Δp $[Pa]$	Δt $[s]$	$A_{e_1}/A_{e_{max}}$
0	7.43	47.17	126.29	0.3181	0.1575
2	7.425	47.133	126.25	0.3180	0.1575
4	7.42	47.04	126.11	0.3176	0.1577
6	7.415	46.88	125.86	0.317	0.1582
8	7.4	46.65	125.52	0.3161	0.1586
10	7.39	46.37	125.08	0.315	0.1593
12.5	7.37	45.93	124.44	0.3134	0.1605
15	7.343	45.39	123.64	0.3114	0.1618

Table 8.7: Result obtained at 17000 m of altitude

Flight path angle [deg]	$A_{e,1}$ $[m^2]$	$A_{e_{max}}$ $[m^2]$	Δp $[Pa]$	Δt $[s]$	$A_{e_1}/A_{e_{max}}$
0	7.63	51.66	117.62	0.3394	0.1477
2	7.63	51.63	117.59	0.3392	0.1478
4	7.63	51.51	117.44	0.3387	0.1481
6	7.627	51.32	117.19	0.338	0.1486
8	7.615	51.07	116.87	0.3371	0.1491
10	7.6	50.73	116.43	0.3358	0.1498
12.5	7.58	50.21	115.77	0.3339	0.151
15	7.55	49.59	115.01	0.3317	0.1522

Table 8.8: Result obtained at 18000 m of altitude

Flight path angle [deg]	$A_{e,1}$ $[m^2]$	$A_{e_{max}}$ $[m^2]$	Δp $[Pa]$	Δt $[s]$	$A_{e_1}/A_{e_{max}}$
0	7.9	56.93	110.12	0.3626	0.1388
2	7.895	56.87	110.05	0.3624	0.1388
4	7.887	56.74	109.91	0.3619	0.1390
6	7.88	56.52	109.66	0.3611	0.1394
8	7.86	56.21	109.34	0.3600	0.1398
10	7.84	55.83	108.93	0.3587	0.1404
12.5	7.815	55.22	108.30	0.3566	0.1415
15	7.78	54.49	107.54	0.354	0.1427

Table 8.9: Result obtained at 19000 m of altitude

Flight path angle [deg]	$A_{e,1}$ $[m^2]$	$A_{e_{max}}$ $[m^2]$	Δp $[Pa]$	Δt $[s]$	$A_{e_1}/A_{e_{max}}$
0	8.18	63.06	103.72	0.3888	0.1297
2	8.188	63.01	103.68	0.3887	0.1298
4	8.18	62.86	103.53	0.3881	0.1301
6	8.17	62.60	103.29	0.3872	0.1304
8	8.152	62.24	102.96	0.386	0.1310
10	8.129	61.786	102.55	0.3844	0.1316
12.5	8.095	61.07	101.93	0.3821	0.1325
15	8.06	60.225	101.17	0.3793	0.1338

Table 8.10: Result obtained at 20000 m of altitude

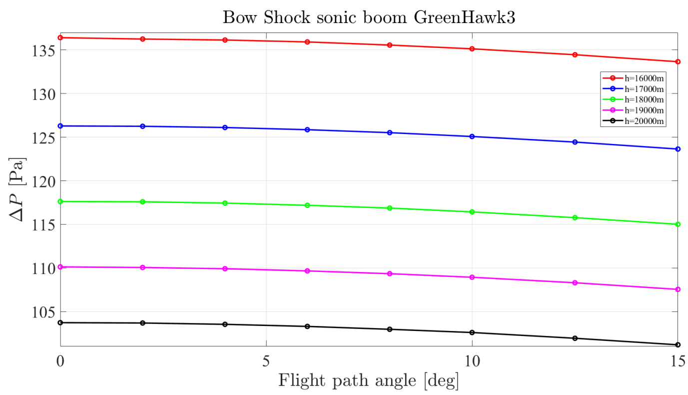

Figure 8.4: Bow shock overpressure with altitude and flight path angle variation

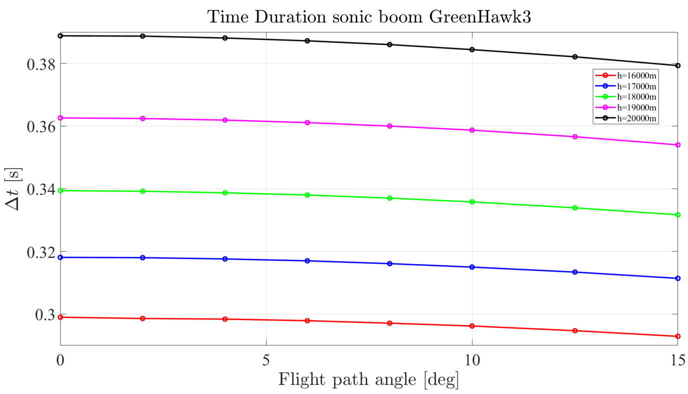

Figure 8.5: Time duration with altitude and flight path variation

About bow shock overpressure it decreases as flight path angle and flight altitude increase. Moreover the increase in flight altitude has a better beneficial effect for the overpressure. Moreover, regarding time duration it increases with increasing flight altitude, as opposed to flight path angle.

8.2.3 Sonic boom analysis by varying flight path angle and Mach number

The third sonic boom analysis was evaluated by varying simultaneously the flight path angle and Mach number.
As for the Mach number, as in the previous case it has been varying between 2.4 and 3.0 while the flight path angle has been varying between 0 and 15 degrees.

Flight path angle [deg]	$A_{e,1}$ $[m^2]$	$A_{e_{max}}$ $[m^2]$	Δp $[Pa]$	Δt $[s]$	$A_{e_1}/A_{e_{max}}$
0	8.66	71.77	104.20	0.405	0.12
2	8.61	71.70	104.16	0.4049	0.1201
4	8.595	71.52	104.01	0.4044	0.1202
6	8.58	71.2	103.76	0.4034	0.1205
8	8.56	70.77	103.40	0.402	0.121
10	8.535	70.22	102.97	0.4003	0.1216
12.5	8.497	69.37	102.29	0.3977	0.1225
15	8.444	68.34	101.50	0.3946	0.1235

Table 8.11: Result obtained with a Mach number equal to 2.4

Flight path angle [deg]	$A_{e,1}$ $[m^2]$	$A_{e_{max}}$ $[m^2]$	Δp $[Pa]$	Δt $[s]$	$A_{e_1}/A_{e_{max}}$
0	8.53	70.12	104.16	0.4017	0.1216
2	8.525	70.06	104.12	0.4015	0.1216
4	8.52	69.88	103.97	0.4009	0.1219
6	8.50	69.58	103.73	0.4000	0.1222
8	8.48	69.17	103.38	0.3986	0.1227
10	8.46	68.63	102.95	0.397	0.1233
12.5	8.42	67.8	102.26	0.3943	0.1242
15	8.37	66.81	101.45	0.3911	0.1253

Table 8.12: Result obtained with a Mach number equal to 2.5

Flight path angle [deg]	$A_{e,1}$ $[m^2]$	$A_{e_{max}}$ $[m^2]$	Δp $[Pa]$	Δt $[s]$	$A_{e_1}/A_{e_{max}}$
0	8.45	68.5	104.09	0.3985	0.1232
2	8.45	68.504	104.05	0.3984	0.1234
4	8.442	68.33	103.90	0.3978 b	0.1236
6	8.43	68.04	103.66	0.3969	0.1239
8	8.41	67.63	103.29	0.3955	0.1244
10	8.385	67.12	102.88	0.3939	0.1249
12.5	8.35	66.32	102.21	0.3914	0.1259
15	8.3	65.35	101.43	0.3883	0.127

Table 8.13: Result obtained with a Mach number equal to 2.6

Flight path angle [deg]	$A_{e,1}$ $[m^2]$	$A_{e_{max}}$ $[m^2]$	Δp $[Pa]$	Δt $[s]$	$A_{e_1}/A_{e_{max}}$
0	8.38	67.08	104.00	0.3957	0.1249
2	8.38	67.02	103.96	0.3955	0.1250
4	8.372	66.85	103.81	0.395	0.1252
6	8.36	66.57	103.57	0.394	0.1256
8	8.34	66.18	103.23	0.3928	0.1260
10	8.31	65.67	102.81	0.3912	0.1265
12.5	8.28	64.9	102.18	0.3888	0.1276
15	8.235	63.97	101.42	0.3859	0.1287

Table 8.14: Result obtained with a Mach number equal to 2.7

Flight path angle [deg]	$A_{e,1}$ $[m^2]$	$A_{e_{max}}$ $[m^2]$	Δp $[Pa]$	Δt $[s]$	$A_{e_1}/A_{e_{max}}$
0	8.316	65.67	103.89	0.3931	0.1266
2	8.314	65.61	103.85	0.3929	0.1267
4	8.305	65.45	103.70	0.3924	0.1269
6	8.292	65.18	103.48	0.3916	0.1272
8	8.275	64.8	103.17	0.3904	0.1277
10	8.25	64.3	102.76	0.3888	0.1283
12.5	8.215	63.56	102.13	0.3864	0.1292
15	8.17	62.66	101.36	0.3835	0.1304

Table 8.15: Result obtained with a Mach number equal to 2.8

Flight path angle [deg]	$A_{e,1}$ $[m^2]$	$A_{e_{max}}$ $[m^2]$	Δp $[Pa]$	Δt $[s]$	$A_{e_1}/A_{e_{max}}$
0	8.25	64.33	103.79	0.3908	0.1282
2	8.249	64.28	103.78	0.3907	0.1283
4	8.241	64.12	103.64	0.3902	0.1285
6	8.23	63.855	103.41	0.3883	0.1289
8	8.21	63.48	103.09	0.3881	0.1293
10	8.19	63.02	102.68	0.3866	0.1300
12.5	8.15	62.29	102.02	0.3841	0.1308
15	8.11	61.41	101.29	0.3811	0.1321

Table 8.16: Result obtained with a Mach number equal to 2.9

Flight path angle [deg]	$A_{e,1}$ $[m^2]$	$A_{e_{max}}$ $[m^2]$	Δp $[Pa]$	Δt $[s]$	$A_{e_1}/A_{e_{max}}$
0	8.19	63.06	103.72	0.3888	0.1297
2	8.188	63.01	103.68	0.3887	0.1298
4	8.18	62.86	103.53	0.3881	0.1301
6	8.17	62.10	103.29	0.3872	0.1305
8	8.152	62.24	102.96	0.386	0.1310
10	8.129	61.786	102.55	0.3844	0.1316
12.5	8.095	61.07	101.93	0.3821	0.1325
15	8.06	60.225	101.17	0.3793	0.1338

Table 8.17: Result obtained with a Mach number equal to 3.0

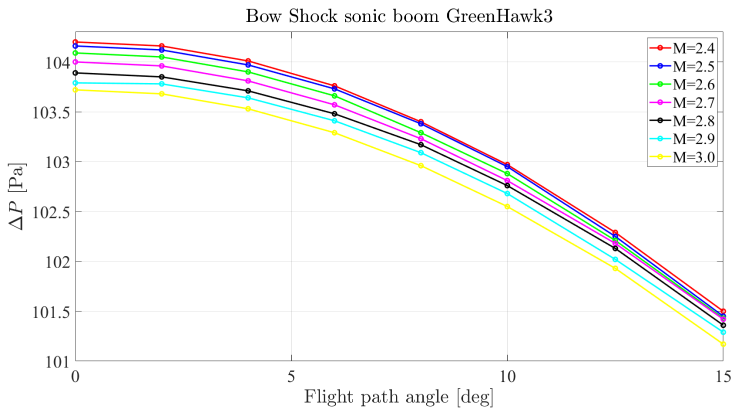

Figure 8.6: Bow Shock overpressure with Mach and flight path angle variation

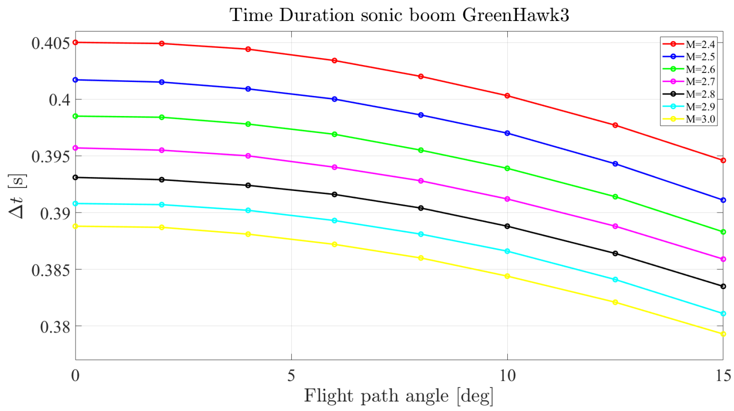

Figure 8.7: Time duration with Mach and flight path angle variation

As can be seen from the figure 8.6, as the Mach number increases, there is a slight decrease in bow shock overpressure (less than one percentage point). This is in contrast to what Carlson's method supports and could be due to the particular distribution of areas. Regarding flight path angle there is a clear decrease in bow shock overpressure as it increase.
Analyzing figure 8.7 an increase in Mach number and flight path angle leads to a reduction in time signature duration.

8.2.4 Sonic boom analysis by varying altitude and aircraft length

A sonic boom analysis was conducted by varying the aircraft altitude and length. In particular the length of the aircraft was varied between 36.5 to 42 meters while flight altitude between 16000 m to 20000m. The operative condition were a Mach number equal to 3 and a flight path angle equal to 0 deg.

Aircraft length $[m]$	$A_{e,1}$ $[m^2]$	$A_{e_{max}}$ $[m^2]$	Δp $[Pa]$	Δt $[s]$	$A_{e_1}/A_{e_{max}}$
36.54	5.61	36.7	130.86	0.2868	0.1529
37.38	5.85	37.7	131.74	0.2887	0.1552
38.22	6.09	38.7	132.6	0.2907	0.1574
39.06	6.35	39.74	133.49	0.2926	0.1597
39.90	6.59	40.76	134.32	0.2944	0.1617
40.95	6.92	42.05	135.38	0.2967	0.1646
42.00	7.25	43.32	136.42	0.299	0.1672

Table 8.18: Result obtained at 16000 m of altitude

Aircraft length $[m]$	$A_{e,1}$ $[m^2]$	$A_{e_{max}}$ $[m^2]$	Δp $[Pa]$	Δt $[s]$	$A_{e_1}/A_{e_{max}}$
36.54	5.77	40.06	121.27	0.3054	0.1441
37.38	6.02	41.14	122.10	0.3075	0.1463
38.22	6.27	42.23	122.94	0.3096	0.1484
39.06	6.51	43.3	123.64	0.3114	0.1502
39.90	6.77	44.42	124.46	0.3135	0.1524
40.95	7.1	45.83	125.42	0.3159	0.1550
42.00	7.43	47.17	126.29	0.3181	0.1575

Table 8.19: Result obtained at 17000 m of altitude

Aircraft length $[m]$	$A_{e,1}$ $[m^2]$	$A_{e_{max}}$ $[m^2]$	Δp $[Pa]$	Δt $[s]$	$A_{e_1}/A_{e_{max}}$
36.54	5.95	44.01	113.12	0.3263	0.1352
37.38	6.2	45.15	113.80	0.3282	0.1373
38.22	6.45	46.33	114.56	0.3304	0.1392
39.06	6.71	47.52	115.27	0.3325	0.1412
39.90	7.00	48.7	115.98	0.3345	0.1431
40.95	7.3	50.2	116.82	0.337	0.1454
42.00	7.63	51.66	117.62	0.339	0.1477

Table 8.20: Result obtained at 18000 m of altitude

Aircraft length $[m]$	$A_{e,1}$ $[m^2]$	$A_{e_{max}}$ $[m^2]$	Δp $[Pa]$	Δt $[s]$	$A_{e_1}/A_{e_{max}}$
36.54	6.17	48.6	106.10	0.349	0.127
37.38	6.425	49.86	106.73	0.3514	0.128
38.22	6.68	51.14	107.43	0.3538	0.1306
39.06	6.94	52.4	108.02	0.3557	0.1324
39.90	7.22	53.706	108.61	0.3576	0.1345
40.95	7.57	55.33	109.39	0.3602	0.1368
42.00	7.9	56.93	110.12	0.3626	0.1388

Table 8.21: Result obtained at 19000 m of altitude

Aircraft length $[m]$	$A_{e,1}$ $[m^2]$	$A_{e_{max}}$ $[m^2]$	Δp $[Pa]$	Δt $[s]$	$A_{e_1}/A_{e_{max}}$
36.54	6.44	53.97	99.84	0.3742	0.1193
37.38	6.67	55.37	100.46	0.3766	0.1207
38.22	6.95	56.76	101.11	0.379	0.1224
39.06	7.21	58.15	101.71	0.3813	0.124
39.90	7.48	59.56	102.30	0.3835	0.1256
40.95	7.84	61.33	103.05	0.3863	0.1278
42.00	8.18	63.06	103.72	0.3888	0.1297

Table 8.22: Result obtained at 20000 m of altitude

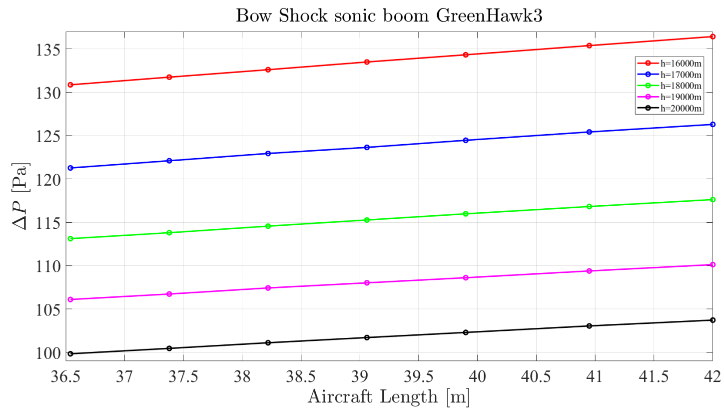

Figure 8.8: Bow Shock overpressure with aircraft length and altitude variation

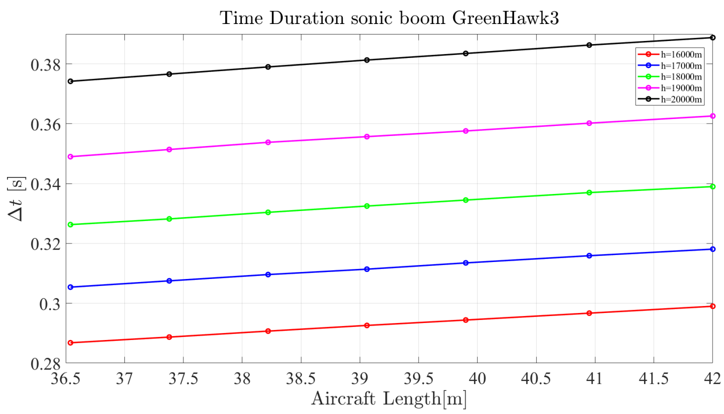

Figure 8.9: Time duration with aircraft length and altitude variation

As can be seen from the figure 8.8, the bow shock overpressure increases as the length of the aircraft grows and decreases at higher altitudes.In particular, the effect of altitude increase is predominant compared to that of aircraft length.
Regarding time duration, it can be seen that it increases as both length and altitude increase.

8.2.5 Sonic boom analysis with Mach number and length variation

Finally a sonic boom analysis was conducted by varying the Mach number and the aircraft length. In particular, the Mach number varied between 2.4 and 3.0 while the aircraft length varied between 36.5 m and 42.0 m.
The test was conducted for an altitude of 20000m and a flight path angle of 0 degrees.

Aircraft length $[m]$	$A_{e,1}$ $[m^2]$	$A_{e_{max}}$ $[m^2]$	Δp $[Pa]$	Δt $[s]$	$A_{e_1}/A_{e_{max}}$
36.54	6.79	61.6	100.48	0.3906	0.1102
37.38	7.06	63.15	101.06	0.3929	0.1118
38.22	7.33	64.7	101.67	0.3953	0.1133
39.06	7.605	66.3	102.25	0.3975	0.1147
39.90	7.89	67.84	102.80	0.3996	0.1163
40.95	8.24	69.8	103.52	0.4025	0.118
42.00	8.61	71.77	104.20	0.4051	0.120

Table 8.23: Result obtained with a Mach number equal to 2.4

Aircraft length $[m]$	$A_{e,1}$ $[m^2]$	$A_{e_{max}}$ $[m^2]$	Δp $[Pa]$	Δt $[s]$	$A_{e_1}/A_{e_{max}}$
36.54	6.72	60.16	100.40	0.3871	0.1118
37.38	6.99	61.67	100.97	0.3894	0.1133
38.22	7.26	63.2	101.63	0.3919	0.1149
39.06	7.53	64.75	102.21	0.3941	0.1163
39.90	7.82	66.28	102.75	0.3962	0.1180
40.95	8.18	68.2	103.47	0.3990	0.1199
42.00	8.53	70.12	104.17	0.4017	0.1216

Table 8.24: Result obtained with a Mach number equal to 2.5

Aircraft length $[m]$	$A_{e,1}$ $[m^2]$	$A_{e_{max}}$ $[m^2]$	Δp $[Pa]$	Δt $[s]$	$A_{e_1}/A_{e_{max}}$
36.54	6.66	58.8	100.36	0.3843	0.1133
37.38	6.92	60.28	100.89	0.3863	0.1148
38.22	7.18	61.77	101.58	0.389	0.1163
39.06	7.46	63.28	102.13	0.391	0.1179
39.90	7.74	64.8	102.68	0.3932	0.1194
40.95	8.09	66.69	103.41	0.3959	0.1213
42.00	8.45	68.56	104.09	0.3985	0.1232

Table 8.25: Result obtained with a Mach number equal to 2.6

Aircraft length $[m]$	$A_{e,1}$ $[m^2]$	$A_{e_{max}}$ $[m^2]$	Δp $[Pa]$	Δt $[s]$	$A_{e_1}/A_{e_{max}}$
36.54	6.599	57.5	100.25	0.3814	0.1147
37.38	6.86	58.95	100.83	0.3837	0.1164
38.22	7.125	60.42	101.46	0.386	0.1180
39.06	7.4	61.9	102.03	0.388	0.1195
39.90	7.67	63.4	102.69	0.3907	0.1208
40.95	8.00	65.25	103.36	0.3933	0.1226
42.00	8.38	67.08	104.00	0.3957	0.1249

Table 8.26: Result obtained with a Mach number equal to 2.7

Aircraft length $[m]$	$A_{e,1}$ $[m^2]$	$A_{e_{max}}$ $[m^2]$	Δp $[Pa]$	Δt $[s]$	$A_{e_1}/A_{e_{max}}$
36.54	6.54	56.25	100.12	0.3788	0.1163
37.38	6.8	57.7	100.71	0.3811	0.1179
38.22	7.06	59.14	101.34	0.3835	0.1194
39.06	7.33	60.58	101.91	0.3856	0.1210
39.90	7.6	62.03	102.47	0.3877	0.1225
40.95	7.96	63.87	103.23	0.3906	0.1246
42.00	8.31	65.65	103.91	0.3932	0.1266

Table 8.27: Result obtained with a Mach number equal to 2.8

Aircraft length $[m]$	$A_{e,1}$ $[m^2]$	$A_{e_{max}}$ $[m^2]$	Δp $[Pa]$	Δt $[s]$	$A_{e_1}/A_{e_{max}}$
36.54	6.485	55.1	99.99	0.3765	0.1177
37.38	6.74	56.5	100.57	0.3787	0.1193
38.22	7.006	57.91	101.22	0.3811	0.1210
39.06	7.27	59.33	101.79	0.3833	0.1226
39.90	7.545	60.76	102.40	0.3856	0.1242
40.95	7.9	62.57	103.14	0.3883	0.1263
42.00	8.26	64.33	103.85	0.3910	0.1282

Table 8.28: Result obtained with a Mach number equal to 2.9

Aircraft length $[m]$	$A_{e,1}$ $[m^2]$	$A_{e_{max}}$ $[m^2]$	Δp $[Pa]$	Δt $[s]$	$A_{e_1}/A_{e_{max}}$
36.54	6.44	53.97	99.84	0.3742	0.1193
37.38	6.67	55.37	100.46	0.3766	0.1207
38.22	6.95	56.76	101.11	0.379	0.1223
39.06	7.21	58.15	101.71	0.3813	0.1240
39.90	7.48	59.56	102.30	0.3835	0.1256
40.95	7.84	61.33	103.05	0.3863	0.1278
42.00	8.18	63.06	103.72	0.3888	0.1297

Table 8.29: Result obtained with a Mach number equal to 3.0

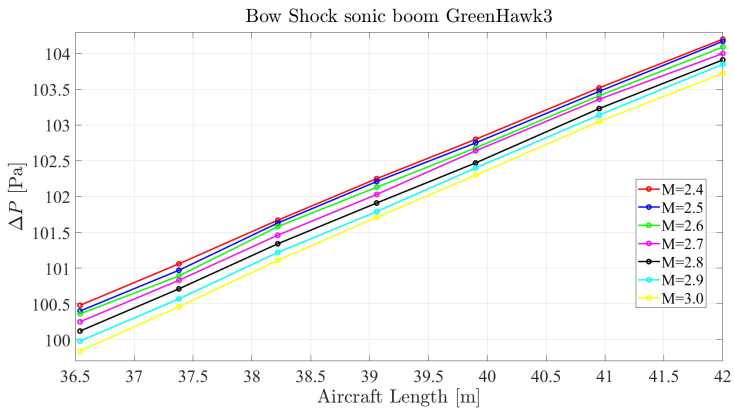

Figure 8.10: Bow Shock overpressure with Mach number and length variation

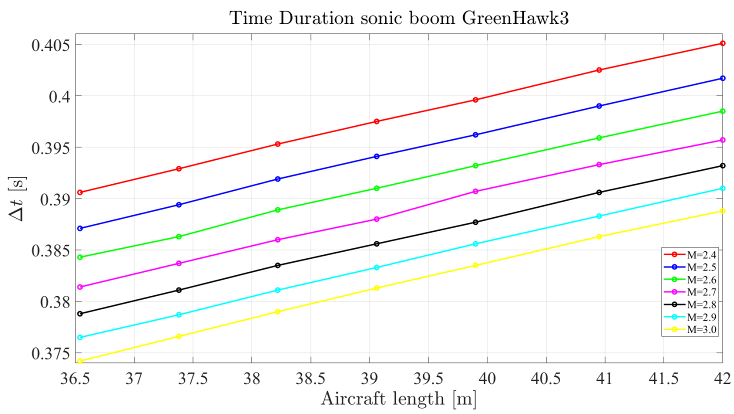

Figure 8.11: Time duration with Mach number and length variation

As can be seen from the figure 8.10, as the Mach number increase, the bow shock overpressure remains more or less constant, while it increase as the length of the aircraft grows.
As far as time duration is concerned, it increases with the Mach number and the aicraft length growth.

9

Conclusion

9.1 Method evaluations

This thesis assessed the impact of certain flight conditions and aircraft geometry on bow shock overpressure and time signature duration for a primary sonic boom. Different types of aircraft with quite different aerodynamic and performance characteristics were investigated in order to determine whether certain measures would be beneficial for all aircraft.
In particular, the aircraft studied were:

i. Stratofly, a hypersonic aircraft capable of flying at a hypersonic Mach number equal to 8 and with much greater dimensions and weight

ii. A shorter version with a length of 66.3 m instead of the 94.6 m of the reference aircraft

iii. Concorde, the first and only occidental supersonic civil aircraft with a cruising Mach number equal to 2.02

iv. GreenHawk3, a conceptual design of a supersonic business jet capable of flying at Mach 3 made by eleven students from the Politecnico di Torino between 2020 and 2021.

v. A version of this by translating the two halfwings forward to study this change in terms of sonic boom response

vi. A version of this with a Canard configuration, in order to compare which is the best benefit in terms of Sonic Boom response

(a) Concorde (b) GreenHawk3 (c) Stratofly

Figure 9.1: Aircraft studied

The methodologies that have been studied are applicable to both the design phase of the aircraft and the operational phase. The study varied the length of the aircraft, the Mach number, the flight altitude and the angle of the flight path.

Effect of altitude

As can be seen from the results proposed in the previous chapters, it is clear that increasing the flight altitude has a considerable effect on decreasing bow shock overpressure for all aircraft. On the other hand, an increase in altitude leads to an evident increase in sonic boom duration and is due to the longer time required for the pressure wave to reach the ground. Since it is thought that in the future there will be overpressure values (probably over 0.5 lb/ft^2) above which it will not be possible to operate, the increase in flight altitude could be important to allow these aircraft to fly over the land.
Consequently, a study to maximise operational flight altitude already in the design phase would bring considerable benefits in terms of reducing sonic boom overpressure. Moreover, the effect related to the increase in altitude is the most important effect for overpressure.
The reason why the influence of flight altitude is so predominant on bow shock overpressure can be found in Carlson's own simplified formulation:

$$\Delta p_{max} = K_P \cdot K_R \cdot \sqrt{p_v p_g} \cdot \left(M^2 - 1\right)^{\frac{1}{8}} \cdot h_e^{-\frac{3}{4}} \cdot l^{\frac{3}{4}} \cdot K_s \tag{9.1}$$

This consideration was understandable by analysing Carlson's simplified formulation in which the contribution of the altitude was present both in terms of the atmospheric effects given by the product $\sqrt{p_v \cdot p_g}$ and by the presence of the effective altitude h_e itself elevated with a negative exponent. In order to emphasize the variation of pressure as a function of flight altitude, a graph has been presented:

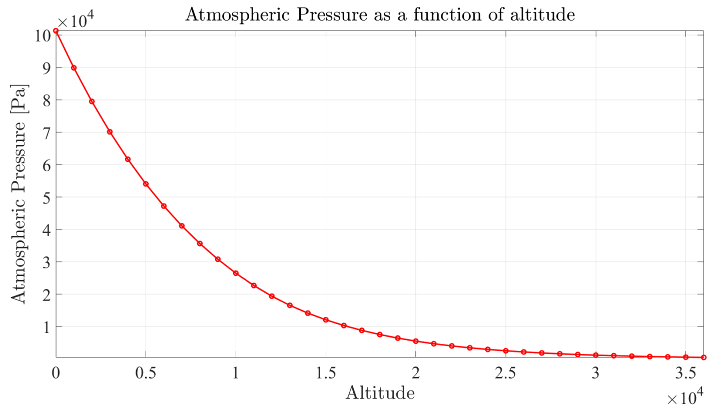

Figure 9.2: Development of atmospheric pressure with flight altitude

Effect of aircraft length

Regarding aircraft length, a reduction in aircraft length leads to a reduction in sonic boom overpressure and time signature duration duration.
Analysing the graphs for the previous chapters, it can be seen that the reduction in bow shock overpressure with the reduction in aircraft length is much smaller than with the change in altitude. Consequently, the aircraft dimensions are not the most important factor in terms of bow shock overpressure but rather the operating conditions.
Moreover, in the shape factor parameter K_S derived through figure 2.4 the length of the aircraft

in the denominator involves a compensation with the term $l^{\frac{3}{4}}$.

Effect of flight path angle

As far as the flight path angle and ray path azimuth angle are concerned, its growth leads to an important reduction in bow shock overpressure for higher value of these angles. This is due to the fact that as the inclination from the horizontal increases, the ray paths will have to take a longer trajectory to reach the ground and will result in a higher relative altitude.
Consequently, the effective flight altitude h_e will not simply be given by the difference between the flight altitude and the ground altitude but will have to take into account a new horizontal component d_x.
As already mentioned in chapter 2 the effective flight altitude for the on track case is equal to:

$$h_e = d_x \cdot \sin\gamma + h \cdot \cos\gamma \tag{9.2}$$

As can be seen from the graphs for the aircraft's in the previous chapters for high values of flight path angle and ray path azimuth angle the decrease in bow shock ovepressure is very marked. This may be due to the fact that the method is applicable in the case of level flight or with moderate descents or ascents, so high flight path angle values may fall outside the validity range of the method.
As the flight path angle increases, the rate of decrease of the bow shock overpressure value increases. In particular, it can be seen that for the values of 10,12.5 and 15 degrees the rate of decrease is very evident.
According to the above graphs, the reduction in bow shock ovepressure as flight path angle increases is more pronounced than a reduction in aircraft length but less pronounced than an increase in altitude.

Effect of Mach number

Regarding the variation of bow shock overpressure and time duration as the Mach number changes, the evaluation is very complicated and leads to conflicting results. The Mach number is also involved in the evolution of the equivalent area due to lift through the parameter upstream of the integral of the function itself and equal to:

$$B(x) = \frac{\sqrt{M^2 - 1} \cdot W \cdot \cos\gamma \cos\theta}{1.4 \cdot p_v \cdot M^2 S} \tag{9.3}$$

Analysing the numerator and denominator of this function shows that it is approximately proportional to $\frac{1}{M}$ for high Mach numbers.
According to the Carlson method, the bow shock overpressure should increase slightly as the Mach number increases: this statement was found to be true for Concorde and GreenHawk3(and its other version) but not for the other aircraft tested.
The main reason may be due to the aircraft's configuration itself, as an increase in Mach number has led to changes in the ratio of effective area at midpoint and maximum effective area $(A_{e,1}/A_{e,max})$. The increase of this ratio, as can be seen in figure 2.4 leads to a linear decrease of the shape factor K_S.
So it is possible that the decrease in shape factor value is greater than the increase due to the increase in Mach number. In any case, the decrease in the value of bow shock overpressure as the Mach number increases for these cases is very limited (less then a few percentage points) compared to the previously described parameters.
On the other hand for the time duration the value decreases significantly in all cases as the Mach number increases.

9.2 Influence of the Canard

As discussed in chapter 8, a sonic boom analysis was performed by positioning a canard on the GreenHawk3 aircraft.
The canard was positioned 7.90 metres from the nose of the aircraft and corresponding to the beginning of the passenger cabin. In terms of dimensions, it was decided to take the dimensions of the Eurofighter Typhoon Canard which is a multi-role military aircraft and is an example of a canard for supersonic aircraft.
This size was chosen because it is one of the few examples of a supersonic aircraft equipped with a Canard, even though the size of the aircraft itself is much smaller compared to the GreenHawk3. Consequently, the results may not be adequate and a detailed study should be carried out for an appropriately sized canard.
Comparisons are given below for all tests performed. The results are not as expected an improvement, and may be due to the size of the canard itself.

9.2.1 Flight path angle and altitude variation

In this section, the comparison between the classic configuration and the configuration with the canard will be represented graphically.

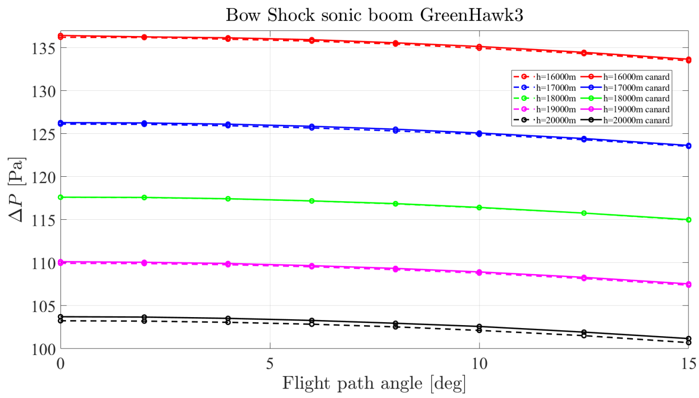

Figure 9.3: Comparison in Bow Shock overpressure with altitude and flight path angle variation

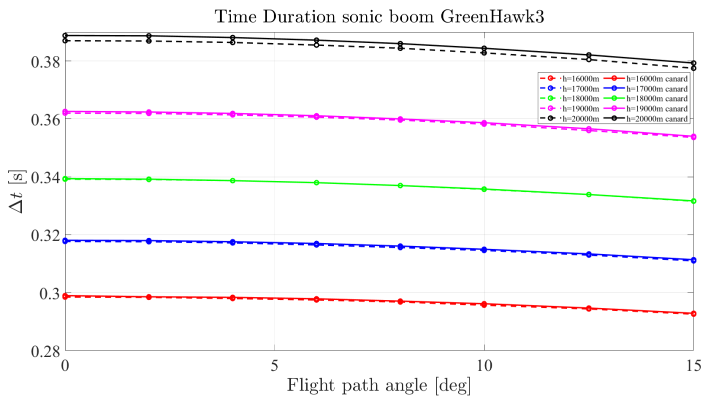

Figure 9.4: Comparison in time duration with altitude and flight path angle variation

As can be seen from the figures 9.3 and 9.4, the introduction of the canard does not cause a noticeable change in bow shock overpressure and time duration. As already pointed out, this may be mainly due to the fact that the canard is small compared to the aircraft.

9.2.2 Mach number and altitude variation

In this scenario, the possible influence of the canard will be analysed in terms of bow shock overpressure and time duration by varying the Mach number and altitude simultaneously.
As in the previous case the range of variation of the parameter were the same.

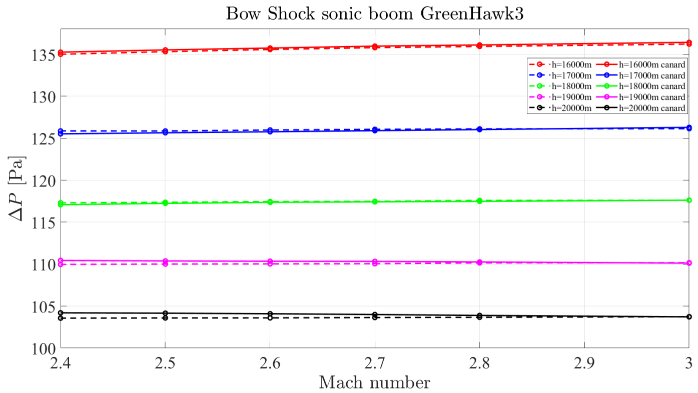

Figure 9.5: Comparison in Bow Shock overpressure with altitude and Mach number variation

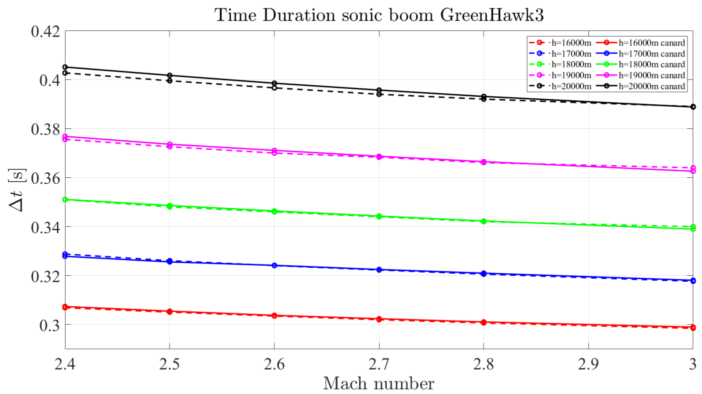

Figure 9.6: Comparison in time duration with altitude and Mach number variation

As in the previous case, the influence of the canard is very slight with a variation of no more than one percentage point.

9.2.3 Aircraft length and altitude variation

It will be studied whether the simultaneous variation of aircraft length and flight altitude will affect the bow shock overpressure and time duration.

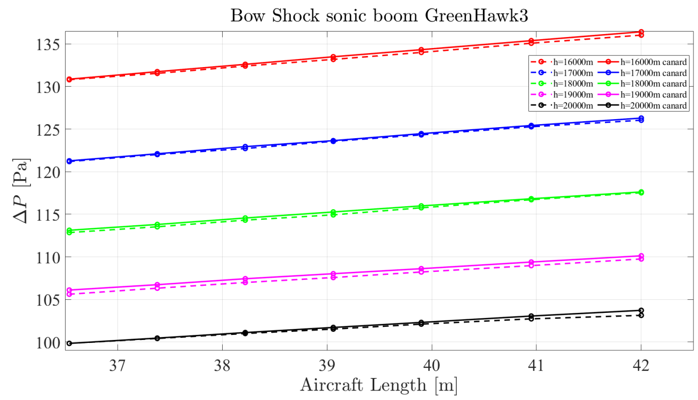

Figure 9.7: Comparison in bow shock overpressure with altitude and aircraft length variation

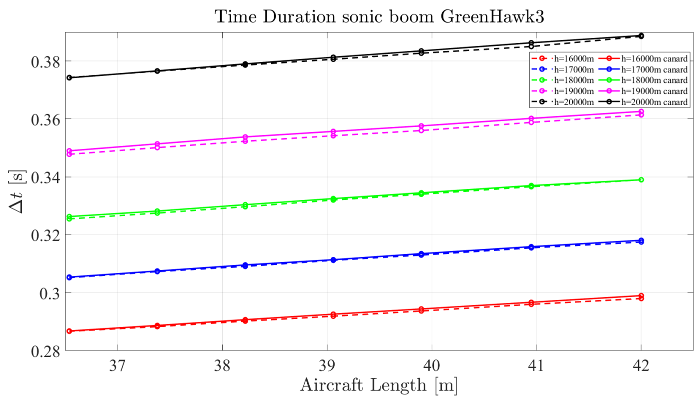

Figure 9.8: Comparison in time duration with altitude and aircraft length variation

As in the previous cases, the presence of the canard does not significantly affect either the bow shock overpressure or the time duration. The greatest difference is again in the time duration for high altitude values, but as in the previous cases it does not exceed one percentage point.

9.2.4 Mach number and aircraft length variation

It will be evaluated whether the presence of the canard together with the variation in Mach number and aircraft length will affect the bow shock overpressure and time duration.

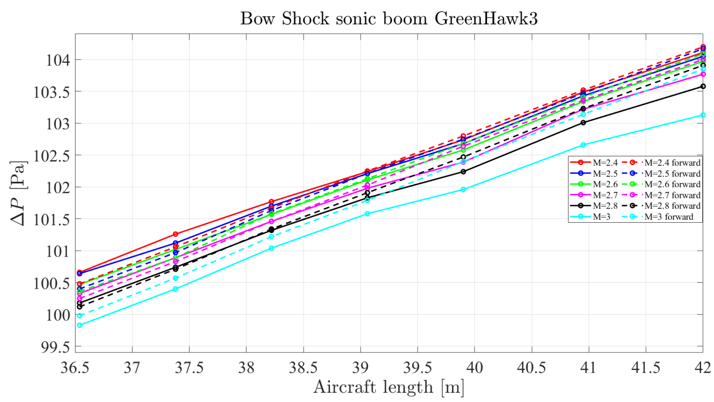

Figure 9.9: Comparison in bow shock overpressure with Mach number and aircraft length variation

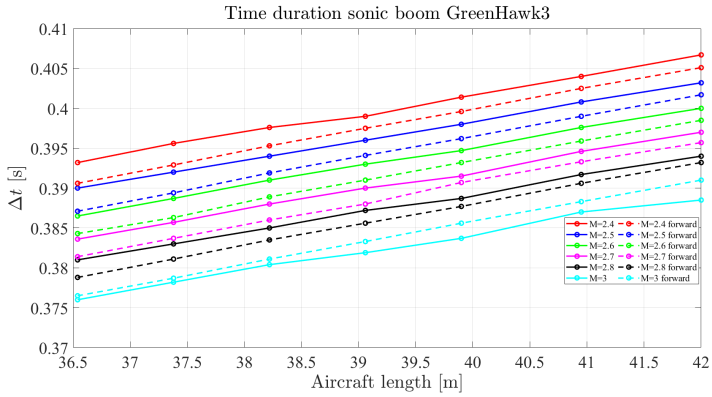

Figure 9.10: Comparison in bow shock overpressure with Mach number and aircraft length variation

As far as time duration is concerned, the presence of the canard has an evident positive effect, with a reduction of more than a few percentage points. About bow shock overpressure the variation given by the canard configuration is very low, with only the case at Mach 3 having a lower value in the nominal case.

9.2.5 Final consideration

The presence of the canard does not vary clearly the response of the bow shock overpressure and time duration. For this studies it was decided to use a canard used on a smaller aircraft just to have a first comparison.
This inevitably led to a reduction and variation of the actual benefits given by this configuration. Clearly there is a reduction in shape factor and the area ratio is greater than the nominal case, however this variation, due to the small size of the canard used, is such that the bow shock and time duration do not vary considerably.

9.3 Influence of wing forward movement

In the chapter 7 a configuration of the GreenHawk3 was analysed with a wing forward displacement of 2 metres. These considerations only concern the analysis of the sonic boom without going into all the other requirements of the aircraft itself.
These analyses were conducted under the same conditions and the same parameters were varied in the same ranges of values.

9.3.1 Flight path angle and altitude variation

In this section a graph will be represented showing the values obtained for both configurations in order to note graphically the relative advantages.

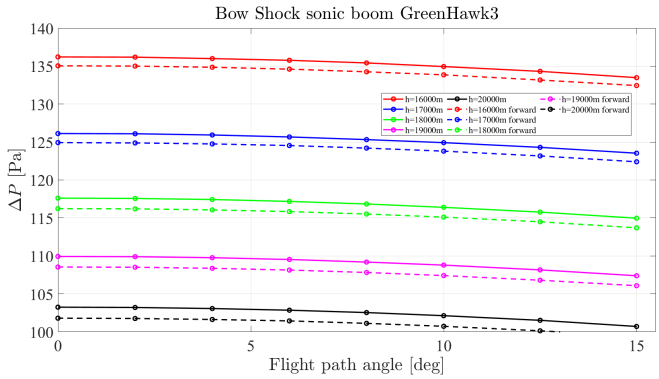

Figure 9.11: Comparison between the two configurations with flight path angle and altitude variation

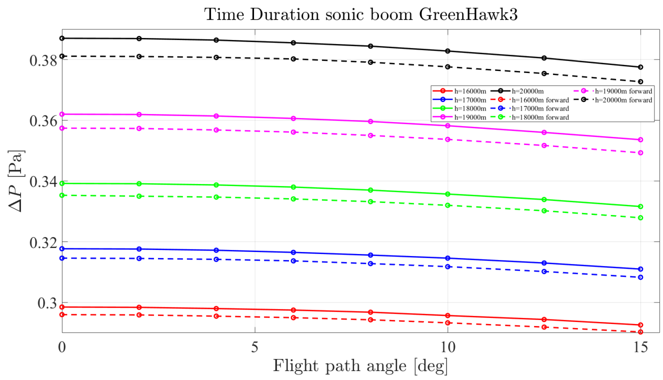

Figure 9.12: Comparison between the two configurations with flight path angle and altitude variation

Comparing the values of the tables in sections 5.2.2 and 7.2.2 it can be seen that the version with the wings positioned two metres forward has lower values of both bow shock overpressure and time duration.
However, in both cases the reduction is not marked and is within a few percentage points.

9.3.2 Mach number and altitude

In this section the advantage of forward positioning will be evaluated by varying the Mach number and flight altitude.

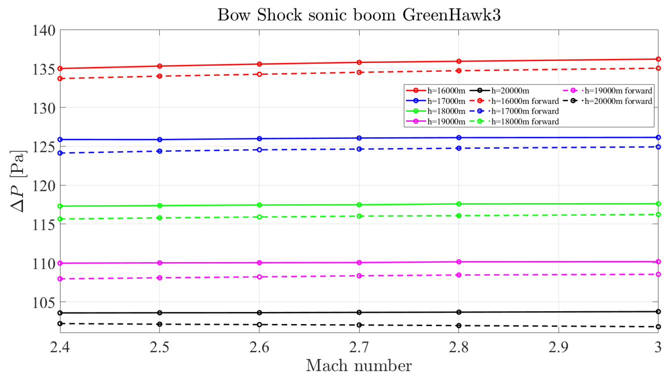

Figure 9.13: Comparison between the two configurations with Mach number and altitude variation

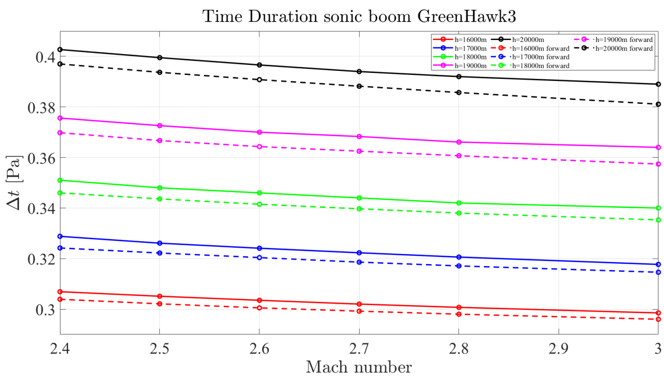

Figure 9.14: Comparison between the two configurations with Mach number and altitude variation

In this case the forward positioning of the wings provides again an advantage for both the bow shock overpressure and the time duration but even in this scenario the values are slightly lower as can be seen in sections 7.2.3 and 5.2.3.

9.3.3 Aircraft length and altitude

This section will examine the possible advantages of forward wing positioning with simultaneous variation of aircraft length and altitude.

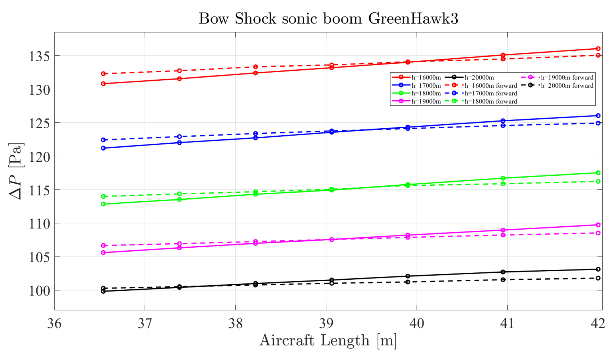

Figure 9.15: Comparison between the two configurations with aircraft length and altitude variation

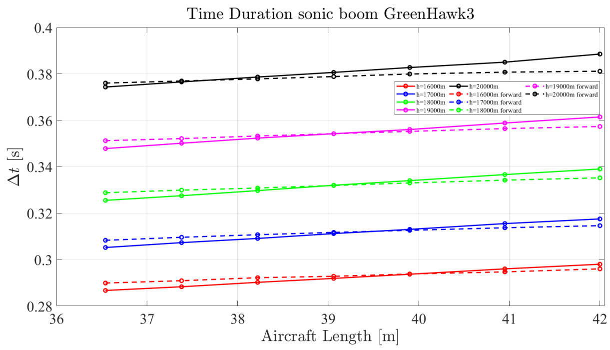

Figure 9.16: Comparison between the two configurations with aircraft length and altitude variation

In this case it can be seen that for lengths shorter than the nominal length a forward positioning of the wing does not bring any advantage, while for the nominal length there is a slight reduction in bow shock overpressure and time duration.

9.3.4 Mach number and Aircraft length

Finally, this section will evaluate the possible benefits of a forward wing configuration by varying the Mach number and aircraft length simultaneously.

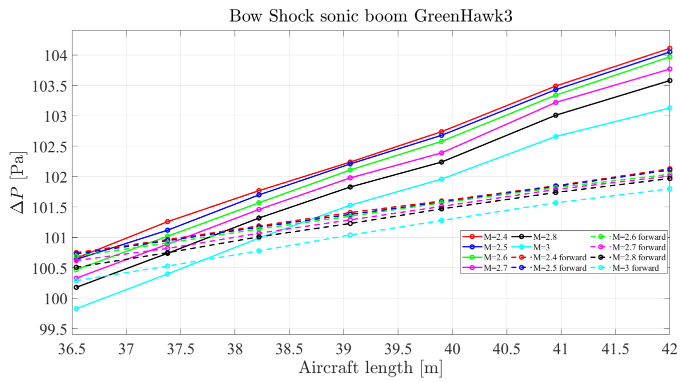

Figure 9.17: Comparison between the two configurations with aircraft length and Mach number variation

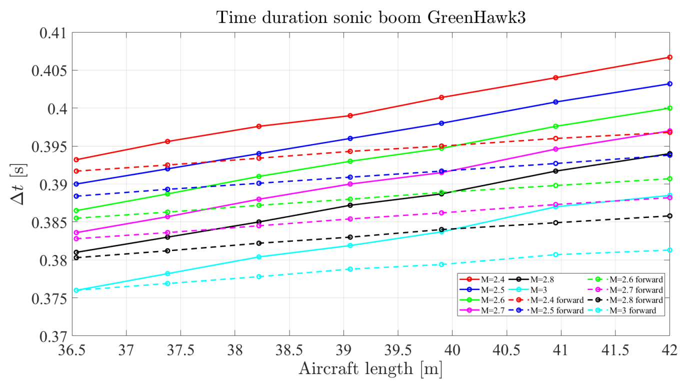

Figure 9.18: Comparison between the two configurations with aircraft length and Mach number variation

As in the previous case, if the aircraft length is less than the nominal one, the forward positioning of the wings leads to disadvantages.
On the other hand, as the length increases, there is a clear advantage for bow shock overpressure and a smaller benefit for time duration.

9.3.5 Final consideration of forward positioning

The same sensitivity analyses were carried out as for the GreenHawk3 aircraft with those of the forward wing positioning aircraft. In all the case studied there is a benefit in terms of bow shock overpressure and time signature duration due to the fact that the area ratio $A_{e,1}/A_{e,max}$ is increased and therefore the shape factor is reduced.
The advantage obtained in all cases is not very evident and does not exceed a few percentage points, but is still an improvement over the nominal case. These analyses were carried out without analysing the aircraft's airworthiness behaviour as a result of the change in geometry distribution. Consequently, during conceptual design phase it would be necessary to study possible issues (especially with regard to the positioning of the centre of gravity) due to wing movement.

9.4 Role of altitude in Stratofly

Two different configurations were studied for Stratofly aircraft:

1. A 94 meters nominal version capable of flying at 36000m and with a Mach number of 8

2. A 30% shorter version capable of flying at Mach 5 and 30 km of altitude

To evaluate the effect of altitude, bow shock overpressure and time duration were evaluated by varying altitude and flight path angle.
For the nominal version of Stratofly a Mach number of 7 has been considered, while for the shorter version the Mach number was equal to 5.

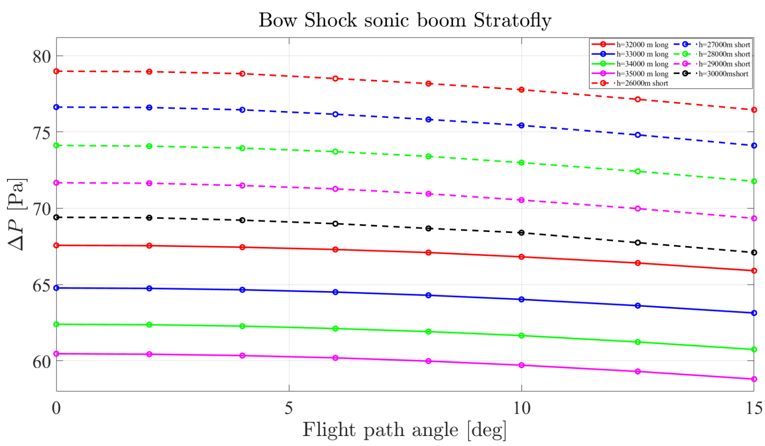

Figure 9.19: Role of altitude for the two different configuration of Stratofly

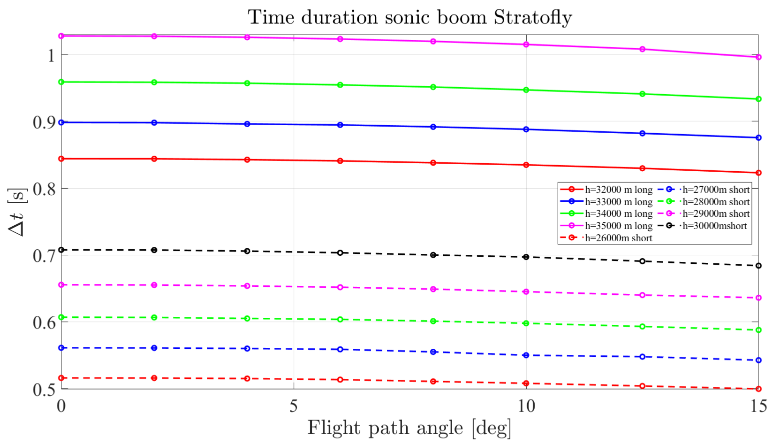

Figure 9.20: Role of altitude for the two different configuration of Stratofly

As can be seen from the figure 9.19, the longer 94.6 meters version, flying at a higher altitude than the second model, has slightly lower bow shock overpressure values. This implies that in Stratofly the effect of altitude is predominant than the effect given by the increase in length of the aircraft and the growth of Mach number.
Concerning time duration, an increase in altitude leads to an evident increase. In particular, it has already been shown that a rise in the length of the aircraft leads to an increase in the time duration, while, as can be seen in figure 9.20, the combined effect of altitude and length leads to a very evident increase.

Acknowledgements

First of all, I would like to personally thank Professors Viola and Fusaro for having always followed me throughout this thesis work.
I would like to thank all my family members who decided to invest in me by allowing me to study away from home and who never stopped believing in me.
I would like to thank the Politecnico di Torino for the many lessons it has given me over this period of time despite the arrival of the coronavirus and despite an Erasmus programme that did not materialise due to the pandemic itself.
Last but not least, I want to thank all my friends and all those who have supported me during these 5 years at university. They have been my strength and determination to achieve all my goals.

Bibliography

[1] *Review of Sonic-Boom generation theory and prediction methods* Acoustical Society of America, 1972.

[2] *Research of low boom and low drag supersonic aircraft design* Chinese Journal of Aeronautics, 2014.

[3] *A laboratory study of Subjective Annoyance Response to Sonic Boom and Aircraft Flyovers* NASA, 1994.

[4] *Application of Sonic-Boom Minimization Concepts in Supersonic Transport Design* NASA, 1973.

[5] *Preliminary Optimization of the Sonic-Boom Properties for Civil Supersonic Aircraft* Journal of Aircraft,2013.

[6] *Supersonic Deviations: Assessment of Sonic-Boom-Restricted Flight Routing* Journal of Aircraft, 2014.

[7] *Low-Boom and Low-Drag Optimization of Twin Engine Version of Silent Supersonic Business Jet* Journal of Fluid Science and Technology, 2008.

[8] *Aeroacoustics of Flight Vehicles: Theory and Practice* NASA, 1991.

[9] *Sonic-Boom Minimization With Nose-Bluntness Relaxation* NASA,1979.

[10] *Noise and Sonic Boom Impact Technology: Effects of Aircraft Noise and Sonic Boom on Structures: an Assessment of the Current State-of- Knowledge* 1989.

[11] *Sonic Boom Minimization through Vehicle Shape Optimization and Probabilistic Acoustic Propagation* Georgia Institue of Technology, 2005.

[12] *Preliminary Optimization of the Sonic Boom Properties for Civil Supersonic Aircraft* Journal of Aircraft, 2013.

[13] *Sonic-Boom Propagation through a Stratified Atmosphere* Acoustical Society of America, 1972.

[14] *Sonic Boom, Six Decades of Research* NASA, 2020.

[15] *The influence of wing configuration elements in a civil aircraft on sonic boom parameters* American Institute of Physics, 2018.

[16] *Simplified Sonic-Boom Prediction* NASA, 1978.

[17] *Supersonic Aircraft Optimization for Minimizing Drag and Sonic Boom* 2003.

[18] *Sonic Boom and Drag Evaluation of Supersonic Jet Concepts* AIAA Aviation Forum, 2018.

[19] *Sonic Boom* The Pennsylvania State University, 2010.

[20] *Quieting the Boom* NASA, 2013.

[21] https://www.concordesst.com/

[22] https://www.britannica.com/technology/Concorde

[23] https://www.britishairways.com/it-it/information/about-ba/history-and-heritage/celebrating-concorde

[24] https://www.h2020-stratofly.eu/

[25] https://cordis.europa.eu/project/id/769246/reporting/it

[26] *Stratofly's CAD*

[27] *Exploitation and analysis of available data: Synthesis*, Rumble, 2017.

[28] *Quantification of indoor vibrations* Rumble, 2017.

[29] *Benchmark test case results on implemented sonic boom noise metrics* Rumble, 2017.